NUREG/CR–6428
ANL–95/47

Effects of Thermal Aging on Fracture Toughness and Charpy–Impact Strength of Stainless Steel Pipe Welds

Manuscript Completed: November 1995
Date Published: May 1996

Prepared by
D. J. Gavenda, W. F. Michaud, T. M. Galvin, W. F. Burke, and O. K. Chopra

Argonne National Laboratory
9700 South Cass Avenue
Argonne, IL 60439

M. E. Mayfield, NRC Project Manager

Prepared for
Office of Nuclear Regulatory Research
U.S. Nuclear Regulatory Commission
Washington, DC 20555
NRC FIN A2212

Effects of Thermal Aging on Fracture Toughness and Charpy–Impact Strength of Stainless Steel Pipe Welds

by

D. J. Gavenda, W. F. Michaud, T. M. Galvin,
W. F. Burke, and O. K. Chopra

Abstract

The degradation of fracture toughness, tensile, and Charpy–impact properties of Type 308 stainless steel (SS) pipe welds due to thermal aging has been characterized at room temperature and 290°C. Thermal aging of SS welds results in moderate decreases in Charpy–impact strength and fracture toughness. For the various welds in this study, upper–shelf energy decreased by 50–80 J/cm^2. The decrease in fracture toughness J–R curve or J_{IC} is relatively small. Thermal aging had little or no effect on the tensile strength of the welds. Fracture properties of SS welds are controlled by the distribution and morphology of second–phase particles. Failure occurs by the formation and growth of microvoids near hard inclusions; such processes are relatively insensitive to thermal aging. The ferrite phase has little or no effect on the fracture properties of the welds. Differences in fracture resistance of the welds arise from differences in the density and size of inclusions. Mechanical–property data from the present study are consistent with results from other investigations. The existing data have been used to establish minimum expected fracture properties for SS welds.

Contents

Figures

Tables

Executive Summary

Stainless steels (SSs) are used extensively in light water reactor (LWR) systems because of their excellent ductility, high notch toughness, corrosion resistance, and good formability. Although these steels are completely austenitic in the wrought condition, welded and cast SSs have a duplex structure consisting of austenite and ferrite phases. The ferrite phase provides additional benefits, e.g., it increases tensile strength and improves the resistance to stress corrosion cracking. However, the duplex steels are susceptible to thermal embrittlement after extended service at reactor operating temperatures, i.e., typically 282°C (540°F) for boiling water reactors, 288–327°C (550–621°F) for pressurized water reactor (PWR) primary coolant piping, and 343°C (650°F) for PWR pressurizers.

It is well established that thermal embrittlement of cast duplex SSs at reactor temperatures increases hardness and tensile strength; decreases ductility, impact strength, and fracture toughness; and shifts the Charpy transition curve to higher temperatures. Thermal embrittlement is caused primarily by formation of the Cr–rich α' phase in the ferrite and, to some extent, by precipitation and growth of carbides at phase boundaries. It results in brittle fracture associated with either cleavage of the ferrite or separation of the ferrite/austenite phase boundary. Predominantly brittle failure occurs when either the ferrite phase is continuous (e.g., in material with a large ferrite content) or the ferrite/austenite phase boundary provides an easy path for crack propagation (e.g., in materials with high C content). The amount, size, and distribution of the ferrite phase in the duplex structure, and the presence of phase–boundary carbides are important parameters in controlling the degree or extent of thermal embrittlement.

A procedure and correlations have been developed for estimating fracture toughness, tensile, and Charpy–impact properties of cast SS components during service from known material information. Although SS welds have a duplex structure and their chemical compositions are similar to those of cast SSs, the estimation scheme is not applicable to SS welds. The degradation of fracture toughness, tensile, and Charpy–impact properties of Type 308 pipe welds due to thermal aging has been characterized in this report. The welds were aged for 7,000–10,000 h at 400°C to simulate saturation conditions, i.e., lowest impact energy that would be achieved by the material after long–term aging. The results have been compared with fracture–property data from other studies.

Thermal aging of the SS welds resulted in moderate decreases in Charpy–impact strength and fracture toughness at both room temperature and 290°C. For the various welds, USE decreased by 50–80 J/cm^2 (30–47 ft·lb.). The decrease in the fracture toughness J–R curve or J_{IC} is relatively small. Metallographic examination of the specimens indicates that failure occurs by the formation and growth of microvoids near hard inclusions. Differences in the fracture resistance of the welds arises from differences in the density and size of inclusions. In this study, the effect of thermal aging on fracture properties is minimal because of the relatively low ferrite content (4–6% ferrite) and thin vermicular ferrite morphology in the welds.

The Charpy–impact, tensile, and fracture toughness results from this study have been compared with available data on SMAWs, SAWs, and GTAWs prepared with Types 308 or 316 SS filler metal. The data are consistent with results from other investigations. The fracture properties of SS welds are insensitive to filler metal. The welding process has a significant effect. In general, GTAWs exhibit higher fracture resistance than SMAWs or SAWs, and there is no difference between SAW and SMAW J–R curves. The Charpy–impact energy of some welds may be as low as 40 J.

The results indicate that the decrease in impact strength due to aging depends on the ferrite content and initial impact strength of the weld. Welds with relatively high strength show a large decrease whereas those with poor strength show minimal change. In SS welds with poor strength, failure occurs by the formation and growth of microvoids. Such processes are relatively insensitive to thermal aging. The existing data indicate that at reactor temperatures, the fracture toughness J_{IC} of thermally aged welds can be as low as 40 kJ/m^2. A conservative estimate of J–R curve for aged SS welds may be given by $J = 40 + 83.5\ \Delta a^{0.643}$.

Acknowledgments

This work was supported by the Office of the Nuclear Regulatory Research in the U.S. Nuclear Regulatory Commission (NRC), under FIN A2212, Program Manager: Michael McNeil.

1 Introduction

Stainless steels (SSs) are used extensively in light water reactor (LWR) systems because of their excellent ductility, high notch toughness, corrosion resistance, and good formability. Although these steels are completely austenitic in the wrought condition, welded and cast SSs have a duplex structure consisting of austenite and ferrite phases. The ferrite phase provides additional benefits, e.g., it increases tensile strength and improves resistance to stress corrosion cracking. However, duplex steels are susceptible to thermal embrittlement after extended service at reactor operating temperatures, i.e., typically 282°C (540°F) for boiling water reactors, 288–327°C (550–621°F) for pressurized water reactor (PWR) primary coolant piping, and 343°C (650°F) for PWR pressurizers.

It is well established[1–7] that thermal aging of cast SSs at 250–350°C (482–662°F) increases hardness and tensile strength; decreases ductility, impact strength, and fracture toughness; and shifts the Charpy transition curve to higher temperatures. Aging of cast SSs at temperatures <500°C (<932°F) leads to precipitation of additional phases in the ferrite, e.g., formation of a Cr–rich α' phase by spinodal decomposition; nucleation and growth of α'; precipitation of a Ni– and Si–rich G phase, $M_{23}C_6$, and γ_2 (austenite); and additional precipitation and/or growth of existing carbides at ferrite/austenite phase boundaries.[8–12] Thermal embrittlement is caused primarily by formation of the Cr–rich α' phase in the ferrite and, to some extent, by precipitation and growth of carbides at phase boundaries. Thermal embrittlement of cast SSs results in brittle fracture associated with either cleavage of the ferrite or separation of the ferrite/austenite phase boundary. Predominantly brittle failure occurs when either the ferrite phase is continuous (e.g., in cast material with a large ferrite content) or the ferrite/austenite phase boundary provides an easy path for crack propagation (e.g., in high–C grades of cast steel with large phase–boundary carbides). The amount, size, and distribution of the ferrite phase in the duplex structure, and the presence of phase–boundary carbides are important parameters in controlling the degree or extent of thermal embrittlement. In general, the low–C CF–3 steels are the most resistant to thermal embrittlement, and the Mo–bearing, high–C CF–8M steels are the least resistant. The extent of thermal embrittlement increases with increased ferrite content.

A procedure and correlations have been developed at Argonne National Laboratory (ANL) for estimating fracture toughness, tensile, and Charpy–impact properties of cast SS components during service from known material information.[13,14] The ANL estimation scheme is applicable to compositions within the ASTM Specifications A 351 for Grades CF–3, CF–3A, CF–8, CF–8A, and CF–8M. A correlation for Charpy–impact energy at saturation, i.e., the mini mum impact energy that would be achieved for the material after long–term aging, is given in terms of chemical composition. Change in impact energy as a function of time and temperature of service is estimated from saturation impact energy and from the correlations that describe the kinetics of embrittlement, which are also given in terms of chemical composition. The fracture toughness J–R curve for the material is then obtained from the correlation between the fracture toughness parameters and the Charpy–impact energy. Tensile yield and flow stresses, and Ramberg/Osgood parameters are estimated from the flow stress of the unaged material and the kinetics of embrittlement.[3]

Although SS welds have a duplex structure and their chemical compositions are similar to those of cast SSs, the ANL correlations are not applicable to these welds. The ANL correlations account for mechanical–property degradation of typical heats of cast SS. They do not consider the effects of compositional or structural differences that may arise from differences in processing or heat treatment of the steels. Type 308 SS welds generally contain 5–15% ferrite but their mechanical properties typically differ from those of cast SSs. For a given ferrite content, the tensile strength of SS welds is higher and fracture toughness is lower than that of cast SSs. Experimental data[15] indicate that cast SSs with poor fracture toughness are relatively insensitive to thermal aging, i.e., fracture toughness of the material would not change significantly during service. In these steels, failure is controlled by void formation near inclusions or other flaws in the material, i.e., by processes that are not sensitive to thermal aging. These results suggest that SS welds with poor fracture toughness, e.g., shielded metal arc welds (SMAWs) or submerged arc welds (SAWs), should be relatively insensitive to thermal aging.

Degradation of fracture toughness and Charpy–impact energy of several SS pipe welds has been characterized in this report. The welds were aged for 7,000–10,000 h at 400°C to simulate saturation conditions, i.e., the lowest impact energy that would be achieved by the material after long–term aging. The results are compared with data from other studies.

2 Material Characterization

Five pipe weldments were procured for the study. The composition and ferrite content of the welds are given in Table 1. The ferrite content was measured with a ferrite scope and calculated from the chemical composition in terms of Hull's equivalent factors.[16] Fabrication and procurement history of the weldments is as follows:

PWWO: 12–in. Type 304 Schedule 100 pipe mockup weldment with overlays was supplied by Georgia Power and NUTECH.[17] The weld was fabricated with Type 308L filler metal and conventional butt welding procedures. On one side of the weld the prep geometry of the weld was long and smooth, i.e., typical of that used in the Hatch–1 reactor. On the other side, the prep geometry was short, typical of that used in the Hatch–2 reactor. The overlay was similar to that applied to the recirculation piping in the Hatch–2 reactor.

PWCE: 28–in., Type 304/308 pipe weldment was obtained from the Boston Edison Power Co.

Table 1. Composition and ferrite content of austenitic stainless steel welds

Material	Composition (wt.%)										Ferrite[b] (%)	
ID[a]	C	N	Si	Mn	P	S	Ni	Cr	Mo	Cu	Calc.	Meas.
PWWO	0.030	0.072	0.44	2.12	0.018	0.018	10.72	20.35	0.27	0.20	4.1	6.8
PWCE	0.050	0.060	0.44	1.79	0.003	0.002	9.54	20.22	0.05	0.04	5.4	6.1
PWER	0.020	0.074	0.36	1.78	0.018	0.009	10.29	20.12	0.19	0.12	4.8	5.2
PWDR	0.080	–	0.75	1.00	0.022	0.010	9.74	20.72	0.08	0.08	5.9	–
PWMS	0.021	–	0.40	1.61	0.025	0.006	9.56	19.80	0.19	0.11	8.3	–

[a] PWWO: 12–in. schedule 100 pipe mockup weldment with overlays supplied by Georgia Power and NUTECH.
PWCE: 28–in.–diameter Type 304 stainless steel pipe weldment obtained from Boston Edison.
PWER: 20–in.–diameter Type 304 stainless steel pipe weldment prepared for EPRI at Southwest Fabricating.
PWDR: 10–in.–diameter Type 304 stainless steel weldment after service in Dresden reactor.
PWMS: 28–in.–diameter pipe weldment treated by Mechanical Stress Improvement Process (MSIP).
[b] Calculated from the composition with Hull's equivalent factor.
Measured by Ferrite Scope, Auto Test FE, Probe Type FSP–1.

PWER: 20–in., Type 304/308 pipe weldment was supplied by the Electric Power Research Institute (EPRI). It was prepared at Southwest Fabricating by the heat sink welding (HSW) technique.[18]

PWDR: 10–in., Type 304 SS pipe weldment was obtained from the emergency core–spray system of the Dresden–2 reactor. It was prepared by shielded metal arc welding with coated electrodes; the root pass was made by gas tungsten arc welding. The insert and filler metals were Type ER308. The pipe had been in service for ≈4.5 y. Water temperature in the core spray line is 204–260°C during normal operation.[19]

PWMS: 28–in., seamless Type 304 SS pipe weldment was treated by the Mechanical Stress Improvement Process (MSIP).[20] The filler metal was Type ER308L. The MSIP treatment is intended to produce a more favorable state of residual stress on the inner surface of the pipe welds, particularly near heat–affected zones. The weld undergoes monotonic compressive loading that is produced by a split–ring–like tool mounted on the pipe. The favorable residual stresses are induced by plastic compression of the weld.

Although the welding process is not specified for all of the weldments, the welds of large–diameter pipes are typically prepared by shielded metal arc welding. All of the welds consisted of a duplex austenite and ferrite structure; the ferrite phase was at the core of the dendritic branches in the weld. Typical microstructures of the welds are shown in Fig. 1. All of the welds exhibit a vermicular ferrite morphology. The ferrite content of the welds is relatively low (in the range of 4–6%).

3 Mechanical Properties

Charpy–impact tests were conducted on standard V–notch specimens (Fig. 2) according to American Society for Testing and Materials (ASTM) Specification E 23. A Dynatup Model 8000A drop–weight impact machine with an instrumented tup and data readout system was used for the Charpy–impact tests. Load– and energy–time data were obtained from an instrumented tup and recorded on a dual–beam storage oscilloscope. The load–time traces from each test were digitized and stored on a floppy disk for analysis. Total energy was computed from the load–time trace; the value was corrected for the effects of tup velocity.

The instrumented tup and data readout instrumentation were calibrated by fracturing standard V–notch specimens fabricated from 6061–T6 Al and 4340 steel with a hardness of Rockwell R_C 54. Accuracy of the impact–test machine was also checked with Standard Reference Materials 2092 and 2096 obtained from the National Institute of Standards and Technology. Tests on the reference materials were performed in accordance with the testing procedures of Section 11 of ASTM E23. The specimens for high–temperature tests were heated by resistance heating. Pneumatic clamps were used to make electrical connections and hold the specimens in position on the anvils. The temperature was monitored and controlled by a thermocouple attached to the specimen. Specimens for the low–temperature tests were cooled in either a refrigerated bath or liquid N.

The fracture toughness J–R curve tests were conducted according to ASTM Specification E 1152–87. Compact–tension specimens (Fig. 3), 25.4 mm thick, were used for the tests. The experimental procedure and data for the fracture toughness tests are given in the Appendix.

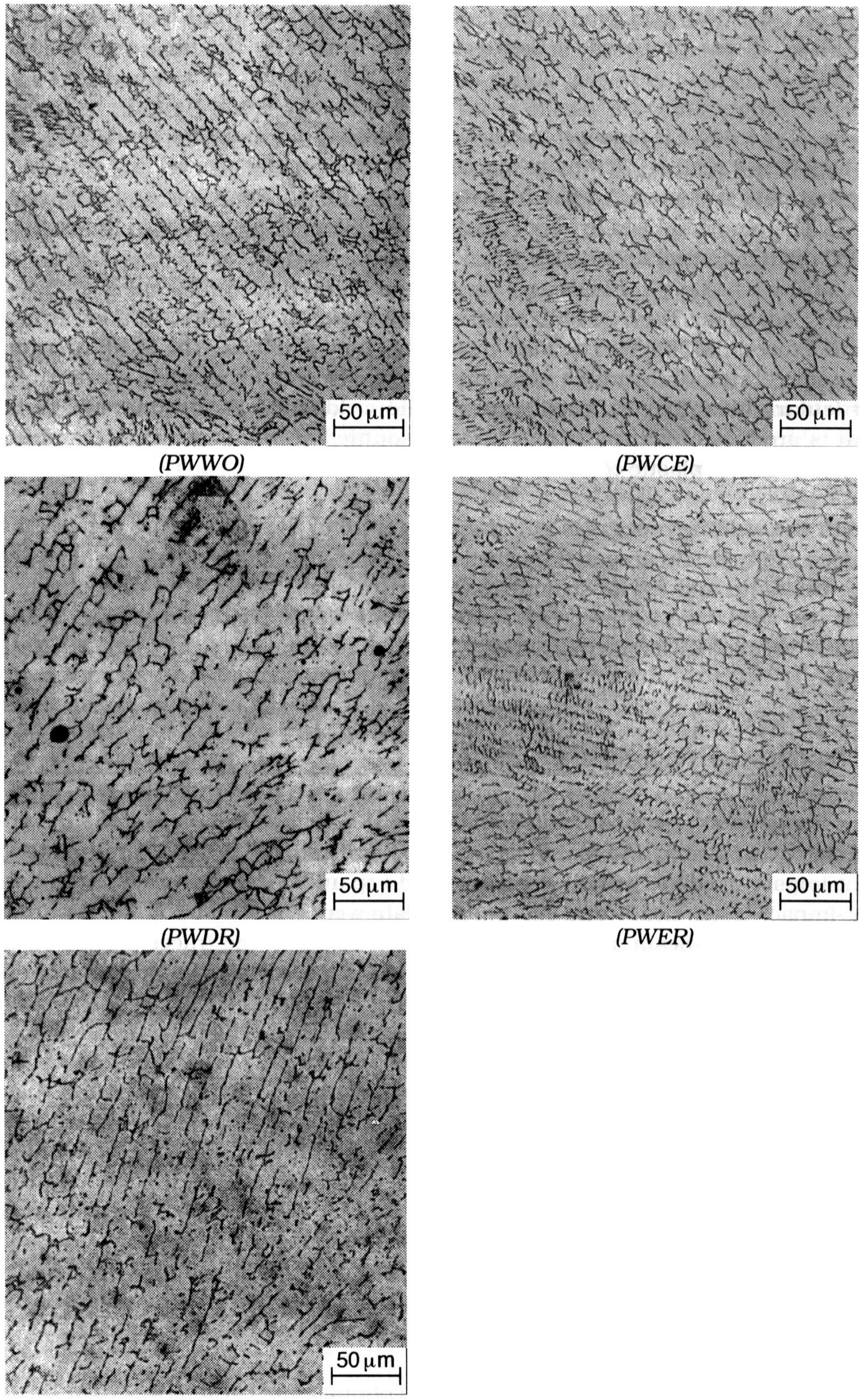

Figure 1. Typical ferrite morphology of the various welds of this study

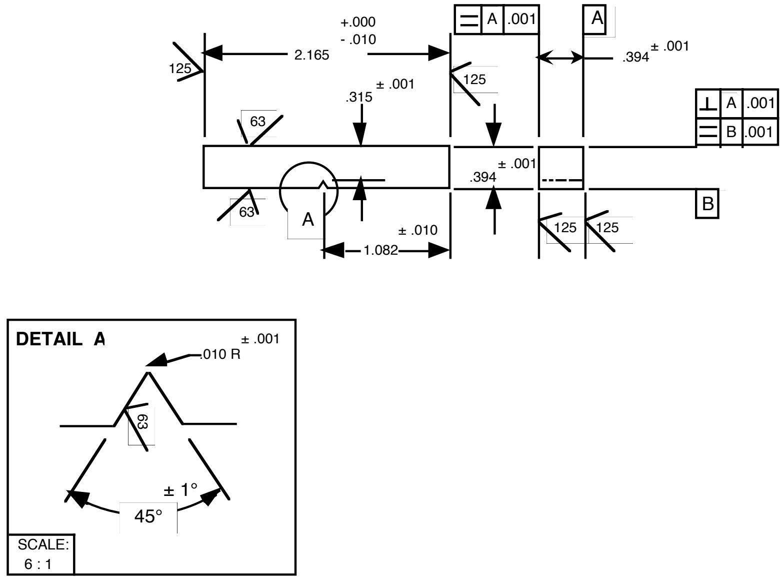

Figure 2. Configuration of Charpy–impact test specimen: units of measure are inches

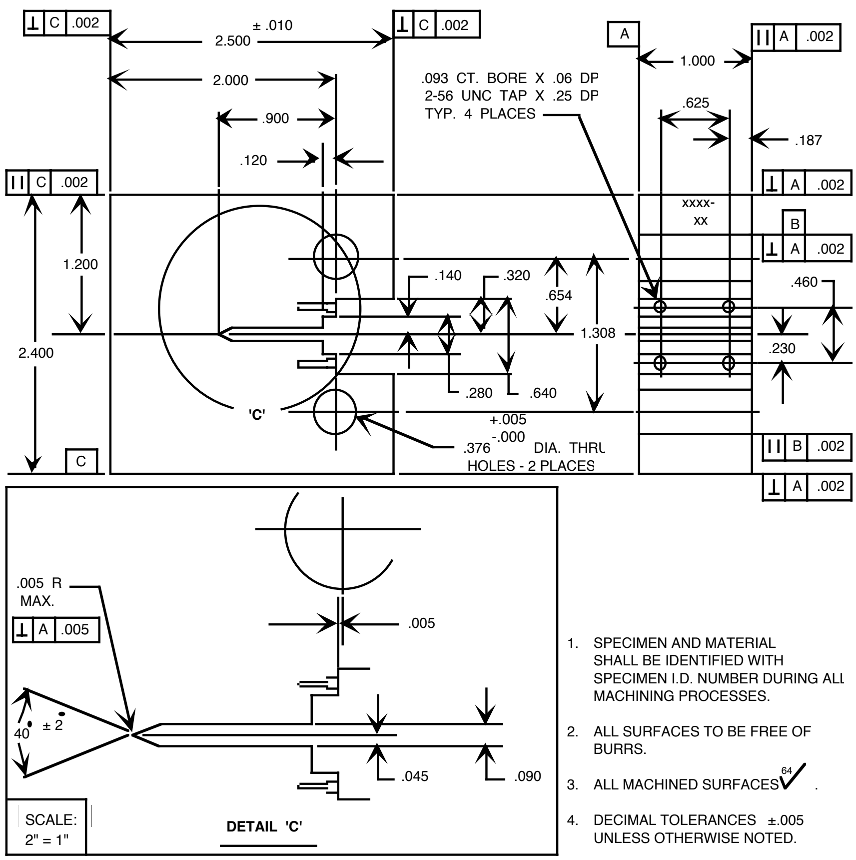

Figure 3. Configuration of compact–tension test specimen: units of measure are inches

The orientation and location on the weldment where the Charpy–impact and fracture toughness test specimens were taken are shown in Fig. 4. In all cases, the fracture plane is in the center of the weld. The variation in ferrite content in the center of all of the welds was minimal; the variation in the PWWO weld is shown in Fig. 5. Some of the materials were aged in the laboratory for 8,000–10,000 h at 400°C (752°F) to simulate the saturation condition, i.e., the condition when the lowest impact strength is achieved by the material after long–term service at reactor temperatures.

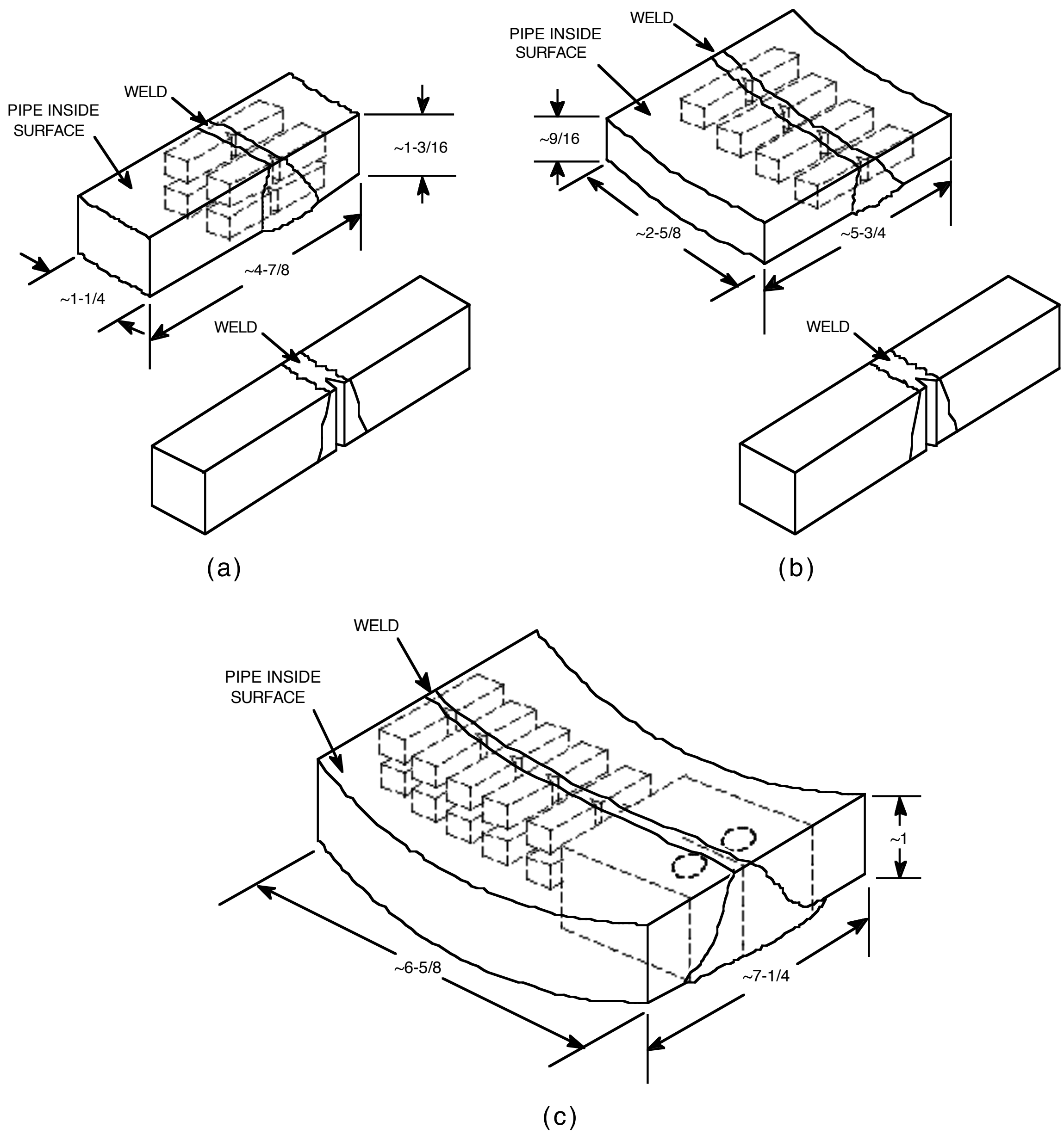

Figure 4. Orientation and location on weldments where mechanical test specimens were taken: (a) and (c) ≥1 in.–thick pipe sections and (b) <1 in.–thick pipe sections

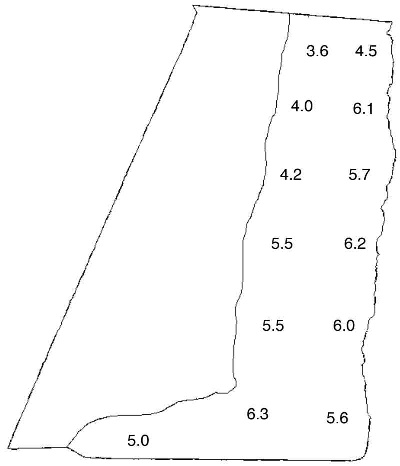

Figure 5. Variations in ferrite content of PWWO weld

3.1 Charpy–Impact Energy

Charpy impact data for the PWCE, PWWO, PWDR, and PWMS welds are given in Table 2. A complete Charpy transition curve was obtained only for the PWWO weld; other welds were tested at room temperature and 290°C. Transition curves for the unaged and aged PWWO weld are shown in Fig. 6. The Charpy data were fitted with a hyperbolic tangent function of the form

$$C_V = K_o + B\left[1 + \tanh\left(\frac{T - C}{D}\right)\right], \quad (1)$$

where K_o is the lower–shelf energy, T is the test temperature in °C, B is half the distance between the upper– and lower–shelf energy, C is the mid–shelf Charpy transition temperature (CTT) in °C, and D is the half width of the transition region. The results indicate that thermal aging increased the mid–shelf CTT by 47°C, i.e., from –105°C to –58°C, and decreased upper–shelf energy (USE) by 50 J/cm^2 (30 ft·lb.).

The Charpy–impact data for aged materials represent the saturation condition, i.e., the condition when the lowest impact strength is achieved by the material after long–term service at reactor temperatures. The results indicate that thermal aging results in moderate decreases in impact energy at both room temperature and 290°C. For the various welds, USE decreased by 50–80 J/cm^2 (30–47 ft·lb); from 187 to 137 J/cm^2 (110 to 81 ft·lb) for PWWO, from 353 to 271 J/cm^2 (208 to 160 ft·lb) for PWCE, and from 169 to 98 J/cm^2 (100 to 58 ft·lb) for PWDR. Similar decreases were observed at room temperature. Even in the fully embrittled condition, all of the welds exhibit adequate impact strength, e.g., >90 J/cm^2 (53 ft·lb) at 290°C and >75 J/cm^2 (44 ft·lb) at room temperature.

The results are consistent with the data from other investigations. Mechanical–property data on Charpy–impact, tensile, and fracture toughness properties of SMAWs, SAWs, and gas tungsten arc welds (GTAWs) prepared from Types 308 or 316 filler metal are compiled in Table 3.[21–38] The Charpy–impact data for unaged and aged welds are shown in Fig. 7. The results for unaged welds show large variation; impact energy of some welds may be as low as

Table 2. Charpy–impact test results for stainless steel welds

Test Number	Specimen ID	Aging Temp. (°C)	Aging Time (h)	Test Temp. (°C)	Impact Energy (J/cm^2)	Yield Load (kN)	Maximum Load (kN)
CS-2878	PWWO-05	-	-	-180	59.2	17.615	23.493
CS-2880	PWWO-06	-	-	-100	100.8	14.598	19.607
CS-2879	PWWO-07	-	-	-50	125.4	16.121	21.335
CS-2863	PWWO-08	-	-	25	175.1	12.928	17.244
CS-2864	PWWO-09	-	-	25	162.8	14.539	19.588
CS-2875	PWWO-10	-	-	75	212.2	11.512	16.092
CS-2876	PWWO-11	-	-	150	186.4	12.284	16.053
CS-2871	PWWO-12	-	-	290	189.7	8.622	12.108
CS-2872	PWWO-13	-	-	290	183.4	10.145	13.866
WIN-2882	PWWO-14	400	7,700	-197	9.8	13.836	13.836
WIN-2883	PWWO-15	400	7,700	-180	9.5	14.285	14.285
WIN-2884	PWWO-16	400	7,700	-100	44.1	15.594	18.474
WIN-2885	PWWO-17	400	7,700	-50	82.9	16.248	20.437
WIN-2886	PWWO-18	400	7,700	0	111.3	13.973	18.347
WIN-2887	PWWO-19	400	7,700	25	126.3	14.412	18.221
WIN-2888	PWWO-20	400	7,700	25	130.9	13.397	17.879
WIN-2893	PWWO-21	400	7,700	75	157.4	13.163	17.430
WIN-2894	PWWO-22	400	7,700	150	143.4	11.512	15.428
WIN-2895	PWWO-23	400	7,700	200	152.4	11.542	15.340
WIN-2896	PWWO-24	400	7,700	290	121.8	9.540	13.153
WIN-2897	PWWO-25	400	7,700	290	151.9	10.575	14.305
CS-2861	PWCE-05	-	-	25	255.6	12.948	18.855
CS-2862	PWCE-06	-	-	25	281.9	11.776	18.533
WIN-2889	PWCE-09	400	10,000	25	187.2	13.524	19.011
WIN-2890	PWCE-10	400	10,000	25	149.3	12.167	17.937
CS-2869	PWCE-07	-	-	290	340.5	9.149	12.577
CS-2870	PWCE-08	-	-	290	366.0	7.890	12.430
WIN-2898	PWCE-11	400	10,000	290	291.7	10.155	14.178
WIN-2899	PWCE-12	400	10,000	290	250.8	8.544	14.334
CS-2865	PWDR-06	-	-	25	138.7	12.616	17.537
CS-2866	PWDR-07	-	-	25	140.2	12.791	17.859
WIN-2891	PWDR-01	400	10,000	25	78.8	12.938	15.184
WIN-2892	PWDR-02	400	10,000	25	84.4	12.821	15.028
CS-2873	PWDR-08	-	-	290	148.4	8.310	11.893
CS-2874	PWDR-09	-	-	290	189.5	8.515	12.596
WIN-2900	PWDR-03	400	10,000	290	93.4	8.583	11.493
WIN-2901	PWDR-04	400	10,000	290	102.4	8.866	12.303
CS-2859	PWMS-01	-	-	25	191.4	13.885	18.953
CS-2860	PWMS-02	-	-	25	185.6	13.504	18.861
CS-2867	PWMS-03	-	-	290	202.7	9.872	13.524
CS-2868	PWMS-04	-	-	290	186.9	9.159	12.977

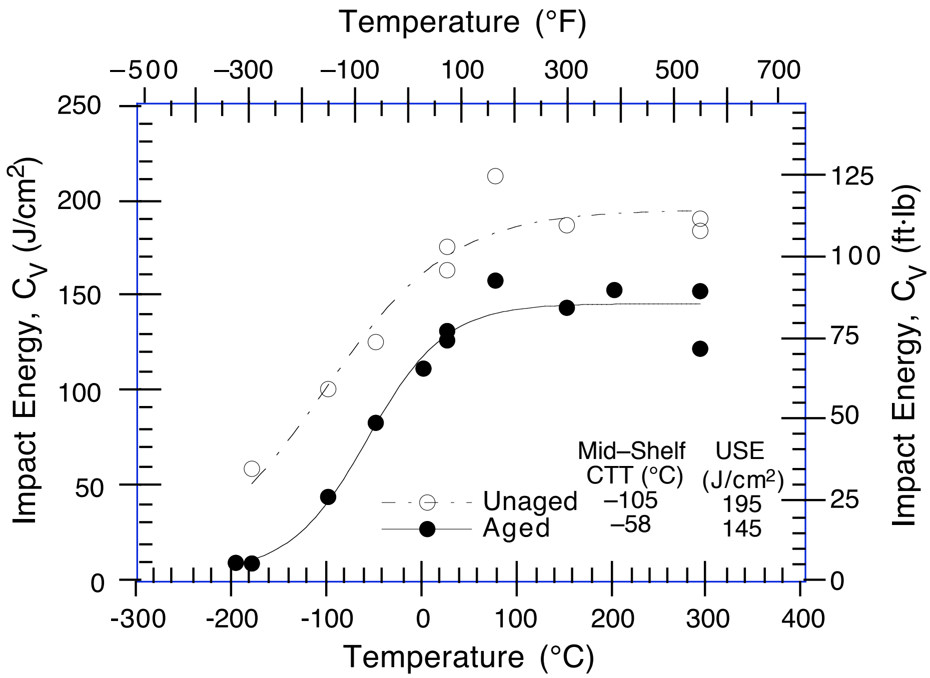

Figure 6. Effect of thermal aging on Charpy–transition curve for PWWO weld

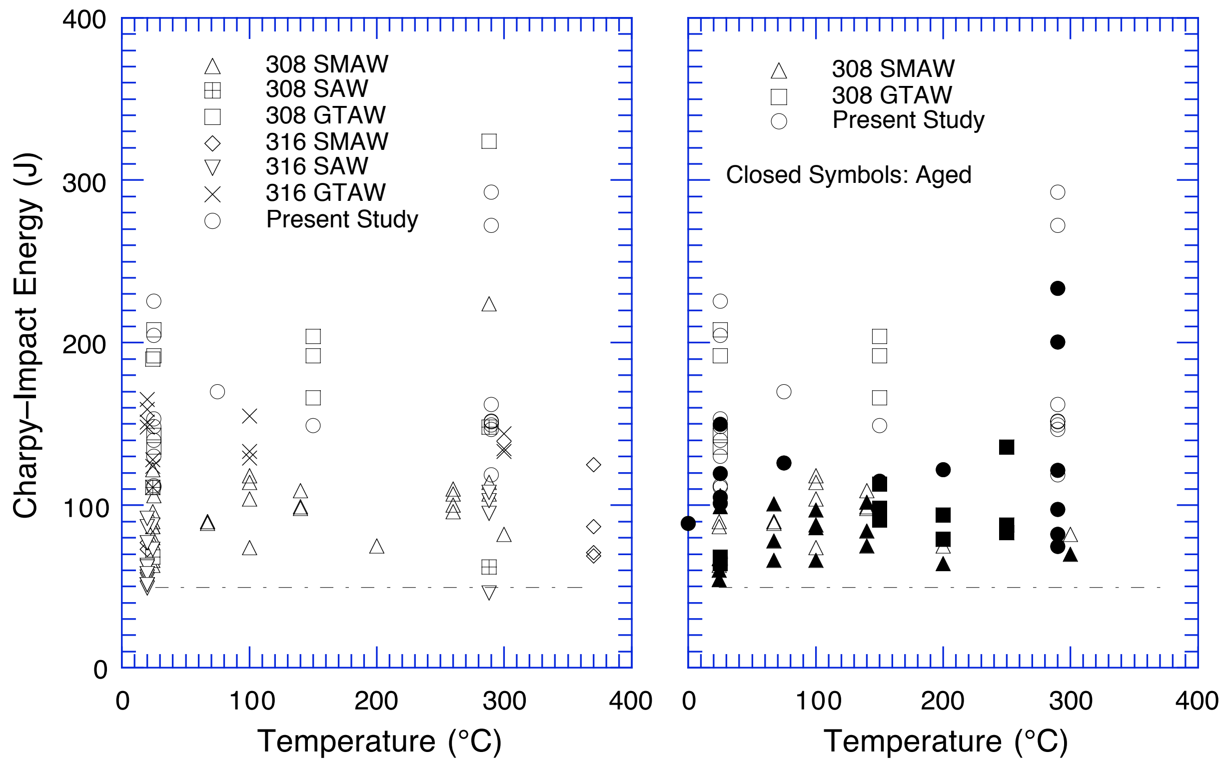

Figure 7. Charpy–impact energy of unaged and aged stainless steel welds

Table 3. Summary of mechanical–property data for austenitic stainless steel welds

Authors	Ref.	Mater. & Process[a]	Heat Treat–ment[b]	Ferrite Content (FN/%)	Test Temp. (°C)[c]	Impact Energy (J)[d]	Yield Strength (MPa)	Ultimate Strength (MPa)	J_{IC} (kJ/m^2)	Tearing Modulus
Horn, et al.	22	308, SMAW	–		RT	122, 111	–	–	–	–
					288	107	315	449	194, 215	–
			SA		RT	–	–	–	–	–
					288	224	192	425	169	–
		316, SAW	–		RT	73	–	–	–	–
					288	95, 103	309	434	170	–
			SA		RT	–	–	–	–	–
					288	108	192	401	221	–
Chipperfield	24	316, SMAW	–	7.0–9.0	370	71	401	486	56	–
			a	3.5–6.5	370	69	286	431	42, 50	–
			b	1.0–3.0	370	87	261	423	40	–
			c	0–0.5	370	125	184	449	67	–
Ould, et al.	25	316L, MMAW/ SAW	I	8.5	20	63, 54	468	605	–	–
					343	–	356	471	–	–
			F	7.5	20	51, 62	465	613	–	–
					343	–	375	474	–	–
			H1	7.5	20	56, 58	425	592	147, 168	–
					343	–	379	464	–	–
		308L, MMAW/ SAW	C	6.0	20	62, 51	439, 452	541, 544	–	–
					343	–	344, 363	391, 390	–	–
			B	6.0	20	49, 51	420, 436	535, 545	153	–
					343	–	325, 341	385, 390	–	–
			D	5.0	20	58, 51	398	563	130	–
					343	–	324, 345	394, 431	–	–
Landes & McCabe	26	308, SAW	–		24	111, 68	348	600	81	190
					288	148, 62	248	426	47	150
		308, GTAW	–		24	190	354, 475	595, 624	195	610
					288	324	239, 372	429, 437	558	500
		308, SMAW	–		24	96	432, 414	605, 597	259	170
					288	114	323, 341	423, 446	168	140
		316, SAW	–		24	88	414	633	116	120
					288	46	281	485	105	90
Mills	27, 28, 29	308, SMAW	–	6.8	24	–	455	634	–	–
					427	–	323	472	154±41	310
					538	–	303	412	154±41	310
		308, GTAW	–	9.9	427	–	278	477	266±20	373
					538	–	268	401	266±20	373
		308, SAW	–	10.7	24	–	365	627	198±17	107
					427	–	344	474	76±17	167
					538	–	290	384	76±17	167
		16–8–2, GTAW	–	5.7	24	–	360	668	392±107	249
					427	–	265	388	266±20	373
					482	–	281	385	266±20	373
					538	–	263	359	266±20	373
		16–8–2, SAW	–	9.0	24	–	391	627	198±17	107
					427	–	297	476	76±17	167
					538	–	321	439	76±17	167

Table 3. (Contd.)

Authors	Ref.	Mater. & Process[a]	Heat Treat–ment[b]	Ferrite Content (FN/%)	Test Temp. (°C)[c]	Impact Energy (J)[d]	Yield Strength (MPa)	Ultimate Strength (MPa)	J_{IC} (kJ/m^2)	Tearing Modulus
Vitek, et al.	30	308L, GTAW	–	10.0	25	208, 136 143, 192	399±56	606±24	480, 773	–
					150	192, 166, 204	–	–	–	–
Alexander, et al.	31	308, SMAW	–	4.0	RT	106			–	–
					140	109	–	–	–	–
				8.0	RT	90			–	–
					140	98	–	–	–	–
				12.0	RT	87			–	–
					140	99	–	–	–	–
Hale & Garwood	32	308L, SMAW	–	5–9	24	63	497±24	606±11	–	–
					300	82	–	–	92±25	75
Garwood	33	316, SAW	–		370	–	325	473	120	–
		316, MMAW	–		370	–	386	471	70	–
Vassilaros, et al.	34	308L, GTAW	–		RT	–	465	612	521	289
					149	–	356	476	400	277
					288	–	338	452	163, 227, 375	152, 363, 437
Gudas & Anderson	35	308L, SMAW	–		RT	–	–	–	243, 168	109, 105
					149	–	–	–	159, 96	89, 71
					288	–	–	–	214, 174	134, 121
Hawthorne & Menke	36	308, SMAW	–	5.2	24	87	478	628	–	–
					260	110	382	474	–	–
					482	108	325	430	–	–
				10.4	24	77	534	693	–	–
					260	100	420	521	–	–
					482	–	358	478	–	–
				15.7	24	66	518	683	–	–
					260	96	415	521	–	–
					482	92	362	482	–	–
				19.0	24	80	557	718	–	–
					260	107	447	563	–	–
					482	102	376	517	–	–
		316, SAW	–	7–10.5	24				–	–
					260				–	–
Faure, et al.	37	316L, GTAW	–		24	111, 124, 128	507, 518	603, 626	–	–
					100	129, 133, 155	458, 482	536, 552	281	–
					300	133, 135, 144	409, 415	470, 480	215	–
Wilkowski, et al.	38	308, SAW	–		288		325	466	–	–
			SA		288		195	465	–	–
Nagasaki, et al.	39	308, GTAW	–		288		298	447	–	–

Table 3. (Contd.)

Authors	Ref.	Mater. & Process[a]	Heat Treat–ment[b]	Ferrite Content (FN/%)	Test Temp. (°C)[c]	Impact Energy (J)[d]	Yield Strength (MPa)	Ultimate Strength (MPa)	J_{IC} (kJ/m^2)	Tearing Modulus
European Community	40	316, GMAW	–		20	159, 165 148, 165 151, 151	518, 361	644, 607	–	–
					550	193, 264 209, 209 219, 159	217, 151	428, 402	–	–
		316, MMAW	–		20	77, 73	469, 469, 428, 437	585, 586, 608, 608	–	–
					550	77, 82	292, 307, 178, 178	403, 413, 421, 422	–	–
		316, SAW	–		20	87, 92, 77	397, 407, 405, 347, 359, 358	566, 568, 567, 584, 596, 590	–	–
					550	64, 87, 87	–	–	–	–

[a] SMAW: Shielded metal arc weld; SAW: Submerged arc weld; MMAW: Manual metal arc weld; and GTAW: Gas tungsten arc weld.
[b] SA: solution annealed; other designations are heat treatment code that are defined in the reference.
[c] RT: room temperature.
[d] All values represent impact energy for a standard Charpy V–notch specimen, i.e., 10 x 10 mm size.

50 J (37 ft·lb). The GTAWs generally exhibited higher impact strength than the SMAWs or SAWs. The results indicate that the welds that were investigated in the present study have relatively high impact strength; the PWCE weld exhibited the highest and PWDR the lowest impact strength.

In Fig. 7 the impact energies of aged welds[25,30–32] fall within the large scatter band of the unaged welds. The results indicate that the effect of thermal aging on Charpy–impact strength depends on the initial impact strength of the welds. Welds with relatively high impact strength, e.g., the GTAWs, show a large decrease in impact energy whereas those with poor impact strength show minimal change in impact energy. Even in the saturation or fully embrittled condition, austenitic SS welds have ≥50 J (37 ft·lb) of impact energy.

Photomicrographs of the fracture surface of unaged and aged weld metal Charpy specimens tested at room temperature are shown in Fig. 8. The results indicate that the overall fracture behavior of the welds is controlled by the distribution and morphology of second–phase particles. All welds exhibit a dimple fracture. Failure occurs by nucleation and growth of microvoids and rupture of remaining ligaments. High–magnification photomicrographs of unaged and aged PWWO and PWDR specimens are presented in Fig. 9, which shows that nearly every dimple was initiated by decohesion of an inclusion (most likely manganese sili cide). The hard inclusions in the SMAW resist deformation and the buildup of high local stresses leads to decohesion of the particle/matrix interface. Inferior fracture resistance of the PWDR weld may be attributed to the higher density and larger size of inclusions relative to the PWWO or PWCE welds. Metallographic results suggest that the delta ferrite phase has relatively little effect on the fracture properties of the welds.

The results also indicate that thermal aging has no effect on fracture morphology of the specimens tested at room temperature; both unaged and aged welds exhibit a dimple fracture.

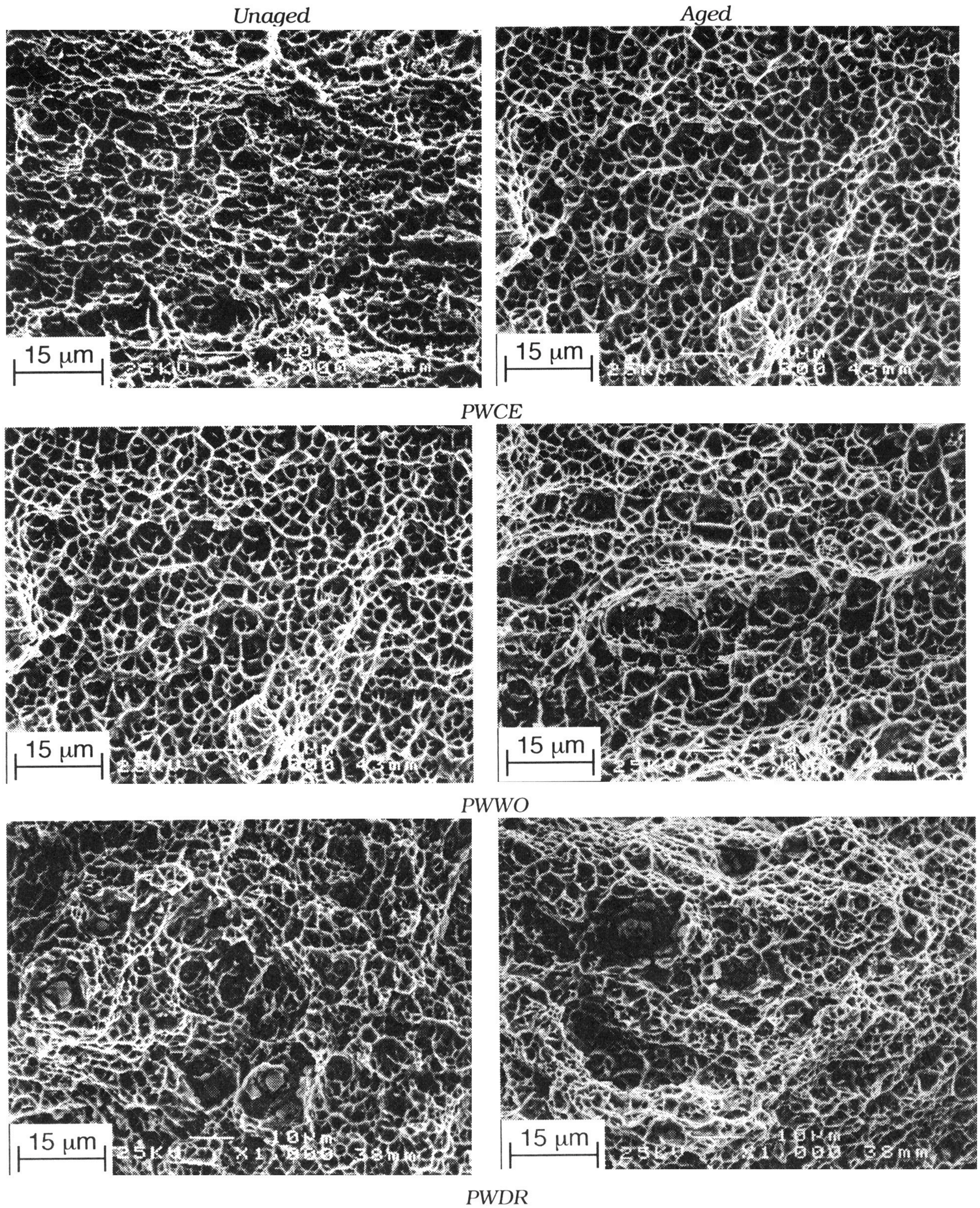

Figure 8. Photomicrographs of fracture surface of unaged and aged Charpy specimens of various welds tested at room temperature

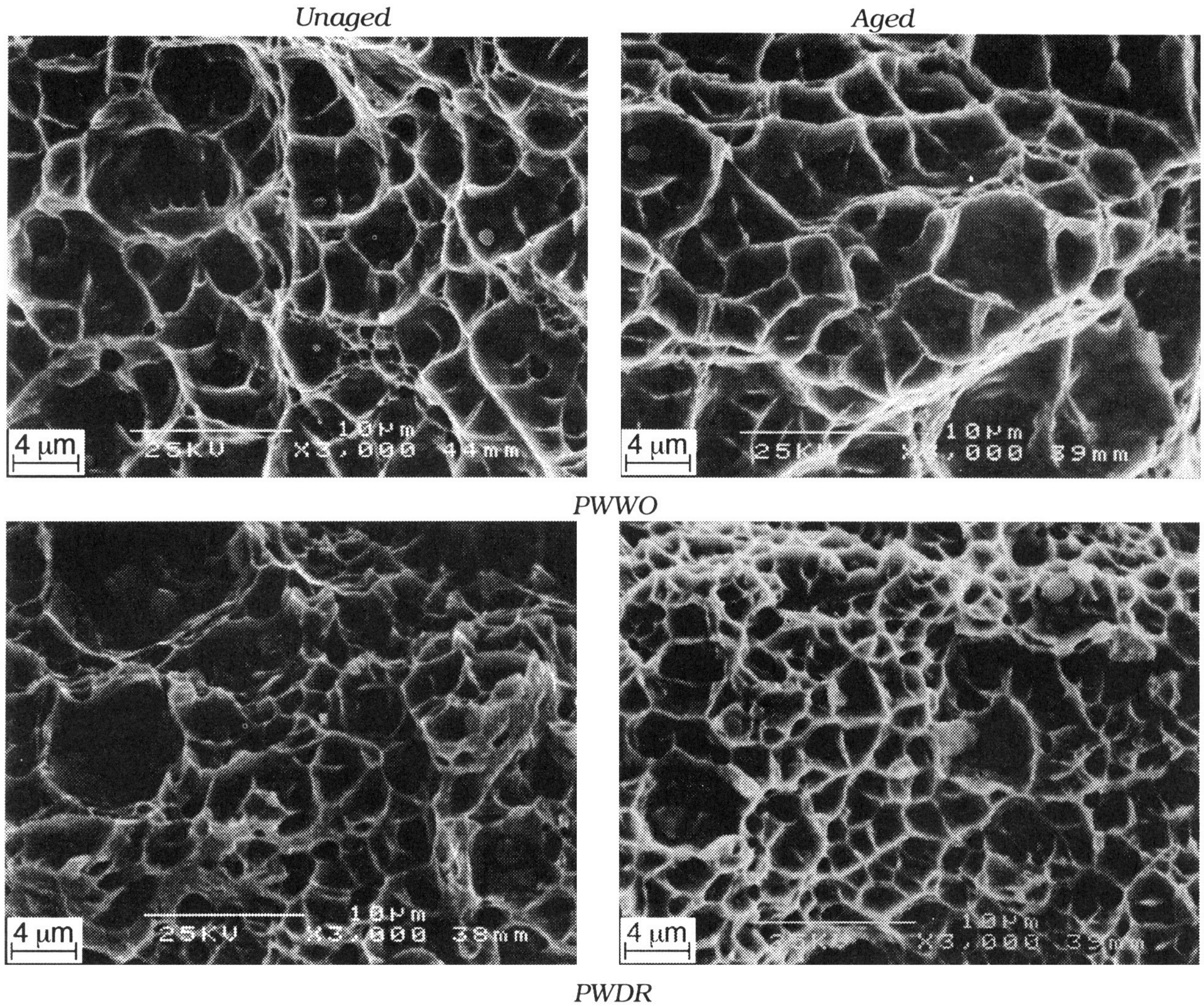

Figure 9. Higher–magnification photomicrographs of fracture surface of unaged and aged Charpy specimens of PWWO and PWDR welds tested at room temperature

It is well known that thermal aging of duplex SSs results in brittle fracture associated with either cleavage of the ferrite or separation of the ferrite/austenite phase boundary.[1,2,11] A brittle fracture was not observed in the welds, most probably because of the relatively low ferrite content and thin vermicular ferrite morphology. However, cleavage of the ferrite phase may occur at very low temperatures. Figure 10 shows cleavage of the ferrite phase in the unaged PWWO weld that was tested at –180°C. The amount of cleavage was slightly larger in the aged specimen than in the unaged specimen.

3.2 Tensile Properties

Tensile tests were not conducted on the welds; tensile properties of the welds were estimated from the Charpy–impact data. The values obtained for 0.2% yield and maximum load in each impact test are listed in Table 2, and may be used to estimate tensile properties of the cast materials. For a Charpy specimen, the yield stress σ_y is estimated from the expression

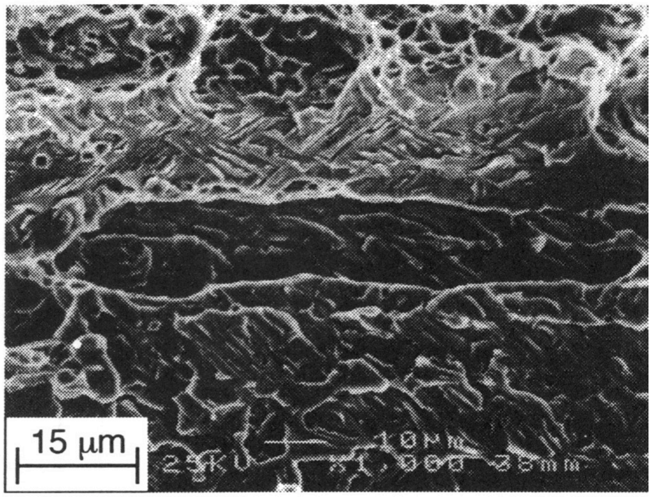

Figure 10.
Photomicrograph of fracture surface of unaged Charpy specimen of PWWO weld tested at –180°C

$$\sigma_y = C_1\ P_y\ B/W\ b^2\ , \tag{2a}$$

and the ultimate stress σ_u is estimated from the expression

$$\sigma_u = C_2\ P_m\ B/W\ b^2\ , \tag{2b}$$

where P_y and P_m are the yield and maximum load, respectively, W is the specimen width, B is the specimen thickness, b is the uncracked ligament, and C_1 and C_2 are constants.[41] The yield and maximum loads were obtained from load–time traces of the Charpy tests. The constants C_1 and C_2 were determined by comparing the Charpy–impact test results with existing tensile properties data for Type 308 and 316 weld metals. The best value of the constants was 2.2 for both C_1 and C_2. The estimated yield and ultimate stress for the various welds are compared with existing data for Type 308 or 316 welds in Fig. 11. Average values of yield and ultimate stress for PWWO, PWCE, PWDR, and PWMS welds are listed in Table 4. Thermal aging has little or no effect on the tensile properties of Type 308 welds. These results are consistent with the data from other studies.[25,30–32]

Table 4. Tensile yield and ultimate stress of various stainless steel welds, estimated from Charpy–impact data

			Room Temp.		290°C	
Material ID	Aging Temp. (°C)	Aging Time (h)	Yield Stress (MPa)	Ultimate Stress (MPa)	Yield Stress (MPa)	Ultimate Stress (MPa)
PWCE	–	–	425	643	315	430
	400	10,000	442	635	321	490
PWWO	–	–	472	633	349	446
	400	7,700	478	620	346	472
PWDR	–	–	437	608	289	421
	400	10,000	443	519	300	409
PWMS	–	–	471	650	327	456

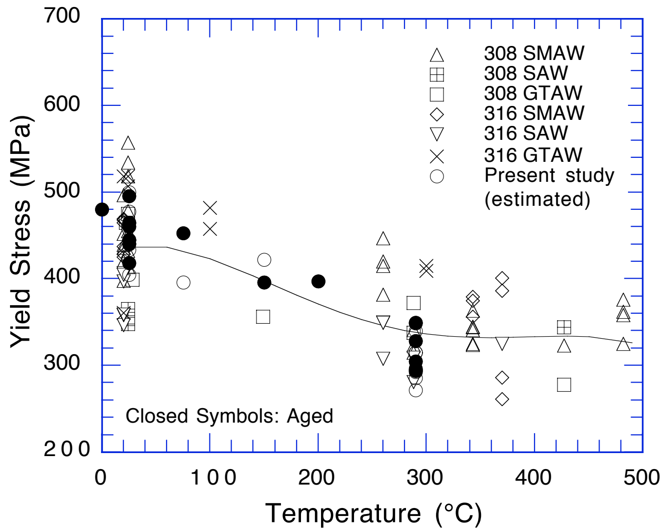

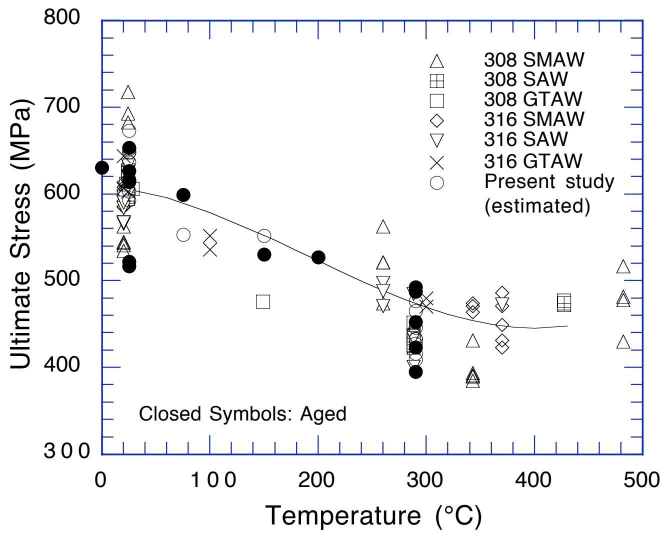

Figure 11. Tensile yield and ultimate stress of stainless steel welds. Solid lines are the best fit to the data.

3.3 Fracture Toughness

Fracture toughness J–R curve tests were conducted at room temperature and 290°C on the PWWO, PWCE, and PWER welds. The fracture toughness results are given in Table 5. The effect of thermal aging on the fracture toughness J–R curves of the various materials is shown in Figs. 12–14. The J–R curves are expressed by the power–law relation $J_d = C(\Delta a)^n$ per ASTM Specifications E 813–85 and E 1152–87. The results indicate that, for all of the welds, the decrease in fracture toughness due to thermal aging is relatively small at room temperature and 290°C. The fracture toughness data are consistent with the Charpy–impact test results. The fracture properties of SMAWs are controlled by the distribution and morphology of second–phase particles. In these welds, failure occurs by the formation and growth of microvoids near hard inclusions. Such processes are relatively insensitive to thermal aging. Fracture resis tance of the PWWO weld is inferior to that of the PWCE weld because of a higher density and a

Table 5. Fracture toughness test results for unaged and aged austenitic stainless steel weldments

Specimen Number	Weld ID	Test No.	Test Temp. (°C)	a/W	Δa Final[a] Comp. (mm)	Δa Final[a] Opt. (mm)	Deformation J[b] J_{IC} (kJ/m²)	Deformation J[b] T_{av}	Deformation J[b] C (kJ/m²)	Deformation J[b] n	Modified J[b] J_{IC} (kJ/m²)	Modified J[b] T_{av}	Modified J[b] C (kJ/m²)	Modified J[b] n	Flow Stress (MPa)	Impact Energy[c] (J/cm²)	Condition Time (h)	Condition Temp. (°C)
PWCE–02	PWCE	125	25	0.555	6.06	6.80	482.4	414	893.3	0.722	481.9	455	924.6	0.763	534	268.8	Unaged	–
PWCE–04	PWCE	129	25	0.550	8.70	8.87	566.0	384	920.2	0.631	562.6	425	948.7	0.676	538	168.3	10,000	400
PWCE–01	PWCE	123	290	0.548	7.49	8.47	363.6	544	648.8	0.713	363.6	599	672.0	0.756	373	353.3	Unaged	–
PWCE–03	PWCE	127	290	0.548	11.10	12.26	363.4	371	614.2	0.611	377.7	385	633.5	0.617	406	271.3	10,000	400
PWWO–03	PWWO	131	25	0.548	11.24	11.43	257.3	193	505.0	0.587	258.0	210	523.7	0.617	549	169.0	7,700	400
PWWO–01	PWWO	130	290	0.571	10.00	10.89	242.7	203	400.9	0.481	242.2	226	416.6	0.520	398	128.6	Unaged	–
PWWO–04	PWWO	128	290	0.550	13.40	13.86	189.3	179	338.8	0.505	190.6	195	351.7	0.533	409	186.6	7,700	400
PWWO–02	PWWO	126	290	0.562	13.73	14.05	154.6	219	330.2	0.621	155.6	235	341.9	0.645	409	136.9	7,700	400
PWER–01	PWER	124	290	0.553	10.18	10.34	276.5	244	459.4	0.509	281.3	269	480.3	0.541	409	–	10,000	400

[a]Final crack extension: Comp. = determined from compliance and Opt. = measured optically.
[b]J_{IC} determined with a slope of four times the flow stress for the blunting line.
[c]Charpy–impact energy at the test temperature.

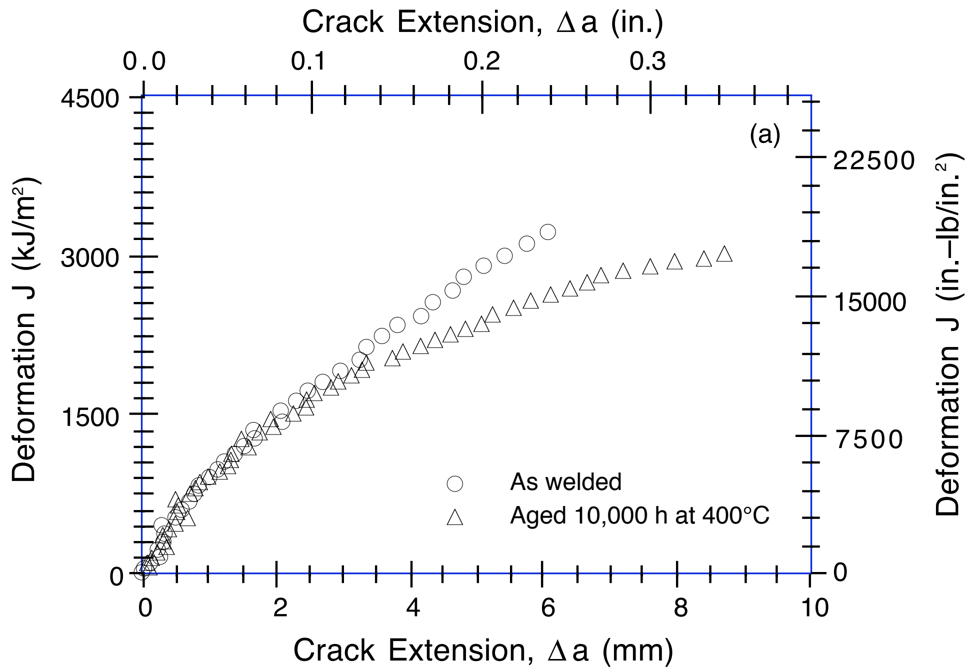

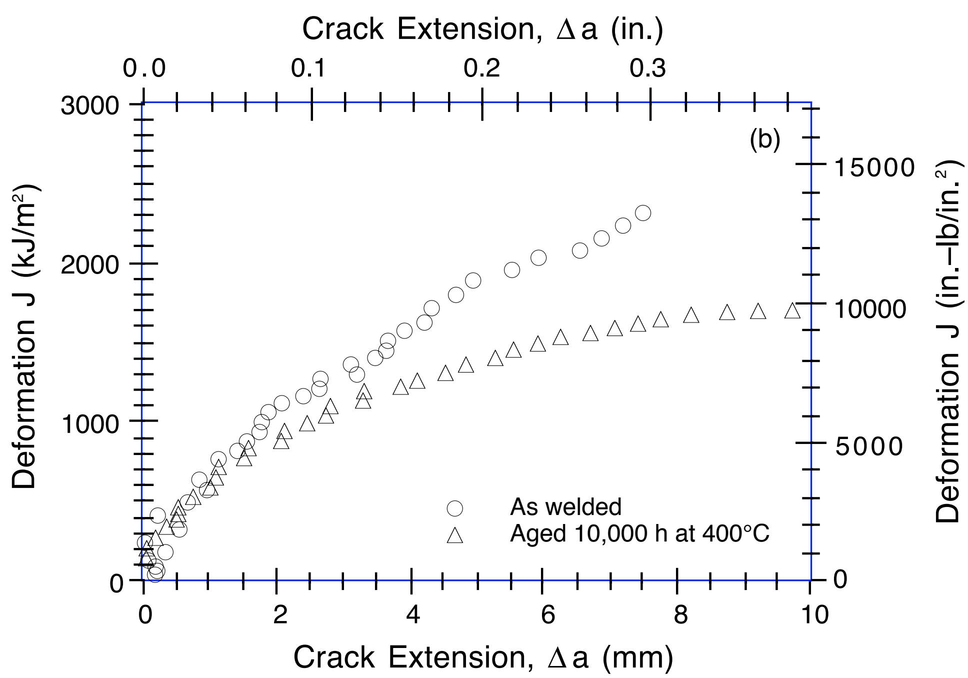

Figure 12. Fracture toughness J–R curve for PWCE weld at (a) room temperature and (b) 290°C

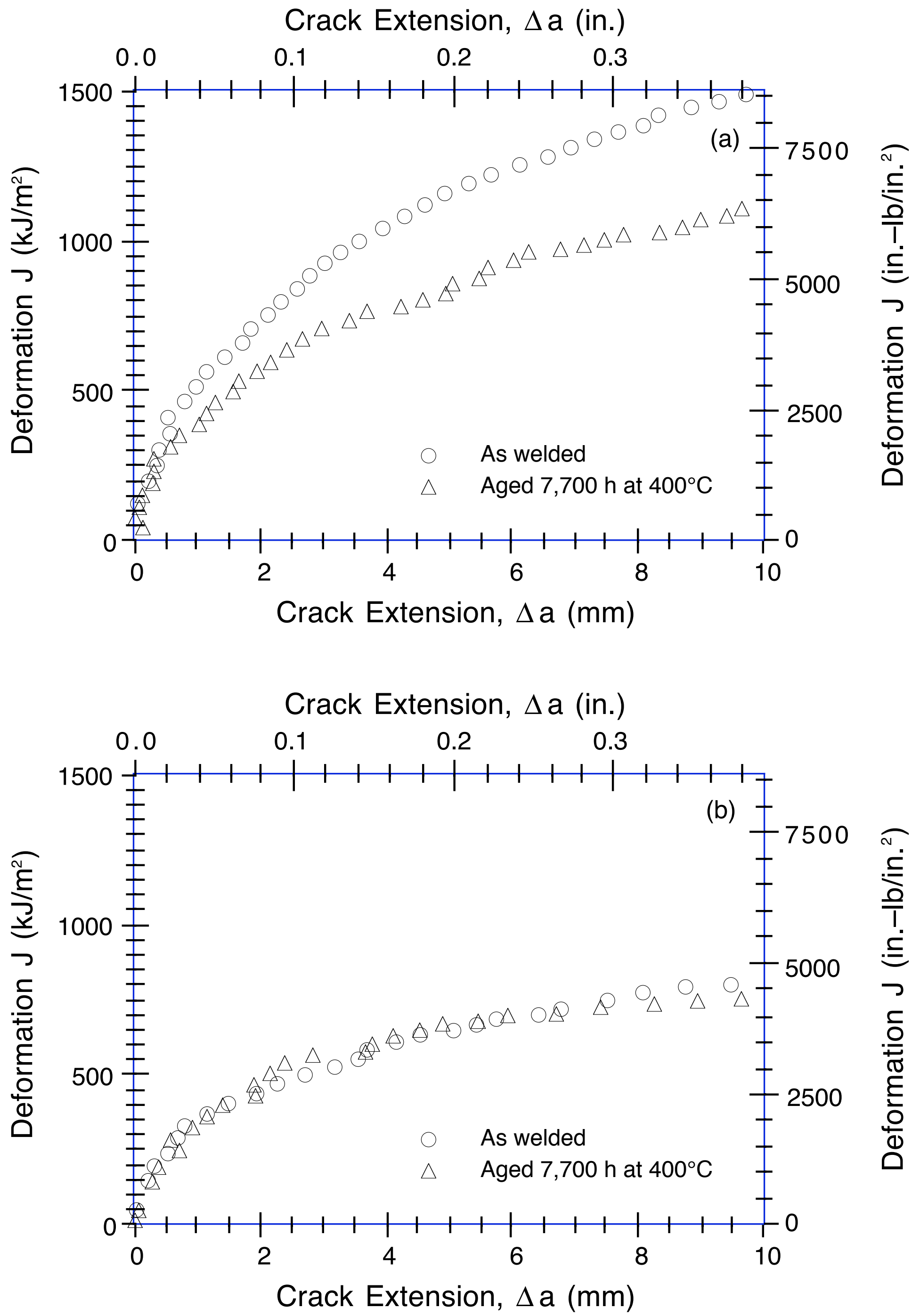

Figure 13. Fracture toughness J–R curve for PWWO weld at (a) room temperature and (b) 290°C

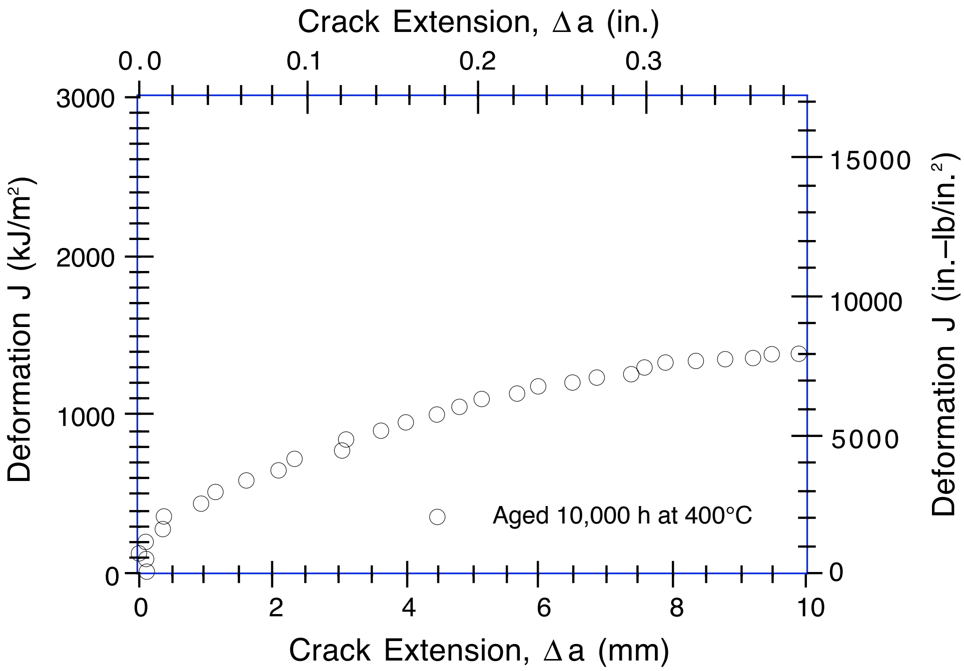

Figure 14. Fracture toughness J–R curve for PWER weld at 290°C

larger size of inclusions. The ferrite phase has little or no effect on the fracture properties of the welds; ferrite is resistant to local failure because of its vermicular morphology and because it constitutes only 4–6% of the weld.

The existing fracture toughness J–R curve data from the work conducted for the U.S. Nuclear Regulatory Commission and compiled in the Pipe Fracture (PIFRAC) Database* and from other sources,[29,30,32–34,37] are shown in Fig. 15. The PIFRAC database, consisting of the data from Refs. 22, 26, 35, 38, and 39, was originally developed at Materials Engineering Associates (MEA),[42] and updated later by Battelle Memorial Institute.[43] The results indicate that fracture properties of SS welds are relatively insensitive to filler metal.[29] However, the welding process significantly affects fracture toughness. In general, GTAWs exhibit higher fracture resistance than SMAWs or SAWs. The statistical differences in SAW and SMAW fracture toughness J–R curves has also been evaluated[44] and results indicate no difference between SAW and SMAW J–R curves. At 288°C, the lower–bound J–R curve for both SAWs and SMAWs, defined as the mean minus one standard deviation J–R curve,[44] is represented by

$$J(kJ/m^2) = 73.4 + 83.5\ \Delta a(mm)^{0.643} \tag{3}$$

where 73.4 kJ/m^2 is the fracture toughness J_{IC}. The lower–bound curve for SAWs and SMAWs shows very good agreement with the data in Fig. 15. The fracture toughness data in the technical basis document for ASME Section XI Article IWB–3640 analysis,[26] are somewhat higher than the curve given by Eq. 3. The available fracture toughness J–R curves for aged SMAWs, SAWs, and GTAWs are shown in Fig. 16.[25,28,32] In these studies, the time and temperature of aging was sufficient to achieve saturation toughness, i.e., the minimum value

* G. Wilkowski and N. Ghadiali, "Short Crack in Piping and Piping Welds," in Technical Data CD–ROM, Battelle Columbus Division, Columbus, OH (May 1995).

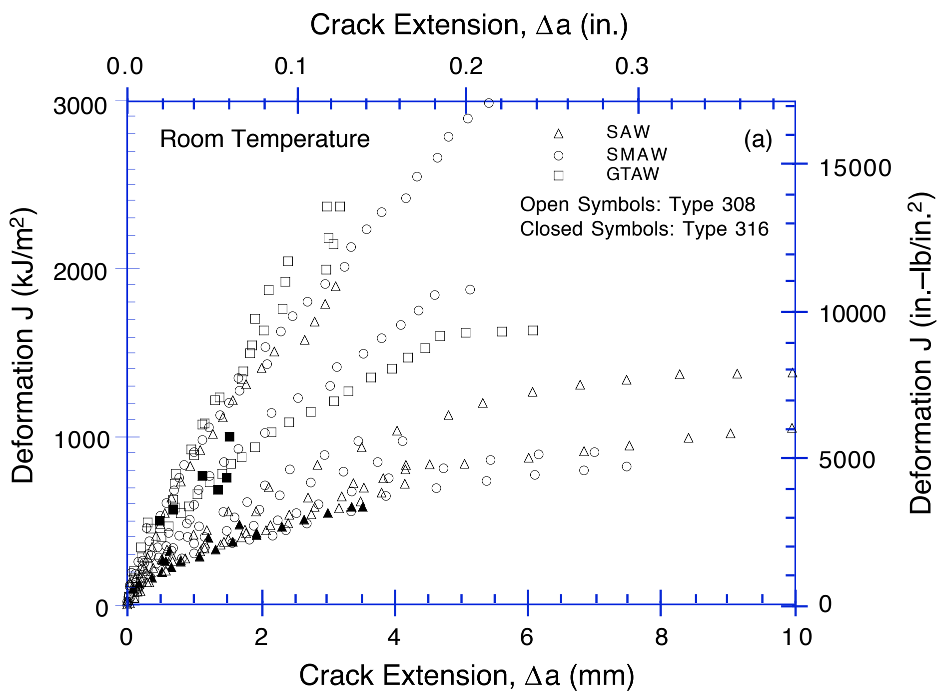

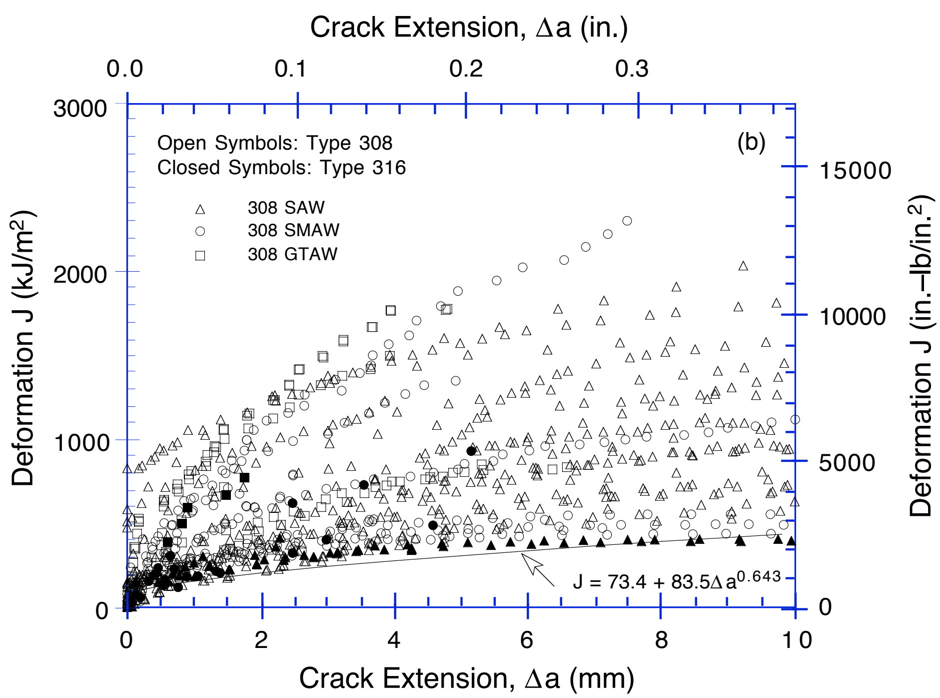

Figure 15. Fracture toughness J–R curves for stainless steel welds at (a) room temperature and (b) 288–427°C. Solid line represents lower–bound curve.

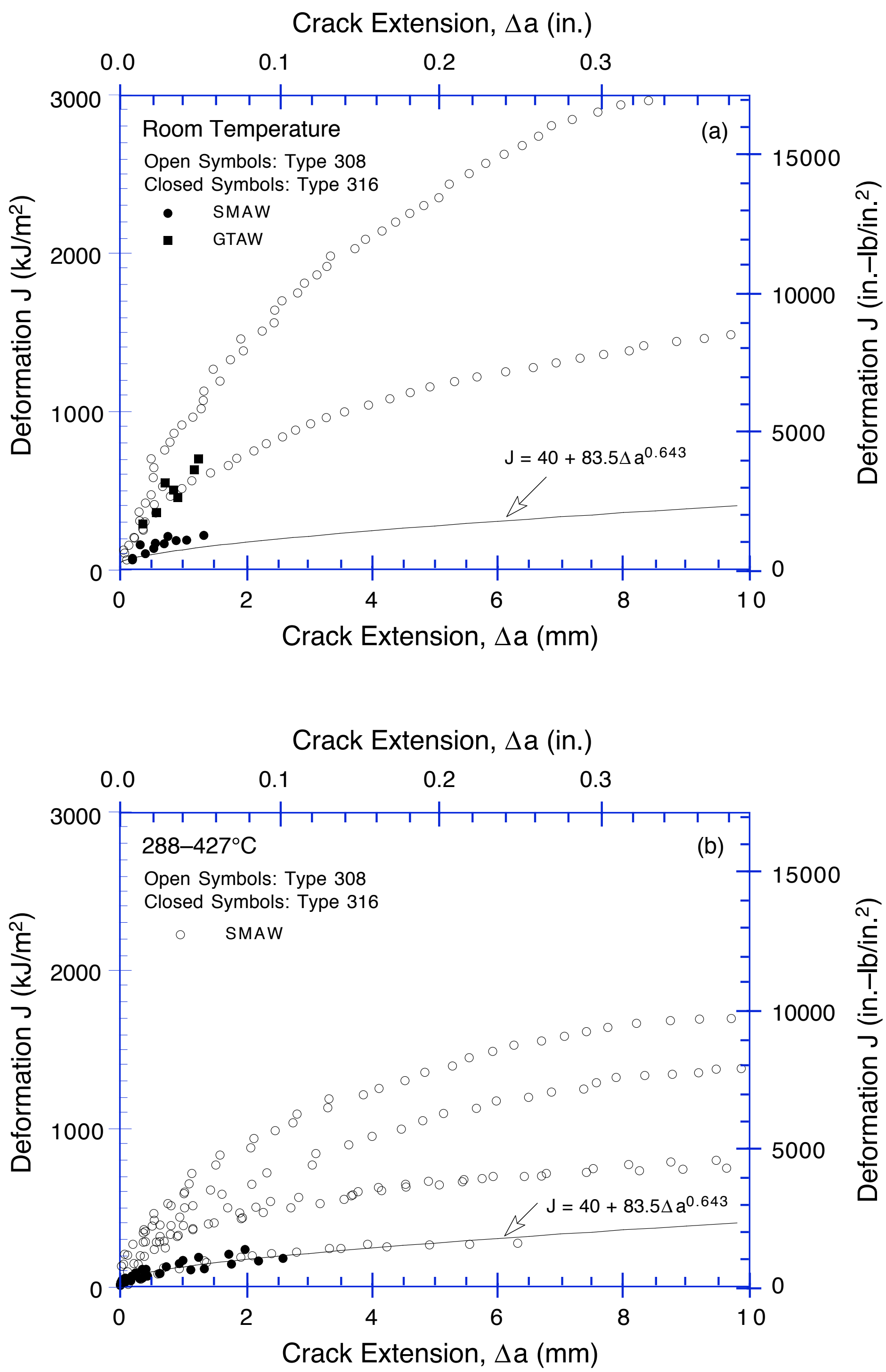

Figure 16. Fracture toughness J–R curves for aged stainless steel welds at (a) room temperature and (b) 288°C. Solid line represents lower–bound curve.

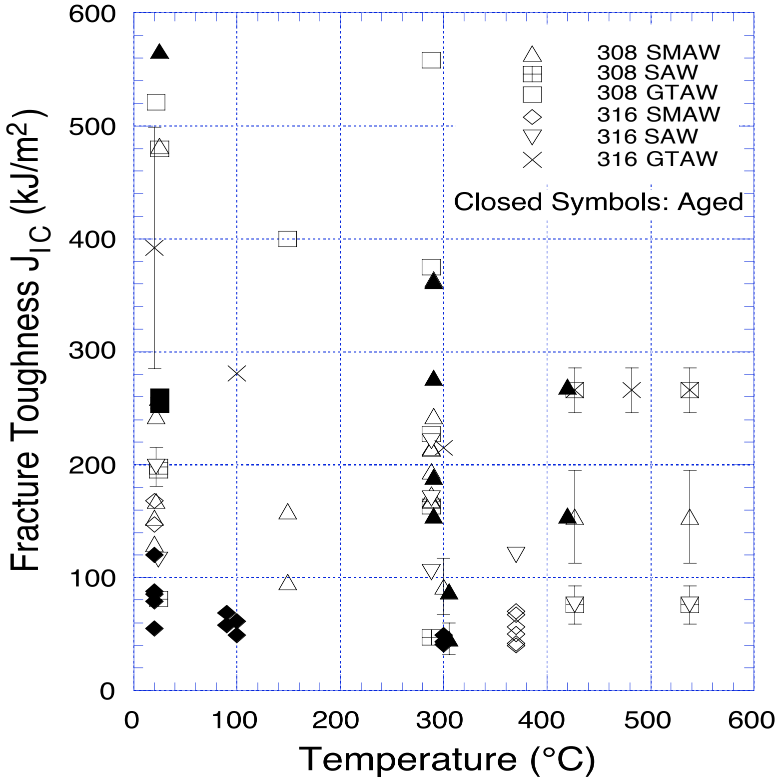

Figure 17. Fracture toughness J_{IC} for unaged and aged stainless steel welds

that could be achieved after long–term aging. The J_{IC} values for unaged and aged welds are plotted in Fig. 17. At reactor temperatures, the fracture toughness J_{IC} of SS welds can be as low as 40 kJ/m^2. Hence, the fracture toughness J–R curves for fully embrittled SMAWs and SAWs can be slightly lower than that predicted by Eq. 3; a conservative estimate for aged welds may be expressed as

$$J(\mathrm{kJ/m^2}) = 40 + 83.5\ \Delta a(\mathrm{mm})^{0.643}. \tag{4}$$

This curve is plotted in Fig. 16. The fracture toughness J–R curves for unaged and aged SS welds, i.e., Eqs. 3 and 4, respectively, are compared in Fig. 18 with the data for aged 316L and CF–3 welds[24,32] and the data in the technical basis document for ASME Section XI Article IWB–3640.[26] Note that the data from Ref. 26 are $J_{modified}$ rather than deformation J. The J–R curve suggested in Ref. 26 is somewhat higher than those predicted by Eqs. 3 and 4.

4 Conclusions

Thermal–aging–induced degradation of fracture toughness and Charpy–impact properties of several Type 304 SS pipe welds has been characterized at room temperature and 290°C. Thermal aging of the welds resulted in moderate decreases in Charpy–impact strength and fracture toughness at both room temperature and 290°C. For the various welds, USE decreased by 50–80 J/cm^2 (30–47 ft·lb.). The decrease in the fracture toughness J–R curve or J_{IC} is relatively small. Although tensile tests were not conducted on the welds, tensile proper–

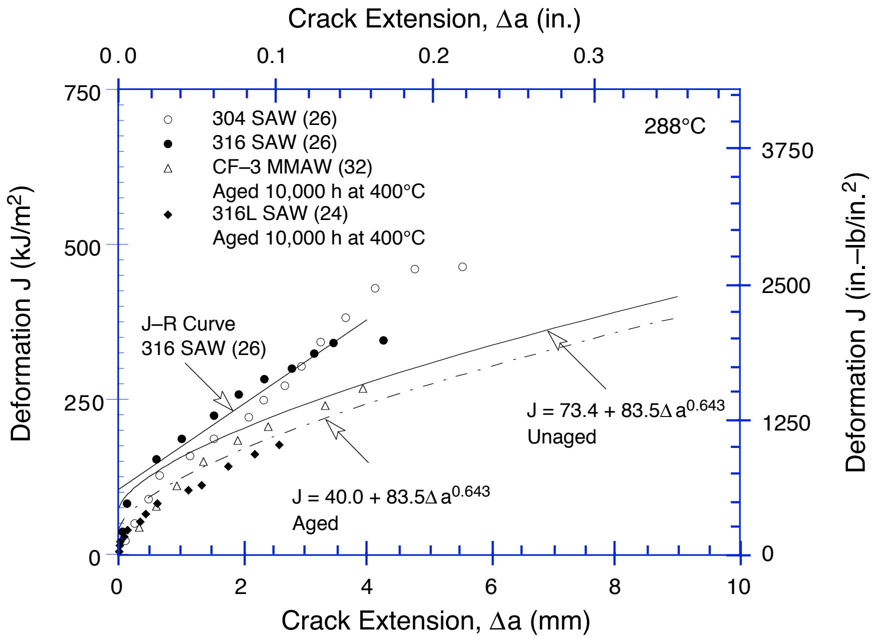

Figure 18. Fracture toughness J–R curves represented by Eqs. 3 and 4 and the data for aged CF–3 and 316L welds and that in the technical basis document for ASME Code IWB–3640 analysis

ties were estimated from the Charpy–impact data. The results indicate little or no effect of thermal aging on tensile strength of the welds. Metallographic examination of the specimens indicates that the fracture properties of SS welds are controlled by the distribution and morphology of second–phase particles. Differences in the fracture resistance of the welds arises from differences in the density and size of inclusions. Failure occurs by the formation and growth of microvoids near hard inclusions. In this study, the effect of thermal aging on fracture properties is minimal because of the relatively low ferrite content (4–6% ferrite) and thin vermicular ferrite morphology in the welds.

The Charpy–impact, tensile, and fracture toughness results from this study have been compared with available data on SMAWs, SAWs, and GTAWs prepared with Types 308 or 316 SS filler metal. The data are consistent with results from other investigations. The fracture properties of SS welds are insensitive to filler metal. The welding process has a significant effect. The large variability in the data makes it difficult to establish the effect of the welding process on fracture properties of SS welds. In general, GTAWs exhibit higher fracture resistance than SMAWs or SAWs, and there is no difference between SAW and SMAW J–R curves. The Charpy–impact energy of some welds may be as low as 40 J.

The results indicate that the decrease in impact strength due to aging depends on the ferrite content and initial impact strength of the weld. Welds with relatively high strength show a large decrease whereas those with poor strength show minimal change. In SS welds with poor strength, failure occurs by the formation and growth of microvoids. Such processes are relatively insensitive to thermal aging. The existing data indicate that at reactor temperatures, the fracture toughness J_{IC} of thermally aged welds can be as low as 40 kJ/m^2. A conservative estimate of J–R curve for aged SS welds may be given by $J = 40 + 83.5\ \Delta a^{0.643}$.

References

1. O. K. Chopra and H. M. Chung, "Effect of Low–Temperature Aging on the Mechanical Properties of Cast Stainless Steels," in *Properties of Stainless Steels in Elevated–Temperature Service*, M. Prager, ed., MPC Vol. 26, PVP Vol. 132, ASME, New York, pp. 79–105 (1988).

2. O. K. Chopra, "Thermal Aging of Cast Stainless Steels: Mechanisms and Predictions," in *Fatigue, Degradation, and Fracture – 1990*, W. H. Bamford, C. Becht, S. Bhandari, J. D. Gilman, L. A. James, and M. Prager, eds., MPC Vol. 30, PVP Vol. 195, ASME, New York, pp. 193-214 (1990).

3. W. F. Michaud, P. T. Toben, W. K. Soppet, and O. K. Chopra, *Tensile–Property Characterization of Thermally Aged Cast Stainless Steels*, NUREG/CR–6142, ANL–93/35 (Feb. 1994).

4. A. Trautwein and W. Gysel, "Influence of Long–Time Aging of CF–8 and CF–8M Cast Steel at Temperatures Between 300 and 500°C on the Impact Toughness and the Structure Properties," in Spectrum, Technische Mitteilungen aus dem+GF+Konzern, No. 5 (May 1981); also in Stainless Steel Castings, V. G. Behal and A. S. Melilli, eds., STP 756, ASTM, Philadelphia, PA, pp. 165–189 (1982).

5. S. Bonnet, J. Bourgoin, J. Champredonde, D. Guttmann, and M. Guttmann, "Relationship between Evolution of Mechanical Properties of Various Cast Duplex Stainless Steels and Metallurgical and Aging Parameters: An Outline of Current EDF Programmes," *Mater. Sci. Technol.*, **6**, 221–229 (1990).

6. P. H. Pumphrey and K. N. Akhurst, "Aging Kinetics of CF3 Cast Stainless Steel in Temperature Range 300–400°C," *Mater. Sci. Technol.*, **6**, 211–219 (1990).

7. Y. Meyzaud, P. Ould, P. Balladon, M. Bethmont, and P. Soulat, "Tearing Resistance of Aged Cast Austenitic Stainless Steel," presented at *Int. Conf. on Thermal Reactor Safety (NUCSAFE 88)*, Oct. 1988, Avignon, France.

8. H. M. Chung and O. K. Chopra, "Kinetics and Mechanism of Thermal Aging Embrittlement of Duplex Stainless Steels," in *Environmental Degradation of Materials in Nuclear Power Systems–Water Reactors*, G. J. Theus and J. R. Weeks, eds., The Metallurgical Society, Warrendale, PA, pp. 359–370 (1988).

9. P. Auger, F. Danoix, A. Menand, S. Bonnet, J. Bourgoin, and M. Guttmann, "Atom Probe and Transmission Electron Microscopy Study of Aging of Cast Duplex Stainless Steels," *Mater. Sci. Technol.*, **6**, 301–313 (1990).

10. M. Vrinat, P. Cozar, and Y. Meyzaud, "Precipitated Phases in the Ferrite of Aged Cast Duplex Stainless Steels," *Scripta Metall.*, **20**, 1101–1106 (1986).

11. P. Joly, R. Cozar, and A. Pineau, "Effect of Crystallographic Orientation of Austenite on the Formation of Cleavage Cracks in Ferrite in an Aged Duplex Stainless Steel," *Scripta Metall.*, **24**, 2235–2240 (1990).

12. J. E. Brown, A. Cerezo, T. J. Godfrey, M. G. Hetherington, and G. D. W. Smith, "Quantitative Atom Probe Analysis of Spinodal Reaction in Ferrite Phase of Duplex Stainless Steel," *Mater. Sci. Technol.*, **6**, 293–300 (1990).

13. O. K. Chopra and W. J. Shack, *Assessment of Thermal Embrittlement of Cast Stainless Steels*, NUREG/CR–6177, ANL–94/2 (May 1994).

14. O. K. Chopra, *Estimation of Fracture Toughness of Cast Stainless Steels during Thermal Aging in LWR Systems – Revision 1*, NUREG/CR–4513 Rev. 1, ANL–93/22 (Aug. 1994).

15. O. K. Chopra, *Long–Term Embrittlement of Cast Duplex Stainless Steels in LWR Systems: Semiannual Report October 1991–March 1992*, NUREG/CR–4744, Vol. 7, No. 1, ANL–92/42 (April 1993).

16. L. S. Aubrey, P. F. Wieser, W. J. Pollard, and E. A. Schoefer, "Ferrite Measurement and Control in Cast Duplex Stainless Steel," in *Stainless Steel Castings*, V. G. Behal and A. S. Melilli, eds., ASTM STP 756, pp. 126–164 (1982).

17. P. S. Maiya and W. J. Shack, in *Environmentally Assisted Cracking in Light Water Reactors: Annual Report*, *October 1983–September 1984*, NUREG/CR–4287, ANL–85–33, pp. 67–70 (Aug. 1985).

18. J. Y. Park, in *Environmentally Assisted Cracking in Light Water Reactors: Annual Report*, *October 1981–September 1982*, NUREG/CR–3292, ANL–83–27, pp. 23–29 (Feb. 1983).

19. D. R. Diercks, *Analysis of Cracked Core Spray Injection Line Piping from the Quad Cities Units 1 and 2 Boiling Water Reactors*, Argonne National Laboratory Report ANL–83–99 (Dec. 1983).

20. P. S. Maiya and W. J. Shack, in *Environmentally Assisted Cracking in Light Water Reactors: Annual Report*, *October 1983–September 1984*, NUREG/CR–4287, ANL–85–33, pp. 67–70 (Aug. 1985).

21. S. Yukawa, *Review and Evaluation of the Toughness of Austenitic Steels and Nickel Alloys After Long–Term Elevated Temperature Exposures*, Welding Research Council Bulletin 378, New York (Jan. 1993).

22. R. M. Horn, H. S. Mehta, W. R. Andrews, and S. Ranganath, *Evaluation of the Toughness of Austenitic Stainless Steel Pipe Weldments*, EPRI NP–4668, Electric Power Research Institute, Palo Alto, CA (June 1986).

23. M. Strangwood and S. G. Druce, "Aging Effects in Welded Cast CF–3 Stainless Steel," *Mater. Sci. Technol.*, **6**, 237–248 (1990).

24. C. G. Chipperfield, "A Toughness and Defect Size Assessment of Welded Stainless Steel Components," *Tolerance of Flaws in Pressurized Components*, Inst. Mech. Eng. pp. 125–137 (1978).

25. P. Ould, P. Balladon, and Y. Mehzaud, "Fracture Toughness of Austenitic Stainless Steel Welds," presented at *Int. Colloquim on Stainless Steels*, Ecole Polytechnique, Mons, Belgium, April 27–28, 1988.

26. J. D. Landes and D. E. McCabe, *Toughness of Austenitic Stainless Steel Pipe Welds*, EPRI NP–4768, Electric Power Research Institute, Palo Alto, CA (Oct. 1986).

27. W. J. Mills, *Fracture Toughness Variations for Stainless Steel Base Metal and Welds*, HEDL–TME 84–11, Hanford Engineering Development Laboratory, Richland, WA (May 1984).

28. W. J. Mills, "Fracture Toughness of Aged Stainless Steel Primary Piping and Reactor Vessel Materials," *J. Press. Vessel Technol.*, **109**, 440–448 (1987).

29. W. J. Mills, "Fracture Toughness of Stainless Steel Welds," in *Fracture Mechanics: Nineteenth Symposium*, T. A. Cruise, ed., ASTM STP 969, American Society for Testing and Materials, Philadelphia, PA, pp. 330–355 (1988).

30. J. M. Vitek, S. A. David, D. J. Alexander, J. R, Keiser, and R. K. Nanstad, "Low Temperature Aging Behavior of Type 308 Stainless Steel Weld Metal," *Acta Metall.*, **39**, 503–516 (1991).

31. D. J. Alexander, K. B. Alexander, M. K. Miller, and R. K. Nanstad, "The Effect of Aging at 343°C on Type 308 Stainless Steel Weldments," in *Fatigue, Degradation, and Fracture – 1990*, W. H. Bamford, C. Becht, S. Bhandari, J. D. Gilman, L. A. James, and M. Prager, eds., MPC Vol. 30, PVP Vol. 195, ASME, New York, pp. 187–192 (1990).

32. G. E. Hale and S. J. Garwood, "Effect of Aging on Fracture Behaviour of Cast Stainless Steel and Weldments," *Mater. Sci. Technol.*, **6**, 230–236 (1990).

33. S. J. Garwood, "Fracture Toughness of Stainless Steel Weldments at Elevated Temperatures," in *Fracture Mechanics: 15th Symposium*, R. J. Sanford, ed., ASTM STP 833, American Society for Testing and Materials, Philadelphia, PA, pp. 333–359 (1984).

34. M. G. Vassilaros, R. A. Hays, and J. P. Gudas, "Investigation of the Ductile Fracture Properties of Type 304 Stainless Steel Plate, Welds, and 4–inch Pipe," in *Proc. 12th Water Reactor Safety Research Information Meeting*, NUREG/CP–0058, Vol. 4, U.S. Nuclear Regulatory Commission, pp. 176–189 (1985).

35. J. P. Gudas and D. R. Anderson, "J_I–R Curve Characteristics of Piping Material and Welds," in *Proc. 9th Water Reactor Safety Research Information Meeting*, Oct. 1981, U.S. Nuclear Regulatory Commission.

36. J. R. Hawthorne and B. H. Menke, "Influence of Delta Ferrite Content and Welding Variables on Notch Toughness of Austenitic Stainless Steel Weldments," in *Structural Materials for*

Service at Elevated Temperatures in Nuclear Power Generation, G. V. Smith, ed., MPC–1, ASME, New York, pp. 351–364 (1975).

37. F. Faure, B. Houssin, and P. Balladon, "Mechanical Properties of Automatic TIG/GTA Welds of Stainless Steel Piping in Nuclear Reactors," in *Trends in Welding Research*, ASM Conf., Gatlinburg, May 14–18, 1989.

38. G. Wilkowski, et al., *Analysis of Experiments on Stainless Steel Flux Welds*, NUREG/CR–4878, BMI–2151 (April 1987).

39. M. Nakagaki, C. Marshall, and F. Brust, *Analysis of Cracks in Stainless Steel TIG Welds*, NUREG/CR–4806, BMI–2144 (Dec. 1986).

40. Mechanical Testing of Austenitic Steel Welded Joints, Joint Final Report–Vol. 2, Commission of the European Communities, Ispra, Italy (1990).

41. W. L. Server, "Impact Three–Point Bend Testing for Notched and Precracked Specimens," *J. Test. Eval.*, **6**, 29 (1978).

42. A. L. Hiser and G. M. Callahan, *A User's Guide to the NRC's Piping Fracture Mechanics Database (PIFRAC)*, NUREG/CR–4894 (May 1987).

43. G. M. Wilkowski, et al., *Short Crcaks in Piping and Piping Welds*, NUREG/CR–4599, Vols. 1 to 3, Nos. 1 and 2 (May 1991 to March 1994).

44. G. M. Wilkowski, et al., *Probabilistic Pipe Fracture Evaluations for Leak–Rate–Dectection Applications*, NUREG/CR–6004 (April 1995).

Appendix

J–R Curve Characterization

The J–R curve tests were performed according to ASTM Specifications E 813–85 (Standard Test Method for J_{IC}, a Measure of Fracture Toughness) and E 1152–87 (Standard Test Method for Determining J–R Curve). Compact–tension (CT) specimens, 25.4 mm (1 in.) thick with 10% side grooves, were used for the tests. The design of the CT specimen is similar to that of the specimen in ASTM Specification E 399, the notch region is modified in accordance with E 813 and E 5112, to permit measurement of load–line displacement by axial extensometer. The extensometer was mounted on razor blades that were screwed onto the specimen along the load line.

Prior to testing, the specimens were fatigue–precracked at room temperature and at load levels within the linear elastic range. The final ratio of crack length to width (a/W) after pre–cracking was ≈0.55. The final 1–mm (≈0.04–in.) crack extension was carried out at a load range of 13–1.3 kN (2.92–0.292 kip), i.e., during precracking, K_{max} was <25 $MPa \cdot m^{1/2}$ (22.6 $ksi \cdot in.^{1/2}$). After precracking, all specimens were side–grooved to 20% of the total specimen thickness, i.e., 10% per side, to ensure uniform crack growth during testing.

The J–R curve tests were performed on an Instron testing machine with 90 kN (20 kip) maximum load capacity. The load and load–line displacement data were digitized with digital voltmeters and stored on a disk for posttest analysis and correction of test data. The single–specimen compliance procedure was used to estimate crack extension. Rotation and modulus corrections were applied to the compliance data. Both deformation theory and modified forms of the J integral were evaluated for each test.

After each test, the specimen was heated to 350°C to heat–tint the exposed fracture surface. The specimen was then fractured at liquid N temperature. The initial (i.e., fatigue precrack) and final (test) crack lengths were measured optically for both halves of the fractured specimen. The crack lengths were determined by the 9/8 averaging technique, i.e., the two near–surface measurements were averaged and the resultant value was averaged with the remaining seven measurements.

The fracture toughness J_{IC} values were determined in accordance with ASTM Specification E 813–81 and E 813–85. For the former, J_{IC} is defined as the intersection of the blunting line given by $J = 2\sigma_f \Delta a$, and the linear fit of the J–vs.–Δa test data between the 0.15– and 1.5–mm exclusion lines. The flow stress σ_f, is the average of the 0.2% yield stress and the ultimate stress. The ASTM Specification E 813–85 procedure defines J_{IC} as the intersection of the 0.2–mm offset line with the power–law fit (of the form $J = C\Delta a^n$) of the test data between the exclusion lines. However, a slope of four times the flow stress ($4\sigma_f$) was used to define the blunting line. The tearing modulus was also evaluated for each test. The tearing modulus is given by $T = E(dJ/da)/\sigma_f^2$, where E is the Young's modulus and σ_f is the flow stress. The ASTM E 813–81 value of tearing modulus is determined from the slope dJ/da of the linear fit to the J–vs.–Δa data. For the power–law curve fits, an average value of dJ/da was calculated[A–1] to obtain the average tearing modulus.

The test data, as well as an analysis and qualification of the data, are presented in Tables A–1 to A–27. Photographs of the fracture surface of the test specimens and deformation and modified J–R curves for the various welds are shown in Figs. A–1 to A–27.

Data Analysis Procedures

The compliance method was used to determine crack length during the tests. The Hudak–Saxena calibration equation[A–2] was used to relate specimen load–line elastic compliance C_i on an unloading/loading sequence with crack length a_i. The compliance, i.e., slope ($\Delta\delta/\Delta P$) of the load–line displacement–vs.–load record obtained during the unloading/loading sequence, is given by

$$U_{LL} = \frac{1}{\left(B_e E_e C_i\right)^{1/2} + 1} \tag{A–1}$$

and

$$a_i/W = 1.000196 - 4.06319\left(U_{LL}\right) + 11.242\left(U_{LL}\right)^2 - 106.043\left(U_{LL}\right)^3 + 464.335\left(U_{LL}\right)^4 - 650.677\left(U_{LL}\right)^5, \tag{A–2}$$

where E_e is the effective elastic modulus, B_e is the effective specimen thickness expressed as $B - (B - B_N)^2/B$, and W is specimen width.

Both rotation and modulus corrections are applied to the compliance data. The modulus correction[A–2] is used to account for the uncertainties in testing, i.e., in the values of initial crack length determined by compliance and measured optically. The effective modulus E_M is determined from

$$E_e = \frac{1}{C_o B_e}\left(\frac{W + a_o}{W - a_o}\right)^{1/2} f\left(\frac{a_o}{W}\right) \tag{A–3}$$

and

$$f\left(\frac{a_o}{W}\right) = 2.163 + 12.219\left(\frac{a_o}{W}\right) - 20.065\left(\frac{a_o}{W}\right)^2 - 0.9925\left(\frac{a_o}{W}\right)^3 + 20.609\left(\frac{a_o}{W}\right)^4 - 9.9314\left(\frac{a_o}{W}\right)^5, \tag{A–4}$$

where C_o is initial compliance, B_e is effective specimen thickness, and a_o is initial physical crack size that has been measured optically.

To account for crack–opening displacement in CT specimens, the crack size should be corrected for rotation.[A–3] The corrected compliance is calculated from

$$\theta = \mathrm{Sin}^{-1}\left[\left(\frac{d_m}{2}+D\right)\Big/\left(D^2+R^2\right)^{1/2}\right]-\tan^{-1}\left(\frac{D}{R}\right) \tag{A–5}$$

and

$$C_c = C_m \Big/ \left[\left(\frac{H^*}{R}\mathrm{Sin}\theta - \mathrm{Cos}\theta\right)\left(\frac{D}{R}\mathrm{Sin}\theta - \mathrm{Cos}\theta\right)\right], \tag{A–6}$$

where C_c and C_m are the corrected and measured elastic compliance at the load line, H^* is the initial half span of load points, R is the radius of rotation of the crack centerline (= (W+a)/2), a is the updated crack length, D is one–half of the initial distance between the displacement points (i.e., one–half of the gage length), d_m is the total measured load–line displacement, and θ is the angle of rotation of a rigid–body element about the unbroken midsection line.

The J value is calculated at any point on the load–vs.–load–line displacement record by means of the relationship

$$\mathbf{J} = \mathbf{J}_{el} + \mathbf{J}_{pl}, \tag{A–7}$$

where J_{el} is the elastic component of J and J_{pl} is the plastic component of J. For a CT specimen, at a point corresponding to the coordinates P_i and δ_i on the specimen load–vs.–load–line displacement record, a_i is ($a_0 + \Delta a_i$), and the deformation J is given by

$$\mathbf{J}_{d(i)} = \frac{(K_i)^2\left(1-\upsilon^2\right)}{E_e} + \mathbf{J}_{pl(i)}, \tag{A–8}$$

where, from ASTM method E 399,

$$K_{(i)} = \left[\frac{P_i}{\left(BB_N W_e\right)^{1/2}}\right] f\left(\frac{a_i}{W}\right), \tag{A–9}$$

with

$$f\left(\frac{a_i}{W}\right) = \left[2+\left(\frac{a_i}{W}\right)\right]\left[0.886+4.64\left(\frac{a_i}{W}\right)-13.32\left(\frac{a_i}{W}\right)^2+14.72\left(\frac{a_i}{W}\right)^3 -5.6\left(\frac{a_i}{W}\right)^4\right]\Big/\left[1-\left(\frac{a_i}{W}\right)\right]^{3/2} \tag{A–10}$$

and

$$\mathbf{J}_{pl(i)} = \left[\mathbf{J}_{pl(i-1)} + \left(\frac{\eta_i}{b_i}\right)\frac{A_{pl(i)}-A_{pl(i-1)}}{B_N}\right]\left[1-\left(\frac{\gamma_i}{b_i}\right)\left(a_i-a_{i-1}\right)\right], \tag{A–11}$$

where υ is Poisson's ratio, b is the uncracked ligament, A_{pl} is the plastic component of the area under the load–vs.–load–line displacement record, η is a factor that accounts for the tensile component of the load as given by

$$\eta_i = 2 + 0.522\, b_i/W, \tag{A–12}$$

and γ, is a factor that accounts for limited crack growth as given by

$$\gamma_i = 1 + 0.76\, b_i/W. \tag{A–13}$$

Modified J values (J_M) are calculated from the relationship (from Ref. A–4)

$$\mathbf{J}_{M(i)} = \mathbf{J}_{d(i)} + \Delta\mathbf{J}_i, \tag{A–14}$$

where

$$\Delta\mathbf{J}_i = \Delta\mathbf{J}_{i-1} + \left(\frac{\gamma_i}{b_i}\right)\mathbf{J}_{pl(i)}\left(a_i - a_{i-1}\right). \tag{A–15}$$

According to ASTM Specification E 1152–87, the J_D–R curves are valid only for crack growth up to 10% of the initial uncracked ligament. Also, they show a dependence on specimen size. The J_M–R curves have been demonstrated to be independent of specimen size and yield valid results for larger crack growth.

Data Qualification

The various validity criteria specified in ASTM Specification E 813–85 for J_{IC} and in ASTM Specification E 1152–87 for J–R curves were used to qualify the results from each test. The various criteria include maximum values of crack extension and J–integrals; limits for initial uncracked ligaments, effective elastic modulus, and optically measured physical crack lengths; and spacing of J–Δa data points. The ω criterion (from Ref. A–5) was also used to ensure that a region of J dominance exists. For the present investigation, all of the welds yielded invalid test results; in most cases because of the shape of the final crack front. In some cases, specimen thickness was inadequate because of the relatively high toughness of the material. The J_{max} limit for the J–vs.–Δa data was ignored in most tests to obtain a good power–law fit of the test data.

Appendix References

A–1. A. L. Hiser, F. J. Loss, and B. H. Menke, *J–R Curve Characterization of Irradiated Low Upper Shelf Welds*, NUREG/CR–3506, MEA–2028, Materials Engineering Associates, Inc., Lanham, MD (April 1984).

A–2. A. Saxena and S. J. Hudak, Jr., "Review and Extention of Compliance Information for Common Crack Growth Specimen," *Int. J. Fracture*, **5**, 453–468 (1978).

A–3. F. J. Loss, B. H. Menke, and R. A. Gray, Jr., "Development of J–R Curve Procedures," in *NRL–EPRI Research Program (RP 886–2), Evaluation and Prediction of Neutron*

Embrittlement in Reactor Pressure Vessel Materials Annual Progress Report for FY 1978, J. R. Hawthorn, ed., NRL Report 8327, Naval Research Laboratory, Annapolis, MD (Aug. 1979).

A–4. H. A. Ernst, "Material Resistance and Instability Beyond J–Controlled Crack Growth," *Elastic–Plastic Fracture: Second Symp., Vol. I: Inelastic Crack Analysis*, ASTM STP 803, American Society for Testing and Materials, Philadelphia (1983).

A–5. J. W. Hutchinson and P. C. Paris, "The Theory of Stability Analysis of J–Controlled Crack Growth," *Elastic Plastic Fracture*, ASTM STP 668, American Society for Testing and Materials, Philadelphia, pp. 37–64 (1983).

Table A–1. Test data for specimen PWCE–02

Test Number	: 0125	Test Temp	: 25˚C
Material Type	: Weld Metal	Heat Number	: PWCE
Aging Temp	: Unaged	Aging Time	: –
Thickness	: 25.36 mm	Net Thickness	: 20.18 mm
Width	: 50.78 mm	Flow Stress	: 534.00 MPa

Unload Number	J_d (kJ/m^2)	J_m (kJ/m^2)	Δa (mm)	Load (kN)	Deflection (mm)
1	15.20	15.20	0.0000	23.443	0.250
2	52.28	52.31	0.0280	36.946	0.502
3	102.22	102.54	0.1172	43.820	0.755
4	157.48	158.72	0.2672	47.057	1.004
5	227.48	228.42	0.2367	48.949	1.305
6	301.95	304.11	0.3225	50.353	1.606
7	377.68	380.14	0.3385	51.045	1.911
8	454.79	456.23	0.2947	51.581	2.210
9	529.58	536.70	0.4997	52.029	2.509
10	603.85	613.98	0.5935	52.481	2.811
11	680.85	695.23	0.7086	52.830	3.116
12	755.23	772.60	0.7808	52.807	3.408
13	833.02	853.72	0.8529	52.943	3.710
14	907.13	935.76	1.0088	52.928	4.010
15	981.59	1016.74	1.1262	52.940	4.310
16	1056.79	1098.06	1.2275	52.844	4.610
17	1128.50	1180.43	1.3912	52.693	4.908
18	1201.74	1262.91	1.5234	52.370	5.212
19	1273.41	1346.72	1.6857	52.211	5.517
20	1352.00	1423.84	1.6673	52.127	5.809
21	1431.84	1540.61	2.0977	51.770	6.208
22	1536.75	1642.96	2.0701	51.538	6.609
23	1628.47	1758.04	2.3059	51.313	7.008
24	1720.16	1867.79	2.4772	50.992	7.411
25	1805.54	1978.68	2.7049	50.287	7.809
26	1912.16	2116.36	2.9638	49.847	8.307
27	2013.56	2254.97	3.2545	49.355	8.808
28	2134.33	2389.33	3.3538	48.396	9.309
29	2239.91	2528.49	3.5853	47.767	9.807
30	2341.12	2664.76	3.8140	47.301	10.307
31	2422.73	2804.41	4.1745	46.812	10.812
32	2553.13	2963.93	4.3445	45.997	11.411
33	2664.57	3129.43	4.6428	45.451	12.008
34	2792.24	3289.24	4.8103	44.687	12.607
35	2897.83	3454.39	5.1055	43.776	13.209
36	2992.22	3614.99	5.4187	43.160	13.808
37	3106.00	3803.53	5.7538	42.271	14.511
38	3218.54	3988.74	6.0633	41.357	15.208

Table A–2. Deformation J_{IC} and J–R curve results for specimen PWCE–02

Test Number	: 0125	Test Temp	: 25˚C
Material Type	: Weld Metal	Heat Number	: PWCE
Aging Temp	: Unaged	Aging Time	: –
Thickness	: 25.36 mm	Net Thickness	: 20.18 mm
Width	: 50.78 mm	Flow Stress	: 534.00 MPa
Modulus E	: 195.06 GPa	(Effective)	
Modulus E	: 193.10 GPa	(Nominal)	
Init. Crack	: 28.2063 mm	Init. a/w	: 0.5554 (Measured)
Final Crack	: 35.0094 mm	Final a/w	: 0.6894 (Measured)
Final Crack	: 34.2695 mm	Final a/w	: 0.6748 (Compliance)

Linear Fit	**$J = B + M(\Delta a)$**		
Intercept B	: 283.992 kJ/m^2	Slope M	: 597.47 kJ/m^3
Fit Coeff. R	: 0.9900	(14 Data Points)	
J_{IC}	: 394.3 kJ/m^2	(2251.4 in.-lb/in.^{2})	
Δa (J_{IC})	: 0.185 mm	(0.0073 in.)	
T average	: 408.7	(J_{IC} at 0.15)	

Power–Law Fit	**$J = C(\Delta a)^n$**		
Coeff. C	: 893.25 kJ/m^2	Exponent n	: 0.7216
Fit Coeff. R	: 0.9962	(14 Data Points)	
J_{IC}(0.20)	: 482.4 kJ/m^2	(2754.9 in.-lb/in.^{2})	
Δa (J_{IC})	: 0.426 mm	(0.0168 in.)	
T average	: 414.3	(J_{IC} at 0.20)	
J_{IC}(0.15)	: 413.0 kJ/m^2	(2358.4 in.-lb/in.^{2})	
Δa (J_{IC})	: 0.343 mm	(0.0135 in.)	
T average	: 419.5	(J_{IC} at 0.15)	
K_{jc}	: 559.4 MPa–$m^{0.5}$		

J_{IC} Validity & Data Qualification (E 813–85)

J_{max} allowed	: 803.70 kJ/m^2	($J_{max} = b_o\sigma_f/15$)
Data Limit	: J_{max} Ignored	
Δa (max) allowed	: 2.251 mm	(at 1.5 exclusion line)
Data Limit	: 1.5 Exclusion line	
Data Points	: Zone A = 5	Zone B = 4
Data Point Spacing	: OK	
B_{net} or b_o size	: OK	
dJ/da at J_{IC})	: OK	
a_o Measurement	: 9 Outside Limit	
a_o Measurement	: 1 Outside Limit	
a_f Measurement	: Near-surface	Outside Limit
Crack size estimate	: Inadequate	(by Compliance)
E Effective	: OK	
J_{IC} Estimate	: Invalid	

J–R curve Validity & Data Qualification (E 1152–86)

J_{max} allowed	: 538.89 kJ/m^2	($J_{max} = B_{net}\ \sigma_f/20$)
Δa (max) allowed	: 2.258 mm	($\Delta a = 0.1b_o$)
Δa (max) allowed	: 6.405 mm	($\omega = 5$)
Data Points	: Zone A = 20	Zone B = 2
Data Point Spacing	: Inadequate	
J-R Curve Data	: Invalid	

Table A–3. Modified J_{IC} and J–R curve results for specimen PWCE–02

Linear Fit	**$J = B + M(\Delta a)$**		
Intercept B	: 255.520 kJ/m^2	Slope M	: 657.42 kJ/m^3
Fit Coeff. R	: 0.9944	(15 Data Points)	
J_{IC}	: 369.1 kJ/m^2	(2107.8 in.-lb/in.^{2})	
Δa (J_{IC})	: 0.173 mm	(0.0068 in.)	
T average	: 449.7	(J_{IC} at 0.15)	
Power–Law Fit	**$J = C(\Delta a)^n$**		
Coeff. C	: 924.64 kJ/m^2	Exponent n	: 0.7629
Fit Coeff. R	: 0.9977	(15 Data Points)	
J_{IC}(0.20)	: 481.9 kJ/m^2	(2751.5 in.-lb/in.^{2})	
Δa (J_{IC})	: 0.426 mm	(0.0168 in.)	
T average	: 454.7	(J_{IC} at 0.20)	
J_{IC}(0.15)	: 406.1 kJ/m^2	(2319.0 in.-lb/in.^{2})	
Δa (J_{IC})	: 0.340 mm	(0.0134 in.)	
T average	: 459.6	(J_{IC} at 0.15)	
K_{jc}	: 585.5 MPa–m$^{0.5}$		

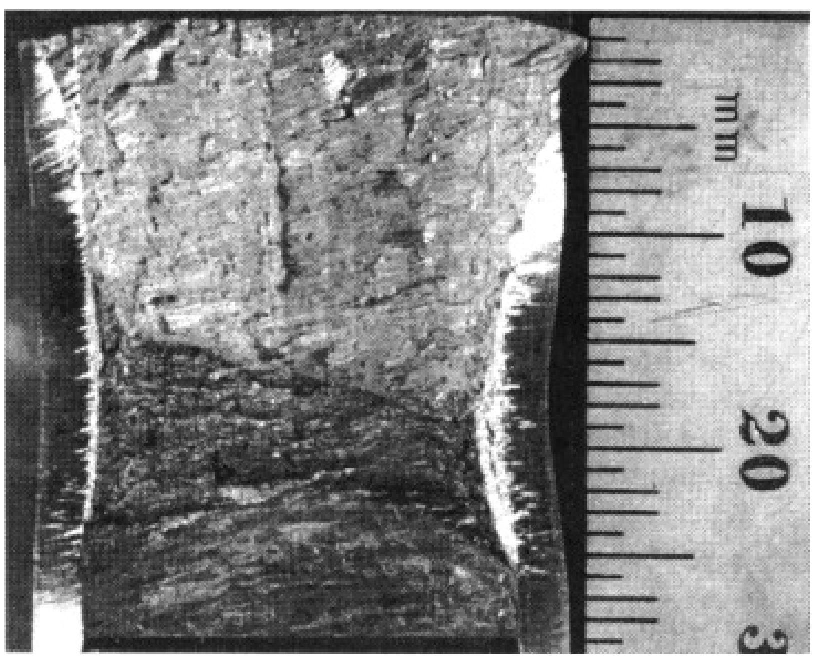

Figure A–1. Fracture surface of unaged weld metal PWCE tested at 25°C

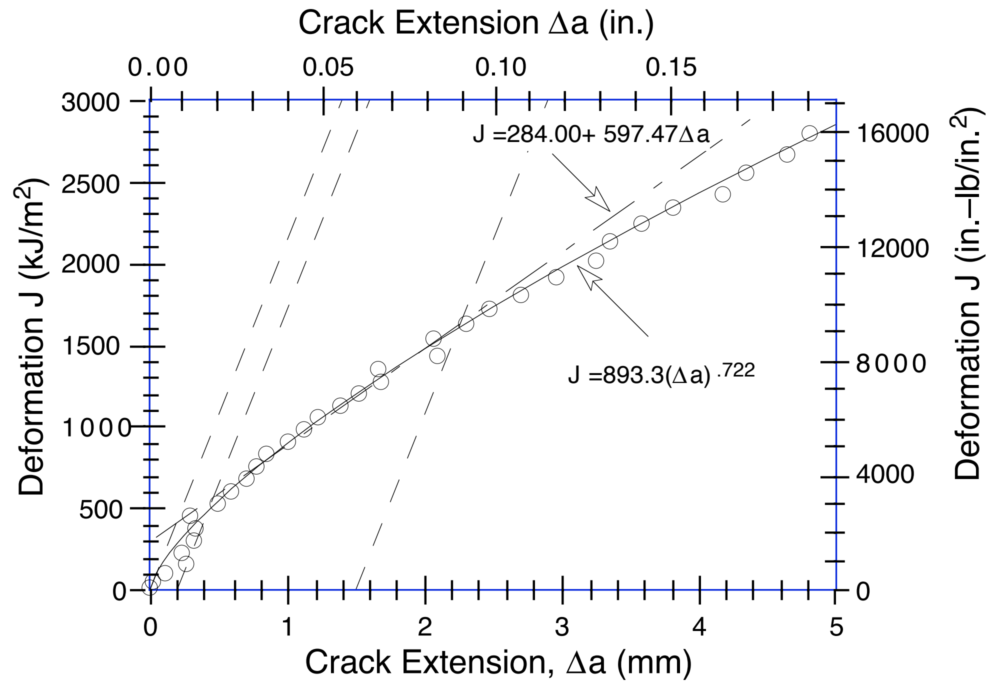

Figure A–2. Deformation J–R curve for unaged weld metal specimen PWCE–02 tested at 25°C. Blunting, 0.2–mm offset, and 1.5–mm offset lines are shown as dashed lines.

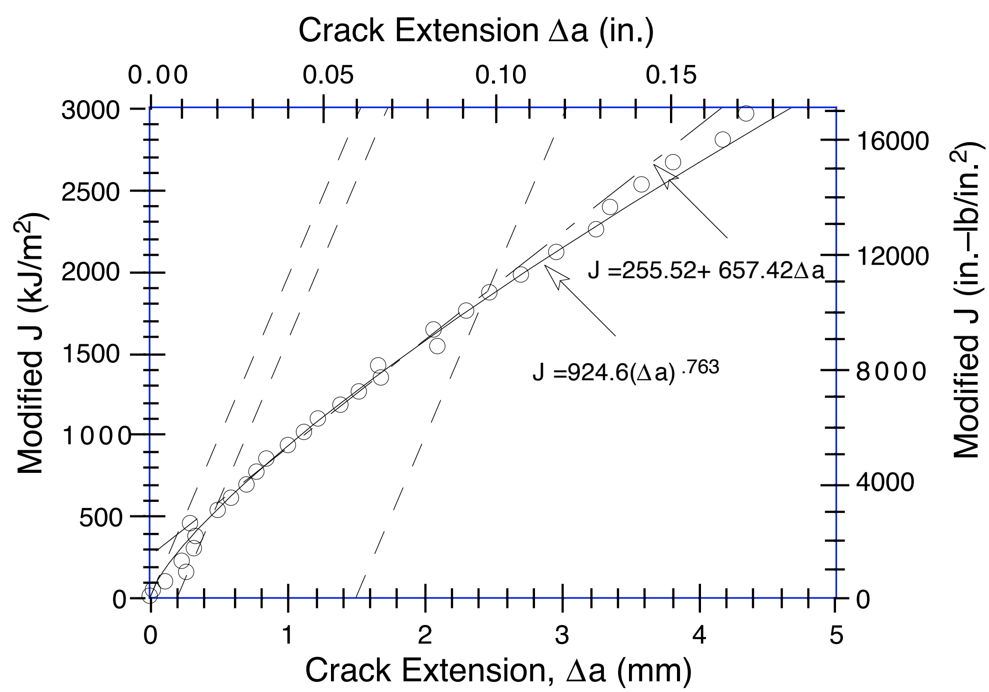

Figure A–3. Modified J–R curve for unaged weld metal specimen PWCE–02 tested at 25°C. Blunting, 0.2–mm offset, and 1.5–mm offset lines are shown as dashed lines.

Table A–4. Test data for specimen PWCE–04

Test Number	: 0129	Test Temp	: 25°C
Material Type	: Weld Metal	Heat Number	: PWCE
Aging Temp	: 400°C	Aging Time	: 10,000 h
Thickness	: 25.37 mm	Net Thickness	: 20.29 mm
Width	: 50.80 mm	Flow Stress	: 538.00 MPa

Unload Number	J_d (kJ/m^2)	J_m (kJ/m^2)	Δa (mm)	Load (kN)	Deflection (mm)
1	16.29	16.28	-0.1303	26.132	0.251
2	58.75	59.01	0.1101	42.335	0.502
3	100.62	100.80	0.0805	48.905	0.703
4	150.27	150.79	0.1433	51.989	0.905
5	201.40	202.58	0.2264	53.926	1.106
6	253.46	256.21	0.3695	55.297	1.306
7	306.00	308.03	0.3180	56.009	1.507
8	362.41	364.26	0.3077	56.437	1.708
9	418.59	422.46	0.4064	57.337	1.911
10	471.26	477.36	0.5011	57.678	2.107
11	524.22	535.12	0.6809	57.882	2.307
12	582.23	588.55	0.5289	58.212	2.510
13	642.26	649.10	0.5442	58.329	2.710
14	700.26	705.55	0.5023	58.455	2.908
15	754.28	768.16	0.7150	58.539	3.112
16	806.09	823.63	0.7990	58.773	3.311
17	860.16	880.65	0.8620	58.739	3.508
18	913.74	940.68	0.9902	58.583	3.710
19	963.16	999.13	1.1594	58.668	3.908
20	1014.99	1058.42	1.2910	58.897	4.111
21	1069.51	1115.39	1.3317	58.766	4.308
22	1128.93	1175.39	1.3408	58.956	4.510
23	1190.65	1254.22	1.5925	58.914	4.759
24	1267.00	1322.92	1.4871	58.483	5.009
25	1328.22	1405.16	1.7607	58.379	5.260
26	1385.09	1478.41	1.9630	57.978	5.510
27	1459.29	1549.27	1.9239	57.701	5.761
28	1510.18	1630.78	2.2657	57.500	6.010
29	1563.64	1701.56	2.4509	57.153	6.258
30	1640.00	1779.10	2.4630	56.718	6.525
31	1701.40	1852.14	2.5761	56.527	6.759
32	1751.71	1929.25	2.8267	55.871	7.008
33	1811.93	2001.16	2.9317	55.320	7.259
34	1865.97	2078.21	3.1307	54.797	7.511
35	1919.87	2151.04	3.2885	54.298	7.759
36	1984.76	2223.78	3.3516	53.726	8.010
37	2029.35	2318.46	3.7392	53.166	8.309
38	2091.51	2402.24	3.9002	52.563	8.611
39	2143.87	2492.01	4.1688	51.562	8.908
40	2200.24	2578.59	4.3782	50.911	9.209
41	2254.35	2666.79	4.6063	50.170	9.510
42	2305.78	2753.14	4.8323	49.266	9.809
43	2354.50	2839.71	5.0698	48.875	10.108
44	2440.92	2954.13	5.2376	48.005	10.508
45	2505.67	3073.20	5.5504	47.293	10.909
46	2570.63	3185.61	5.8132	46.219	11.308
47	2629.74	3299.21	6.1042	45.356	11.707
48	2685.53	3411.48	6.3951	44.138	12.107
49	2745.00	3522.81	6.6529	43.109	12.510
50	2810.56	3631.55	6.8601	41.988	12.909
51	2851.33	3743.30	7.1901	40.930	13.307
52	2896.23	3878.73	7.5957	39.323	13.806
53	2942.63	4008.44	7.9557	37.910	14.306
54	2967.49	4139.43	8.3994	36.226	14.808
55	3015.03	4261.21	8.6994	35.079	15.307

Table A–5. Deformation J_{IC} and J–R curve results for specimen PWCE–04

Test Number	: 0129	Test Temp	: 25˚C
Material Type	: Weld Metal	Heat Number	: PWCE
Aging Temp	: 400˚C	Aging Time	: 10,000 h
Thickness	: 25.37 mm	Net Thickness	: 20.29 mm
Width	: 50.80 mm	Flow Stress	: 538.00 MPa
Modulus E	: 207.57 GPa	(Effective)	
Modulus E	: 193.10 GPa	(Nominal)	
Init. Crack	: 27.9156 mm	Init. a/w	: 0.5495 (Measured)
Final Crack	: 36.7875 mm	Final a/w	: 0.7242 (Measured)
Final Crack	: 36.6151 mm	Final a/w	: 0.7208 (Compliance)
Linear Fit	**$J = B + M(\Delta a)$**		
Intercept B	: 371.765 kJ/m^2	Slope M	: 540.66 kJ/m^3
Fit Coeff. R	: 0.9830	(13 Data Points)	
J_{IC}	: 496.5 kJ/m^2	(2835.1 in.-lb/in.^{2})	
Δa (J_{IC})	: 0.231 mm	(0.0091 in.)	
T average	: 387.7	(J_{IC} at 0.15)	
Power–Law Fit	**$J = C(\Delta a)^n$**		
Coeff. C	: 920.22 kJ/m^2	Exponent n	: 0.6311
Fit Coeff. R	: 0.9839	(13 Data Points)	
J_{IC}(0.20)	: 566.0 kJ/m^2	(3232.2 in.-lb/in.^{2})	
Δa (J_{IC})	: 0.463 mm	(0.0182 in.)	
T average	: 383.8	(J_{IC} at 0.20)	
J_{IC}(0.15)	: 502.6 kJ/m^2	(2870.0 in.-lb/in.^{2})	
Δa (J_{IC})	: 0.384 mm	(0.0151 in.)	
T average	: 389.9	(J_{IC} at 0.15)	
K_{jc}	: 560.8 MPa–$m^{0.5}$		

J_{IC} Validity & Data Qualification (E 813–85)

J_{max} allowed	: 820.79 kJ/m^2	($J_{max} = b_o \sigma_f/15$)
Data Limit	: J_{max} Ignored	
Δa (max) allowed	: 2.204 mm	(at 1.5 exclusion line)
Data Limit	: 1.5 Exclusion line	
Data Points	: Zone A = 3	Zone B = 4
Data Point Spacing	: OK	
B_{net} or b_o size	: Inadequate	
dJ/da at J_{IC}	: OK	
a_o Measurement	: 2, 3, 7, & 8 Outside Limit	
Final crack shape	: OK	
Crack size estimate	: OK	(by Compliance)
E Effective	: OK	
J_{IC} Estimate	: Invalid	

J–R curve Validity & Data Qualification (E 1152–86)

J_{max} allowed	: 545.72 kJ/m^2	($J_{max} = B_{net}\ \sigma_f/20$)
Δa (max) allowed	: 2.288 mm	($\Delta a = 0.1b_o$)
Δa (max) allowed	: 5.694 mm	($\omega = 5$)
Data Points	: Zone A = 23	Zone B = 4
Data Point Spacing	: Inadequate	
J-R Curve Data	: Invalid	

Table A–6. Modified J_{IC} and J–R curve results for specimen PWCE–04

Linear Fit	**$J = B + M(\Delta a)$**		
Intercept B	: 336.028 kJ/m^2	Slope M	: 604.26 kJ/m^3
Fit Coeff. R	: 0.9862	(13 Data Points)	
J_{IC}	: 467.2 kJ/m^2	(2667.9 in.-lb/in.^{2})	
Δa (J_{IC})	: 0.217 mm	(0.0085 in.)	
T average	: 433.3	(J_{IC} at 0.15)	
Power–Law Fit	**$J = C(\Delta a)^n$**		
Coeff. C	: 948.65 kJ/m^2	Exponent n	: 0.6756
Fit Coeff. R	: 0.9865	(13 Data Points)	
J_{IC}(0.20)	: 562.6 kJ/m^2	(3212.3 in.-lb/in.^{2})	
Δa (J_{IC})	: 0.461 mm	(0.0182 in.)	
T average	: 424.6	(J_{IC} at 0.20)	
J_{IC}(0.15)	: 492.4 kJ/m^2	(2811.4 in.-lb/in.^{2})	
Δa (J_{IC})	: 0.379 mm	(0.0149 in.)	
T average	: 430.6	(J_{IC} at 0.15)	
K_{jc}	: 585.0 MPa–m$^{0.5}$		

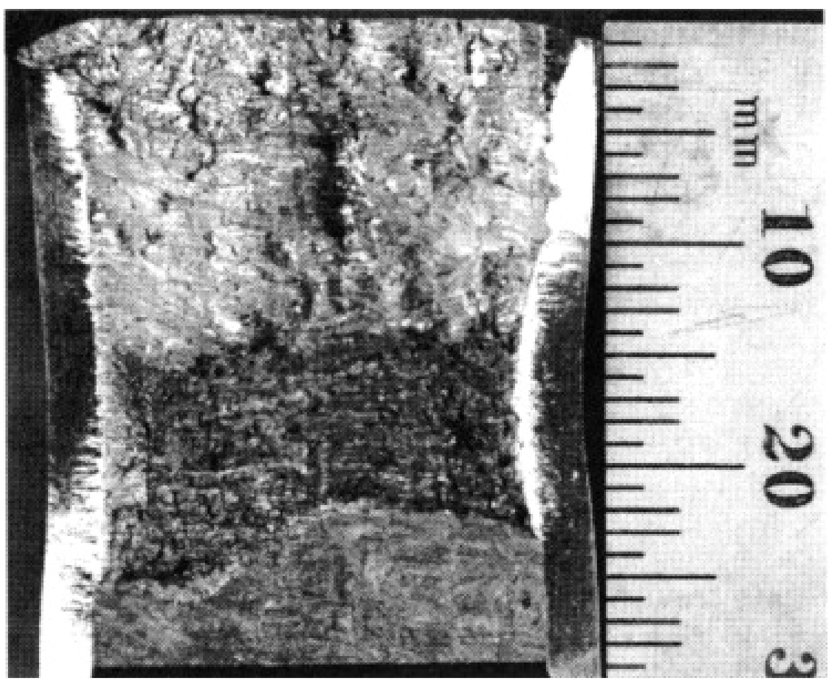

Figure A–4. Fracture surface of aged weld metal PWCE tested at 25°C

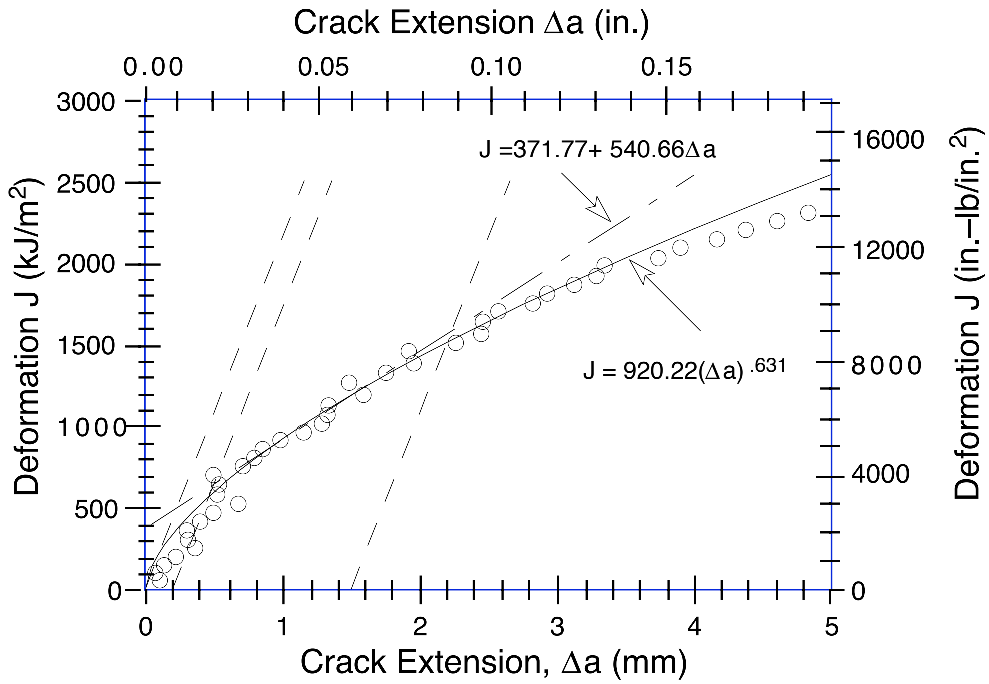

Figure A–5. Deformation J–R curve for weld metal specimen PWCE–04 aged at 400°C for 10,000 h and tested at 25°C. Blunting, 0.2–mm offset, and 1.5–mm offset lines are shown as dashed lines.

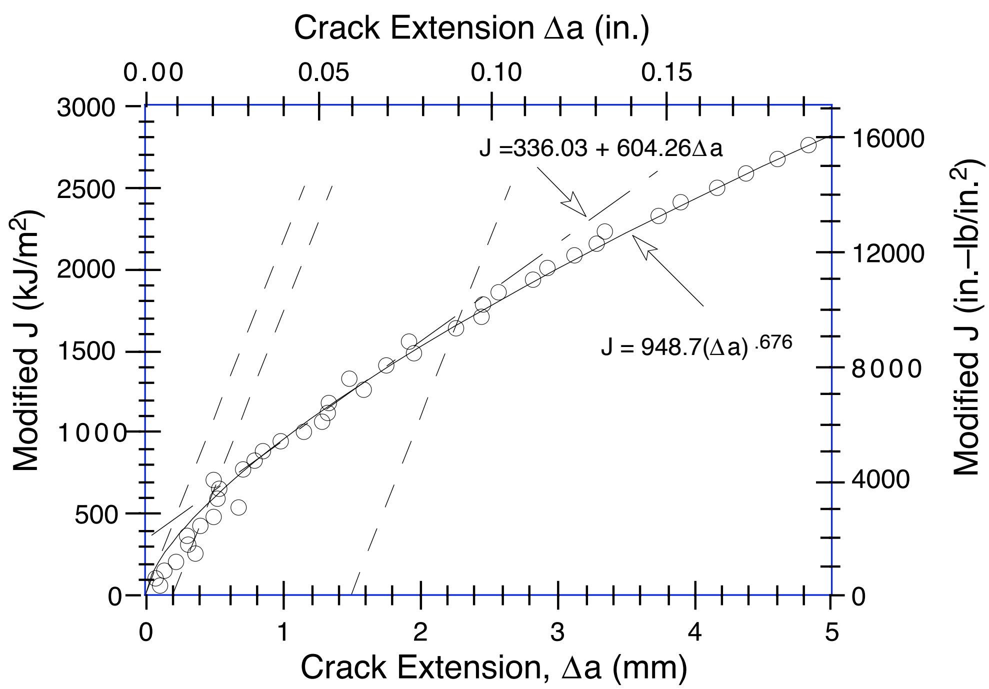

Figure A–6. Modified J–R curve for weld metal specimen PWCE–04 aged at 400°C for 10,000 h and tested at 25°C. Blunting, 0.2–mm offset, and 1.5–mm offset lines are shown as dashed lines.

Table A–7. Test data for specimen PWCE–01

Test Number	: 0123	Test Temp	: 290˚C
Material Type	: Weld Metal	Heat Number	: PWCE
Aging Temp	: Unaged	Aging Time	: –
Thickness	: 25.35 mm	Net Thickness	: 20.23 mm
Width	: 50.81 mm	Flow Stress	: 373.00 MPa

Unload Number	J_d (kJ/m^2)	J_m (kJ/m^2)	Δa (mm)	Load (kN)	Deflection (mm)
1	12.83	12.81	-0.1801	20.644	0.251
2	37.25	37.52	0.1993	30.462	0.439
3	61.29	61.62	0.2326	35.392	0.603
4	87.70	87.93	0.2021	38.210	0.754
5	126.10	125.84	0.1014	40.378	0.955
6	177.86	179.53	0.3499	41.933	1.209
7	238.23	236.54	0.0504	43.008	1.508
8	322.42	328.92	0.5599	43.798	1.907
9	407.13	406.81	0.2347	44.160	2.307
10	490.72	502.15	0.6859	44.638	2.707
11	568.31	588.66	0.9751	44.736	3.106
12	635.35	651.68	0.8596	44.684	3.408
13	762.11	790.63	1.1449	44.379	4.007
14	816.01	857.48	1.4240	44.091	4.309
15	874.14	922.90	1.5692	43.745	4.608
16	933.05	992.24	1.7619	43.685	4.915
17	996.51	1057.48	1.7925	43.150	5.213
18	1057.56	1124.85	1.8940	42.565	5.511
19	1111.88	1192.11	2.0899	42.117	5.810
20	1157.57	1260.04	2.4092	41.654	6.114
21	1203.04	1323.50	2.6550	41.250	6.407
22	1266.45	1387.58	2.6637	40.786	6.710
23	1291.86	1456.96	3.2106	40.198	7.002
24	1357.35	1515.39	3.1271	39.708	7.309
25	1396.36	1586.23	3.4879	39.192	7.609
26	1443.52	1648.33	3.6503	38.738	7.909
27	1504.17	1711.50	3.6766	38.164	8.210
28	1567.96	1800.27	3.9228	37.593	8.609
29	1621.83	1886.05	4.2228	36.760	9.012
30	1712.17	1988.23	4.3275	36.152	9.509
31	1795.79	2116.11	4.6941	34.843	10.108
32	1883.58	2236.71	4.9499	34.106	10.707
33	1949.08	2381.69	5.5332	32.721	11.409
34	2027.78	2516.87	5.9239	31.415	12.108
35	2071.46	2654.72	6.5429	29.993	12.808
36	2149.20	2784.49	6.8670	29.065	13.511
37	2226.28	2917.01	7.1945	28.289	14.207
38	2306.57	3049.09	7.4851	27.281	14.911

Table A–8. Deformation J_{IC} and J–R curve results for specimen PWCE–01

Test Number	: 0123	Test Temp	: 290°C
Material Type	: Weld Metal	Heat Number	: PWCE
Aging Temp	: Unaged	Aging Time	: –
Thickness	: 25.35 mm	Net Thickness	: 20.23 mm
Width	: 50.81 mm	Flow Stress	: 373.00 MPa
Modulus E	: 175.41 GPa	(Effective)	
Modulus E	: 180.00 GPa	(Nominal)	
Init. Crack	: 27.8406 mm	Init. a/w	: 0.5479 (Measured)
Final Crack	: 36.3125 mm	Final a/w	: 0.7147 (Measured)
Final Crack	: 35.3257 mm	Final a/w	: 0.6953 (Compliance)
Linear Fit	**$J = B + M(\Delta a)$**		
Intercept B	: 213.964 kJ/m^2	Slope M	: 430.09 kJ/m^3
Fit Coeff. R	: 0.9833	(10 Data Points)	
J_{IC}	: 300.6 kJ/m^2	(1716.6 in.-lb/in.^{2})	
Δa (J_{IC})	: 0.201 mm	(0.0079 in.)	
T average	: 542.3	(J_{IC} at 0.15)	
Power Fit Law	**$J = C(\Delta a)^n$**		
Coeff. C	: 648.82 kJ/m^2	Exponent n	: 0.7127
Fit Coeff. R	: 0.9783	(10 Data Points)	
J_{IC}(0.20)	: 363.6 kJ/m^2	(2076.1 in.-lb/in.^{2})	
Δa (J_{IC})	: 0.444 mm	(0.0175 in.)	
T average	: 543.7	(J_{IC} at 0.20)	
J_{IC}(0.15)	: 313.2 kJ/m^2	(1788.5 in.-lb/in.^{2})	
Δa (J_{IC})	: 0.360 mm	(0.0142 in.)	
T average	: 550.7	(J_{IC} at 0.15)	
K_{jc}	: 452.8 MPa–m$^{0.5}$		
J_{IC} Validity & Data Qualification (E813-85)			
J_{max} allowed	: 571.17 kJ/m^2	($J_{max} = b_o\sigma_f/15$)	
Data Limit	: J_{max} Ignored		
Δa (max) allowed	: 2.283 mm	(at 1.5 exclusion line)	
Data Limit	: 1.5 Exclusion line		
Data Points	: Zone A = 2	Zone B = 4	
Data Point Spacing	: OK		
B_{net} or b_o size	: Inadequate		
dJ/da at J_{IC}	: OK		
a_f Measurement	: Near-surface	Outside Limit	
Initial crack shape	: OK		
Crack size estimate	: Inadequate	(by Compliance)	
E Effective	: OK		
J_{IC} Estimate	: Invalid		
J–R curve Validity & Data Qualification (E 1152–86)			
J_{max} allowed	: 377.21 kJ/m^2	($J_{max} = b_{net}\,\sigma_f/20$)	
Δa (max) allowed	: 2.297 mm	($\Delta a = 0.1b_o$)	
Δa (max) allowed	: 6.339 mm	($\omega = 5$)	
Data Points	: Zone A = 15	Zone B = 3	
Data Point Spacing	: Inadequate		
J-R Curve Data	: Invalid		

Table A–9. Modified J_{IC} and J–R curve results for specimen PWCE–01

Linear Fit	**$J = B + M(\Delta a)$**		
Intercept B	: 187.921 kJ/m^2	Slope M	: 479.05 kJ/m^3
Fit Coeff. R	: 0.9864	(10 Data Points)	
J_{IC}	: 276.8 kJ/m^2	(1580.5 in.-lb/in.^{2})	
Δa (J_{IC})	: 0.186 mm	(0.0073 in.)	
T average	: 604.0	(J_{IC} at 0.15)	
Power–Law Fit	**$J = C(\Delta a)^n$**		
Coeff. C	: 671.99 kJ/m^2	Exponent n	: 0.7558
Fit Coeff. R	: 0.9816	(10 Data Points)	
J_{IC}(0.20)	: 363.6 kJ/m^2	(2076.2 in.-lb/in.^{2})	
Δa (J_{IC})	: 0.444 mm	(0.0175 in.)	
T average	: 599.2	(J_{IC} at 0.20)	
J_{IC}(0.15)	: 308.2 kJ/m^2	(1760.0 in.-lb/in.^{2})	
Δa (J_{IC})	: 0.357 mm	(0.0140 in.)	
T average	: 605.8	(J_{IC} at 0.15)	
K_{jc}	: 475.1 MPa–m$^{0.5}$		

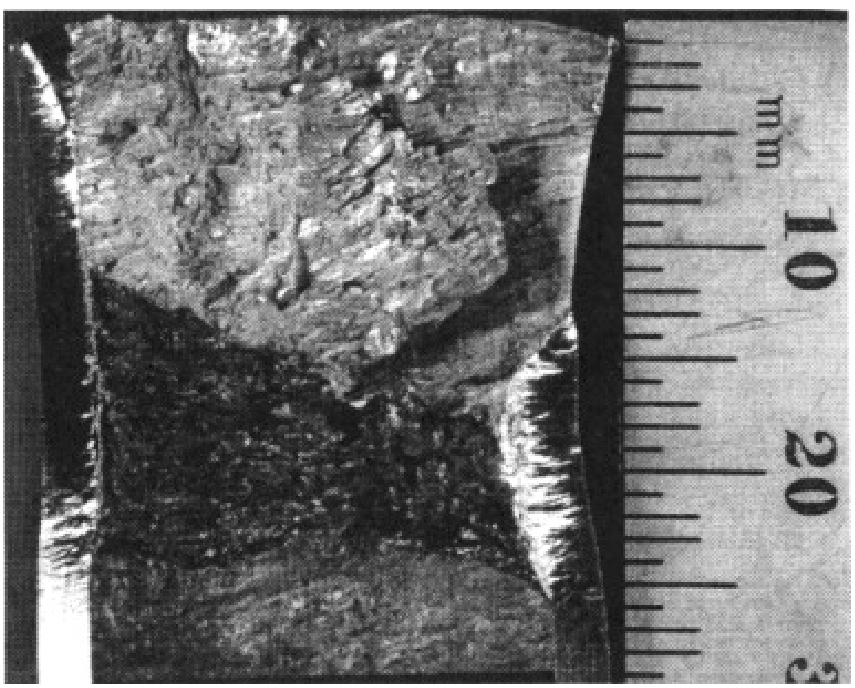

Figure A–7. Fracture surface of unaged weld metal PWCE tested at 290°C

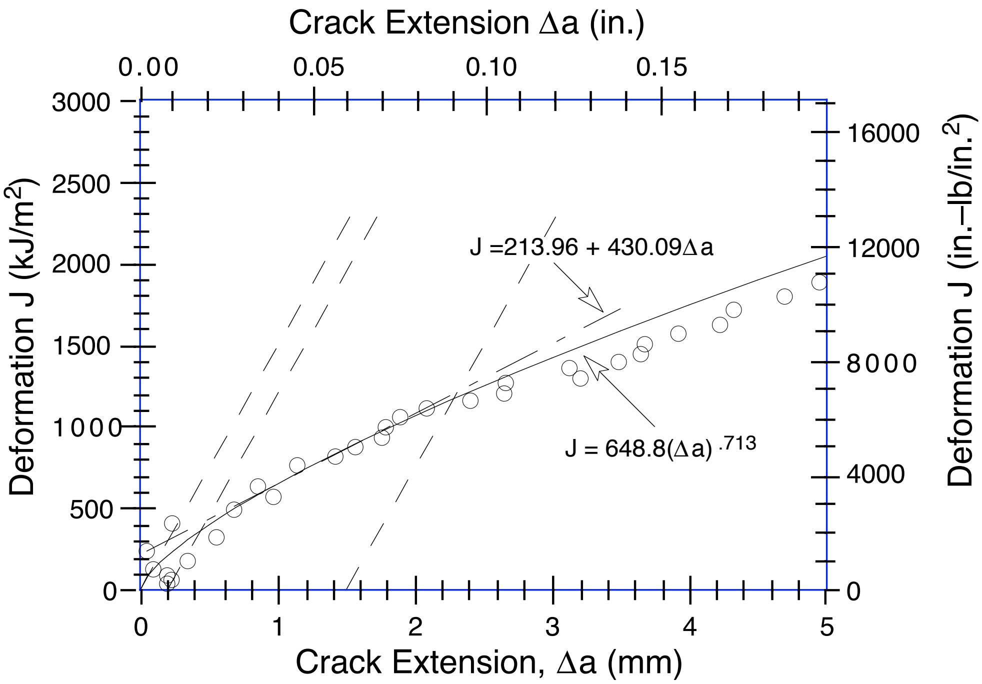

Figure A–8. Deformation J–R curve for unaged weld metal specimen PWCE–01 tested at 290°C. Blunting, 0.2–mm offset, and 1.5–mm offset lines are shown as dashed lines.

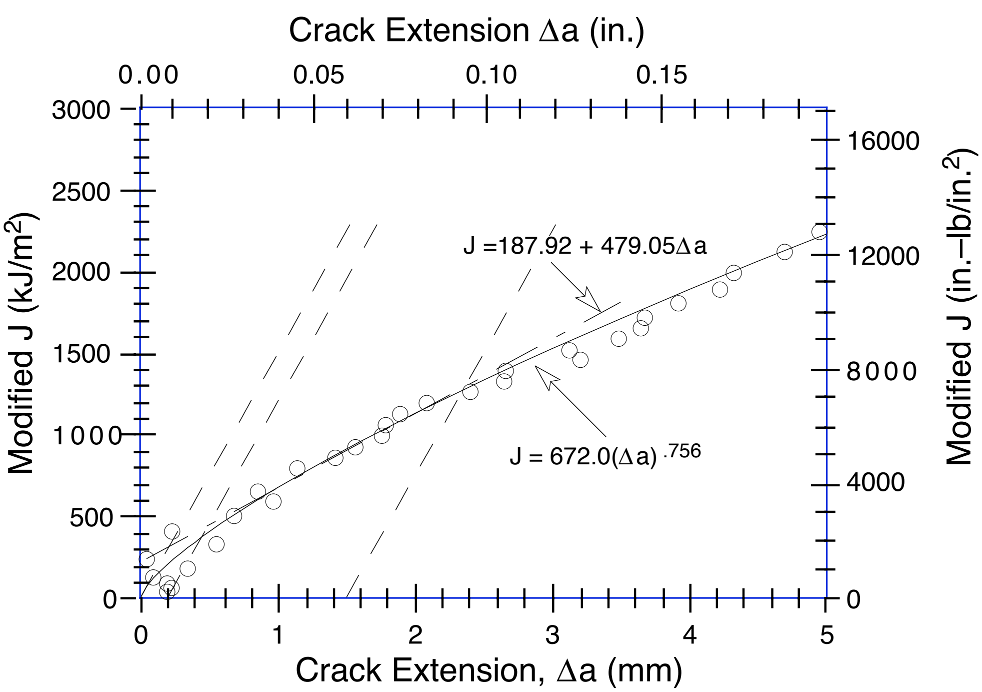

Figure A–9. Modified J–R curve for unaged weld metal specimen PWCE–01 tested at 290°C. Blunting, 0.2–mm offset, and 1.5–mm offset lines are shown as dashed lines.

Table A–10. Test data for specimen PWCE–03

Test Number	: 0127	Test Temp	: 290°C
Material Type	: Weld Metal	Heat Number	: PWCE
Aging Temp	: 400°C	Aging Time	: 10,000 h
Thickness	: 25.35 mm	Net Thickness	: 20.26 mm
Width	: 50.82 mm	Flow Stress	: 406.00 MPa

Unload Number	J_d (kJ/m^2)	J_m (kJ/m^2)	Δa (mm)	Load (kN)	Deflection (mm)
1	13.29	13.26	-0.2959	21.718	0.252
2	48.82	49.04	-0.0594	34.743	0.503
3	92.42	92.59	-0.0738	40.085	0.755
4	142.70	143.64	0.0613	42.514	1.006
5	203.93	204.99	0.0748	44.024	1.305
6	268.19	270.91	0.2063	44.840	1.606
7	340.56	346.12	0.3738	45.440	1.946
8	384.47	392.79	0.5157	45.613	2.157
9	418.08	427.09	0.5480	45.984	2.315
10	461.11	470.04	0.5447	45.862	2.505
11	526.21	541.32	0.7650	45.508	2.809
12	586.62	609.83	1.0197	45.358	3.112
13	649.24	675.58	1.1072	45.006	3.410
14	715.39	743.40	1.1491	44.861	3.711
15	769.56	814.16	1.5298	44.556	4.008
16	831.39	878.96	1.5925	43.992	4.312
17	878.66	951.43	2.0852	43.519	4.612
18	938.35	1013.63	2.1308	42.737	4.916
19	987.24	1082.53	2.4709	42.248	5.208
20	1035.47	1148.47	2.7541	41.333	5.510
21	1094.81	1211.85	2.8147	40.599	5.810
22	1131.50	1282.96	3.3051	39.741	6.114
23	1187.67	1340.28	3.3208	38.887	6.410
24	1215.85	1410.90	3.8681	37.802	6.712
25	1254.21	1469.43	4.1176	37.194	7.011
26	1305.12	1555.82	4.5313	36.101	7.412
27	1356.82	1635.95	4.8448	34.645	7.807
28	1398.49	1719.30	5.2817	33.541	8.212
29	1448.15	1795.89	5.5504	32.323	8.609
30	1488.61	1875.12	5.9200	31.525	9.006
31	1528.97	1952.44	6.2572	30.453	9.408
32	1554.22	2028.49	6.7030	29.254	9.806
33	1584.47	2101.34	7.0628	28.037	10.208
34	1614.20	2174.19	7.4134	26.958	10.609
35	1641.89	2245.24	7.7533	25.676	11.010
36	1668.64	2331.92	8.2042	24.637	11.503
37	1684.56	2422.65	8.7445	23.133	12.038
38	1692.95	2497.17	9.2065	21.699	12.506
39	1696.54	2576.25	9.7165	20.460	13.010
40	1722.21	2650.89	10.0356	19.644	13.510
41	1736.13	2727.87	10.4324	18.589	14.007
42	1752.21	2801.71	10.7837	17.719	14.510
43	1771.22	2873.68	11.0952	16.820	15.008

Table A–11. Deformation J_{IC} and J–R curve results for specimen PWCE–03

Test Number	: 0127	Test Temp	: 290˚C
Material Type	: Weld Metal	Heat Number	: PWCE
Aging Temp	: 400˚C	Aging Time	: 10,000 h
Thickness	: 25.35 mm	Net Thickness	: 20.26 mm
Width	: 50.82 mm	Flow Stress	: 406.00 MPa
Modulus E	: 173.53 GPa	(Effective)	
Modulus E	: 180.00 GPa	(Nominal)	
Init. Crack	: 27.8656 mm	Init. a/w	: 0.5483 (Measured)
Final Crack	: 40.1281 mm	Final a/w	: 0.7896 (Measured)
Final Crack	: 38.9608 mm	Final a/w	: 0.7667 (Compliance)
Linear Fit	**$J = B + M(\Delta a)$**		
Intercept B	: 224.977 kJ/m^2	Slope M	: 378.19 kJ/m^3
Fit Coeff. R	: 0.9815	(9 Data Points)	
J_{IC}	: 293.3 kJ/m^2	(1674.6 in.-lb/in.^{2})	
Δa (J_{IC})	: 0.181 mm	(0.0071 in.)	
T average	: 398.1	(J_{IC} at 0.15)	
Power–Law Fit	**$J = C(\Delta a)^n$**		
Coeff. C	: 614.21 kJ/m^2	Exponent n	: 0.6113
Fit Coeff. R	: 0.9824	(9 Data Points)	
J_{IC}(0.20)	: 363.4 kJ/m^2	(2075.1 in.-lb/in.^{2})	
Δa (J_{IC})	: 0.424 mm	(0.0167 in.)	
T average	: 371.4	(J_{IC} at 0.20)	
J_{IC}(0.15)	: 322.5 kJ/m^2	(1841.6 in.-lb/in.^{2})	
Δa (J_{IC})	: 0.349 mm	(0.0137 in.)	
T average	: 377.7	(J_{IC} at 0.15)	
K_{jc}	: 409.2 MPa–$m^{0.5}$		
J_{IC} Validity & Data Qualification (E 813–85)			
J_{max} allowed	: 621.24 kJ/m^2	($J_{max} = b_o \sigma_f/15$)	
Data Limit	: J_{max} Ignored		
Δa (max) allowed	: 2.094 mm	(at 1.5 exclusion line)	
Data Limit	: 1.5 Exclusion line		
Data Points	: Zone A = 4	Zone B = 2	
Data Point Spacing	: OK		
B_{net} or b_o size	: OK		
dJ/da at J_{IC})	: OK		
a_f Measurement	: Near-surface	Outside Limit	
Initial crack shape	: OK		
Crack size estimate	: Inadequate	(by Compliance)	
E Effective	: OK		
J_{IC} Estimate	: Invalid		
J–R curve Validity & Data Qualification (E 1152–86)			
J_{max} allowed	: 411.26 kJ/m^2	($J_{max} = B_{net}\ \sigma_f/20$)	
Δa (max) allowed	: 2.295 mm	($\Delta a = 0.1 b_o$)	
Δa (max) allowed	: 5.536 mm	($\omega = 5$)	
Data Points	: Zone A = 11	Zone B = 4	
Data Point Spacing	: Inadequate		
J-R Curve Data	: Invalid		

Table A–12. Modified J_{IC} and J–R curve results for specimen PWCE–03

Linear Fit	**$J = B + M(\Delta a)$**		
Intercept B	: 255.972 kJ/m^2	Slope M	: 363.36 kJ/m^3
Fit Coeff. R	: 0.9778	(10 Data Points)	
J_{IC}	: 329.8 kJ/m^2	(1882.9 in.-lb/in.^{2})	
Δa (J_{IC})	: 0.203 mm	(0.0080 in.)	
T average	: 382.5	(J_{IC} at 0.15)	
Power–Law Fit	**$J = C(\Delta a)^n$**		
Coeff. C	: 633.49 kJ/m^2	Exponent n	: 0.6172
Fit Coeff. R	: 0.9864	(10 Data Points)	
J_{IC}(0.20)	: 377.7 kJ/m^2	(2156.5 in.-lb/in.^{2})	
Δa (J_{IC})	: 0.433 mm	(0.0170 in.)	
T average	: 384.9	(J_{IC} at 0.20)	
J_{IC}(0.15)	: 335.1 kJ/m^2	(1913.3 in.-lb/in.^{2})	
Δa (J_{IC})	: 0.356 mm	(0.0140 in.)	
T average	: 391.4	(J_{IC} at 0.15)	
K_{jc}	: 418.1 MPa–m$^{0.5}$		

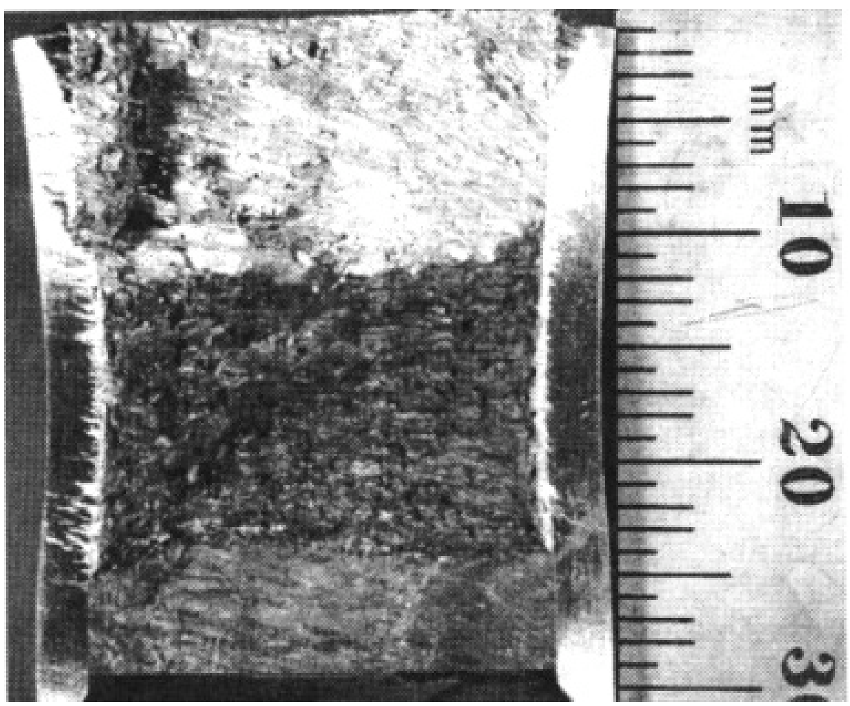

Figure A–10. Fracture surface of aged weld metal PWCE tested at 290°C

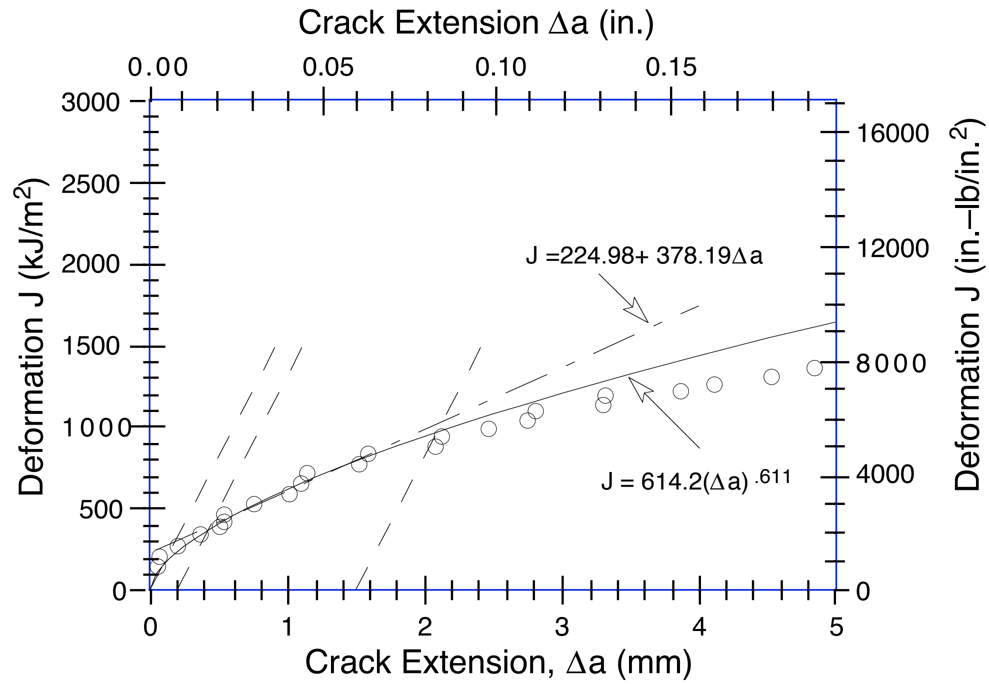

Figure A–11. Deformation J–R curve for weld metal specimen PWCE–03 aged at 400°C for 10,000 h and tested at 290°C. Blunting, 0.2–mm offset, and 1.5–mm offset lines are shown as dashed lines.

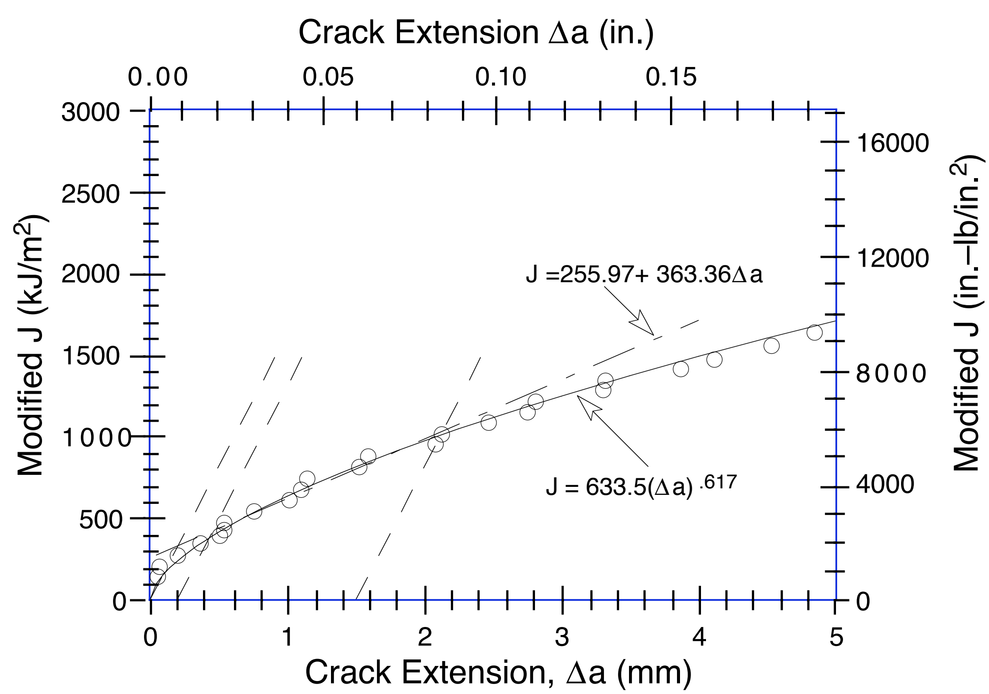

Figure A–12. Modified J–R curve for weld metal specimen PWCE–03 aged at 400°C for 10,000 h and tested at 290°C. Blunting, 0.2–mm offset, and 1.5–mm offset lines are shown as dashed lines.

Table A–13. Test data for specimen PWWO–03

Test Number	: 0131	Test Temp	: 25°C
Material Type	: Weld Metal	Heat Number	: PWWO
Aging Temp	: 400°C	Aging Time	: 7,700 h
Thickness	: 22.84 mm	Net Thickness	: 18.24 mm
Width	: 50.76 mm	Flow Stress	: 549.00 MPa

Unload Number	J_d (kJ/m^2)	J_m (kJ/m^2)	Δa (mm)	Load (kN)	Deflection (mm)
1	14.72	14.71	-0.1327	22.208	0.251
2	54.82	54.89	-0.0506	37.282	0.501
3	121.93	122.42	0.0628	45.593	0.804
4	197.25	199.04	0.2348	48.740	1.105
5	248.49	251.71	0.3722	49.830	1.307
6	301.06	304.73	0.4053	50.334	1.508
7	355.13	361.66	0.5785	50.803	1.708
8	408.54	414.43	0.5465	50.841	1.909
9	462.44	474.26	0.8048	50.723	2.109
10	511.68	528.21	0.9859	50.696	2.308
11	562.26	583.59	1.1511	50.674	2.508
12	611.13	641.88	1.4423	49.896	2.710
13	656.37	697.14	1.7259	49.328	2.911
14	704.03	749.75	1.8546	48.782	3.109
15	750.58	807.86	2.1310	48.012	3.310
16	794.30	860.69	2.3343	47.476	3.508
17	837.91	916.55	2.5895	46.807	3.709
18	881.75	970.78	2.7923	45.981	3.912
19	922.61	1024.84	3.0348	44.773	4.111
20	960.36	1076.86	3.2832	44.133	4.307
21	996.69	1130.87	3.5756	43.191	4.510
22	1038.55	1196.72	3.9496	42.042	4.759
23	1078.32	1259.91	4.2944	40.692	5.009
24	1118.11	1322.82	4.6170	39.197	5.260
25	1155.41	1383.87	4.9324	38.266	5.507
26	1188.08	1446.55	5.3128	36.947	5.759
27	1217.23	1504.98	5.6683	35.671	6.007
28	1250.15	1577.64	6.1262	33.694	6.308
29	1276.82	1644.22	6.5668	32.460	6.606
30	1308.24	1710.28	6.9322	31.030	6.909
31	1336.65	1775.83	7.3079	29.969	7.207
32	1361.38	1839.87	7.6895	28.553	7.506
33	1381.79	1902.79	8.0875	27.549	7.806
34	1415.11	1962.18	8.3221	26.465	8.107
35	1441.41	2049.61	8.8452	24.941	8.508
36	1461.70	2123.18	9.2825	23.576	8.898
37	1485.33	2200.96	9.7080	22.275	9.307
38	1512.30	2272.98	10.0476	21.246	9.704
39	1536.51	2347.13	10.4091	20.376	10.108
40	1565.06	2437.82	10.8374	19.166	10.606

Table A–14. Deformation J_{IC} and J–R curve results for specimen PWWO–03

Test Number	: 0131	Test Temp	: 25°C
Material Type	: Weld Metal	Heat Number	: PWWO
Aging Temp	: 400°C	Aging Time	: 7,700 h
Thickness	: 22.84 mm	Net Thickness	: 18.24 mm
Width	: 50.76 mm	Flow Stress	: 549.00 MPa
Modulus E	: 195.44 GPa	(Effective)	
Modulus E	: 193.10 GPa	(Nominal)	
Init. Crack	: 27.8219 mm	Init. a/w	: 0.5481 (Measured)
Final Crack	: 39.2563 mm	Final a/w	: 0.7734 (Measured)
Final Crack	: 39.0582 mm	Final a/w	: 0.7695 (Compliance)

Linear Fit	**$J = B + M(\Delta a)$**		
Intercept B	: 203.177 kJ/m^2	Slope M	: 285.61 kJ/m^3
Fit Coeff. R	: 0.9654	(9 Data Points)	
J_{IC}	: 233.6 kJ/m^2	(1333.6 in–lb/in^2)	
Δa (J_{IC})	: 0.106 mm	(0.0042 in.)	
T average	: 185.2	(J_{IC} at 0.15)	

Power–Law Fit	**$J = C(\Delta a)^n$**		
Coeff. C	: 504.96 kJ/m^2	Exponent n	: 0.5871
Fit Coeff. R	: 0.9741	(9 Data Points)	
$J_{IC}(0.20)$	: 257.3 kJ/m^2	(1469.4 in–lb/in^2)	
Δa (J_{IC})	: 0.317 mm	(0.0125 in.)	
T average	: 193.2	(J_{IC} at 0.20)	
$J_{IC}(0.15)$	: 225.1 kJ/m^2	(1285.2 in–lb/in^2)	
Δa (J_{IC})	: 0.252 mm	(0.0099 in.)	
T average	: 196.9	(J_{IC} at 0.15)	
K_{jc}	: 375.0 MPa–$m^{0.5}$		

J_{IC} Validity & Data Qualification (E 813–85)		
J_{max} allowed	: 839.50 kJ/m^2	($J_{max} = b_o \sigma_f/15$)
Data Limit	: J_{max}	Ignored
Δa (max) allowed	: 1.828 mm	(at 1.5 exclusion line)
Data Limit	: 1.5 Exclusion line	
Data Points	: Zone A = 4	Zone B = 2
Data point spacing	: OK	
B_{net} and b_o size	: OK	
dJ/da at J_{IC}	: OK	
a_f Measurement	: Near-surface	outside limit
Initial crack shape	: OK	
Crack size estimate	: OK	(by Compliance)
E Effective	: OK	
J_{IC} Estimate	: Invalid	

J–R curve Validity & Data Qualification (E 1152–86)		
J_{max} allowed	: 500.61 kJ/m^2	($J_{max} = B_{net}\, \sigma_f/20$)
Δa (max) allowed	: 2.294 mm	($\Delta a = 0.1 b_o$)
Δa (max) allowed	: 5.334 mm	($\omega = 5$)
Data Points	: Zone A = 4	Zone B = 9
Data point spacing	: OK	
J-R Curve Data	: Invalid	

Table A–15. Modified J_{IC} and J–R curve results for specimen PWWO–03

Linear Fit	**$J = B + M(\Delta a)$**		
Intercept B	: 194.312 kJ/m^2	Slope M	: 313.11 kJ/m^3
Fit Coeff. R	: 0.9728	(9 Data Points)	
J_{IC}	: 226.6 kJ/m^2	(1294.1 in–lb/in^2)	
Δa (J_{IC})	: 0.103 mm	(0.0041 in.)	
T average	: 203.0	(J_{IC} at 0.15)	
Power–Law Fit	**$J = C(\Delta a)^n$**		
Coeff. C	: 523.69 kJ/m^2	Exponent n	: 0.6171
Fit Coeff. R	: 0.9785	(9 Data Points)	
J_{IC}(0.20)	: 258.0 kJ/m^2	(1473.0 in–lb/in^2)	
Δa (J_{IC})	: 0.317 mm	(0.0125 in.)	
T average	: 209.7	(J_{IC} at 0.20)	
J_{IC}(0.15)	: 223.6 kJ/m^2	(1276.8 in–lb/in^2)	
Δa (J_{IC})	: 0.252 mm	(0.0099 in.)	
T average	: 213.4	(J_{IC} at 0.15)	
K_{jc}	: 386.7 MPa–m$^{0.5}$		

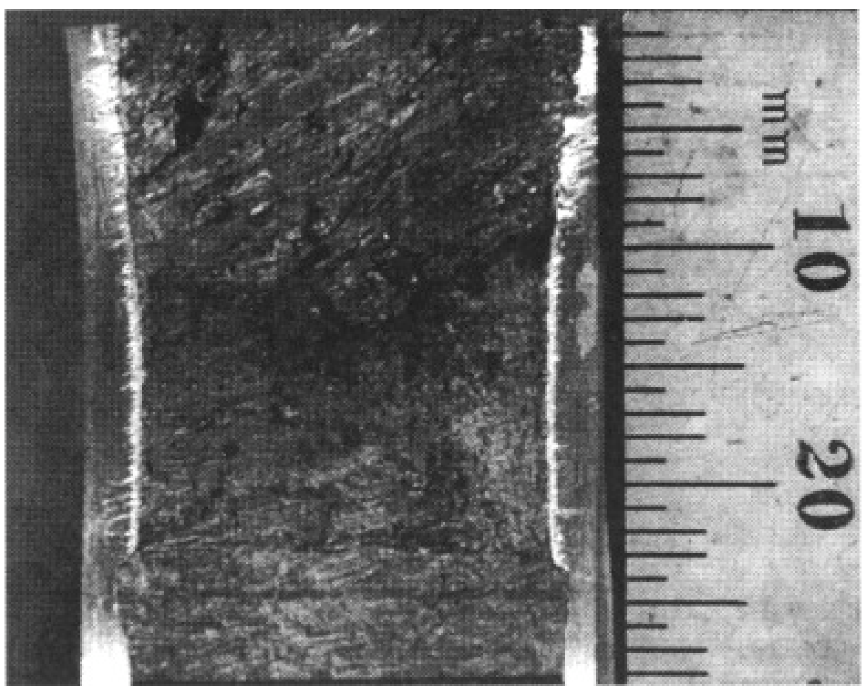

Figure A–13. Fracture surface of aged weld metal PWWO tested at 25°C

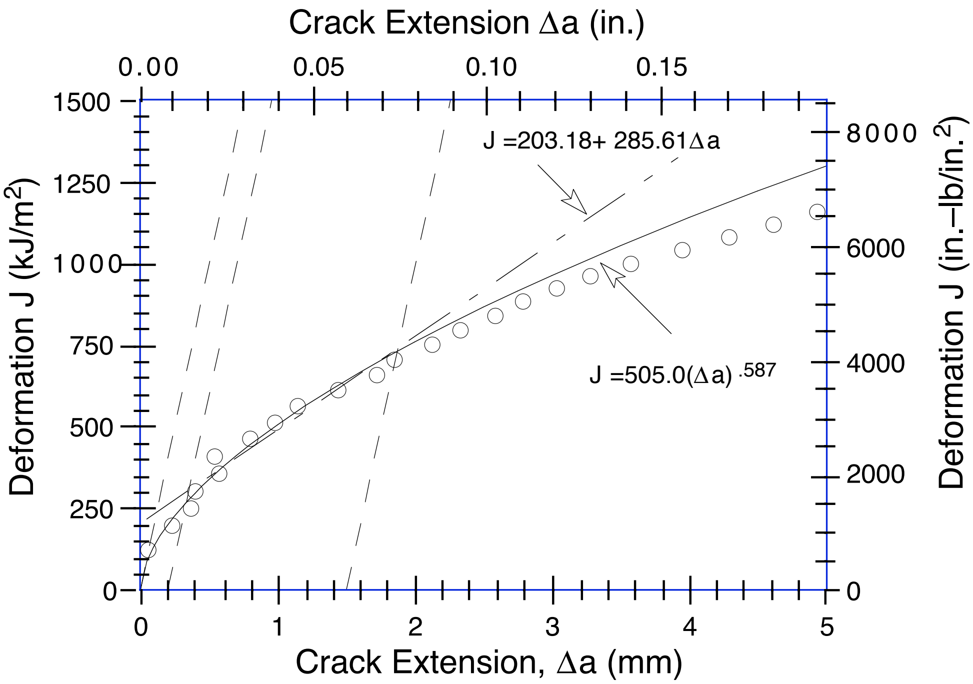

Figure A–14. Deformation J–R curve for weld metal specimen PWWO–03 aged at 400°C for 7,700 h and tested at 25°C. Blunting, 0.2–mm offset, and 1.5–mm offset lines are shown as dashed lines.

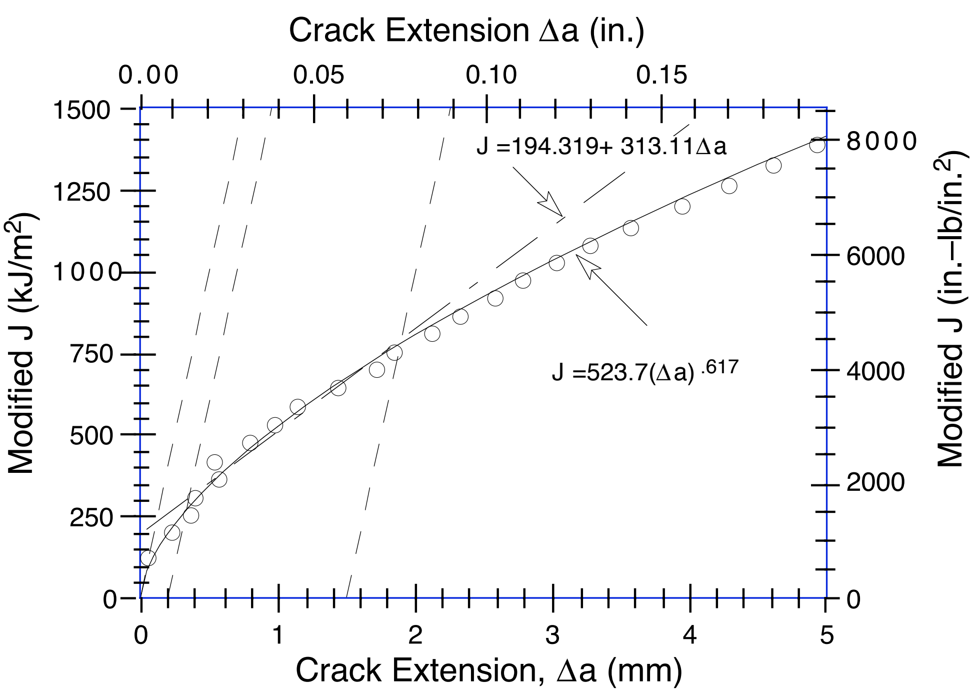

Figure A–15. Modified J–R curve for weld metal specimen PWWO–03 aged at 400°C for 7,700 h and tested at 25°C. Blunting, 0.2–mm offset, and 1.5–mm offset lines are shown as dashed lines.

Table A–16. Test data for specimen PWWO–01

Test Number	: 0130	Test Temp	: 290˚C
Material Type	: Weld Metal	Heat Number	: PWWO
Aging Temp	: Unaged	Aging Time	: –
Thickness	: 22.80 mm	Net Thickness	: 18.25 mm
Width	: 50.77 mm	Flow Stress	: 398.00 MPa

Unload Number	J_d (kJ/m^2)	J_m (kJ/m^2)	Δa (mm)	Load (kN)	Deflection (mm)
1	11.31	11.31	-0.1395	16.399	0.252
2	42.48	42.71	0.1499	27.040	0.503
3	72.94	72.92	0.0260	31.755	0.704
4	111.34	111.56	0.0861	34.229	0.905
5	150.67	151.20	0.1372	35.577	1.107
6	190.78	192.75	0.3069	36.325	1.307
7	230.55	232.69	0.3223	36.468	1.508
8	271.78	273.85	0.3170	36.555	1.707
9	311.93	318.20	0.5812	36.638	1.906
10	350.21	359.05	0.7222	36.527	2.109
11	387.03	402.51	1.0406	35.650	2.309
12	422.93	441.00	1.1521	35.176	2.507
13	459.81	481.65	1.2985	34.566	2.704
14	495.21	524.90	1.5760	34.166	2.910
15	530.23	562.72	1.6671	33.686	3.108
16	563.11	605.09	1.9535	33.057	3.308
17	592.19	641.79	2.1692	32.554	3.498
18	634.02	693.63	2.4292	31.791	3.758
19	671.71	741.77	2.6807	30.656	4.008
20	706.29	789.59	2.9788	29.938	4.257
21	732.25	836.18	3.4159	28.299	4.502
22	762.66	880.74	3.6990	27.370	4.760
23	779.00	925.36	4.2401	26.399	5.002
24	801.04	966.62	4.5902	25.058	5.258
25	822.81	1009.16	4.9525	24.656	5.509
26	855.50	1048.02	5.0550	23.789	5.757
27	872.31	1091.38	5.4786	23.123	5.998
28	909.74	1138.25	5.6214	22.331	6.305
29	933.26	1189.65	6.0237	21.622	6.606
30	961.38	1235.25	6.2647	20.803	6.909
31	970.18	1282.16	6.7711	19.680	7.203
32	983.84	1324.77	7.1424	18.816	7.506
33	1000.88	1367.54	7.4605	18.161	7.804
34	1018.10	1410.95	7.7727	17.396	8.108
35	1025.69	1468.22	8.3404	16.255	8.504
36	1043.64	1519.40	8.7048	15.529	8.905
37	1069.02	1571.89	8.9892	14.939	9.304
38	1080.77	1625.23	9.4086	14.152	9.701
39	1104.44	1673.77	9.6496	13.552	10.100
40	1117.58	1724.96	10.0044	12.873	10.501

Table A–17. Deformation J_{IC} and J–R curve results for specimen PWWO–01

Test Number	: 0130	Test Temp	: 290°C
Material Type	: Weld Metal	Heat Number	: PWWO
Aging Temp	: Unaged	Aging Time	: –
Thickness	: 22.80 mm	Net Thickness	: 18.25 mm
Width	: 50.77 mm	Flow Stress	: 398.00 MPa
Modulus E	: 167.43 GPa	(Effective)	
Modulus E	: 180.00 GPa	(Nominal)	
Init. Crack	: 29.0063 mm	Init. a/w	: 0.5714 (Measured)
Final Crack	: 39.8969 mm	Final a/w	: 0.7859 (Measured)
Final Crack	: 39.0107 mm	Final a/w	: 0.7684 (Compliance)
Linear Fit	**$J = B + M(\Delta a)$**		
Intercept B	: 202.069 kJ/m^2	Slope M	: 191.96 kJ/m^3
Fit Coeff. R	: 0.9927	(7 Data Points)	
J_{IC}	: 229.8 kJ/m^2	(1312.1 in.-lb/in.^{2})	
Δa (J_{IC})	: 0.144 mm	(0.0057 in.)	
T average	: 202.9	(J_{IC} at 0.15)	
Power–Law Fit	**$J = C(\Delta a)^n$**		
Coeff. C	: 400.91 kJ/m^2	Exponent n	: 0.4812
Fit Coeff. R	: 0.9883	(7 Data Points)	
$J_{IC}(0.20)$	: 242.7 kJ/m^2	(1386.1 in.-lb/in.^{2})	
Δa (J_{IC})	: 0.352 mm	(0.0139 in.)	
T average	: 202.9	(J_{IC} at 0.20)	
$J_{IC}(0.15)$	: 220.4 kJ/m^2	(1258.6 in.-lb/in.^{2})	
Δa (J_{IC})	: 0.288 mm	(0.0114 in.)	
T average	: 207.7	(J_{IC} at 0.15)	
K_{jc}	: 299.9 MPa–$m^{0.5}$		
J_{IC} Validity & Data Qualification (E 813–85)			
J_{max} allowed	: 577.39 kJ/m^2	($J_{max} = b_o\sigma_f/15$)	
Data Limit	: J_{max} Ignored		
Δa (max) allowed	: 1.837 mm	(at 1.5 exclusion line)	
Data Limit	: 1.5 Exclusion line		
Data Points	: Zone A = 1	Zone B = 3	
Data Point Spacing	: OK		
B_{net} and b_o size	: OK		
dJ/da at J_{IC}	: OK		
a_f Measurement	: Near-surface	Outside Limit	
Initial crack shape	: OK		
Crack size estimate	: Inadequate	(by Compliance)	
E Effective	: OK		
J_{IC} Estimate	: Invalid		
J–R curve Validity & Data Qualification (E 1152–86)			
J_{max} allowed	: 363.08 kJ/m^2	($J_{max} = B_{net}\ \sigma_f/20$)	
Δa (max) allowed	: 2.176 mm	(Δa = 0.1b_o)	
Δa (max) allowed	: 4.457 mm	(ω = 5)	
Data Points	: Zone A = 7	Zone B = 9	
Data Point Spacing	: OK		
J-R Curve Data	: Invalid		

Table A–18. Modified J_{IC} and J–R curve results for specimen PWWO–01

Linear Fit	**$J = B + M(\Delta a)$**		
Intercept B	: 193.262 kJ/m^2	Slope M	: 216.13 kJ/m^3
Fit Coeff. R	: 0.9939	(7 Data Points)	
J_{IC}	: 223.6 kJ/m^2	(1276.9 in.-lb/in.^{2})	
Δa (J_{IC})	: 0.140 mm	(0.0055 in.)	
T average	: 228.5	(J_{IC} at 0.15)	
Power–Law Fit	**$J = C(\Delta a)^n$**		
Coeff. C	: 416.63 kJ/m^2	Exponent n	: 0.5196
Fit Coeff. R	: 0.9896	(7 Data Points)	
J_{IC}(0.20)	: 242.2 kJ/m^2	(1383.3 in.-lb/in.^{2})	
Δa (J_{IC})	: 0.352 mm	(0.0139 in.)	
T average	: 226.4	(J_{IC} at 0.20)	
J_{IC}(0.15)	: 217.7 kJ/m^2	(1243.2 in.-lb/in.^{2})	
Δa (J_{IC})	: 0.287 mm	(0.0113 in.)	
T average	: 231.4	(J_{IC} at 0.15)	
K_{jc}	: 310.4 MPa–$m^{0.5}$		

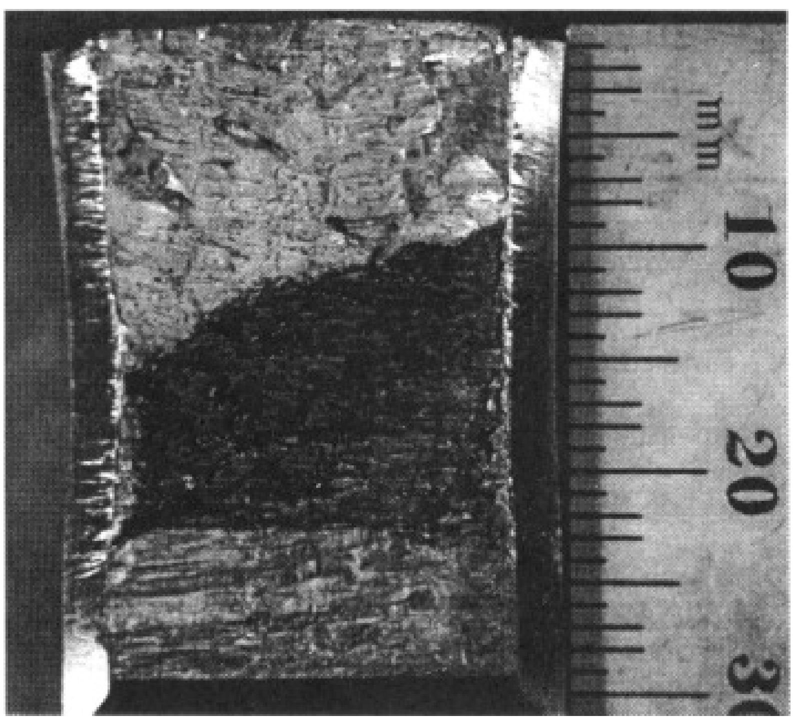

Figure A–16. Fracture surface of unaged weld metal PWWO tested at 290°C

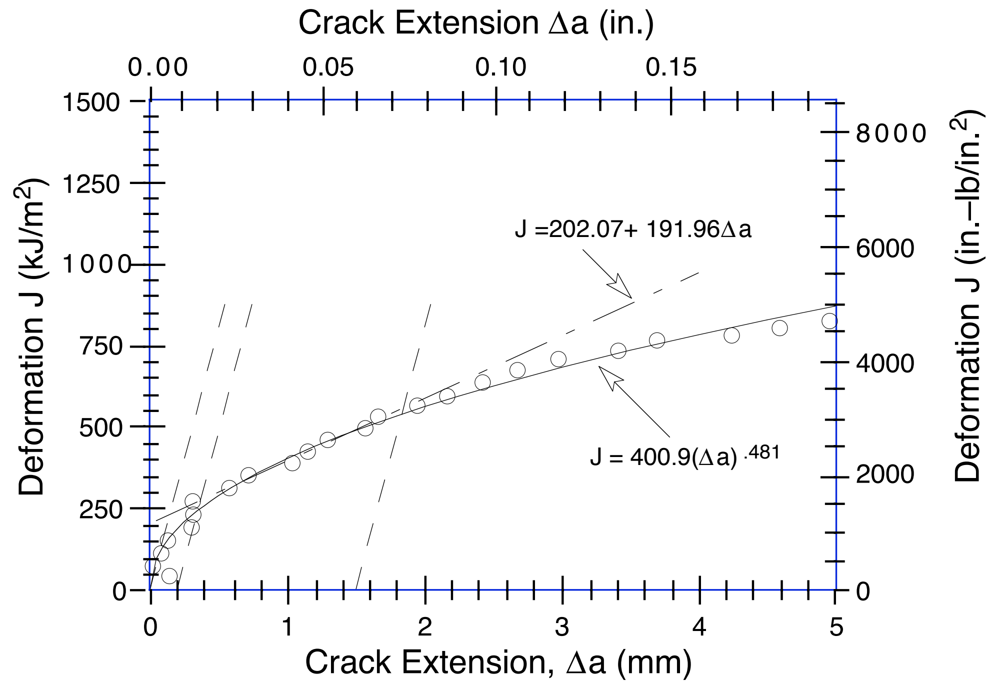

Figure A–17. Deformation J–R curve for unaged weld metal specimen PWWO–01 tested at 290°C. Blunting, 0.2–mm offset, and 1.5–mm offset lines are shown as dashed lines.

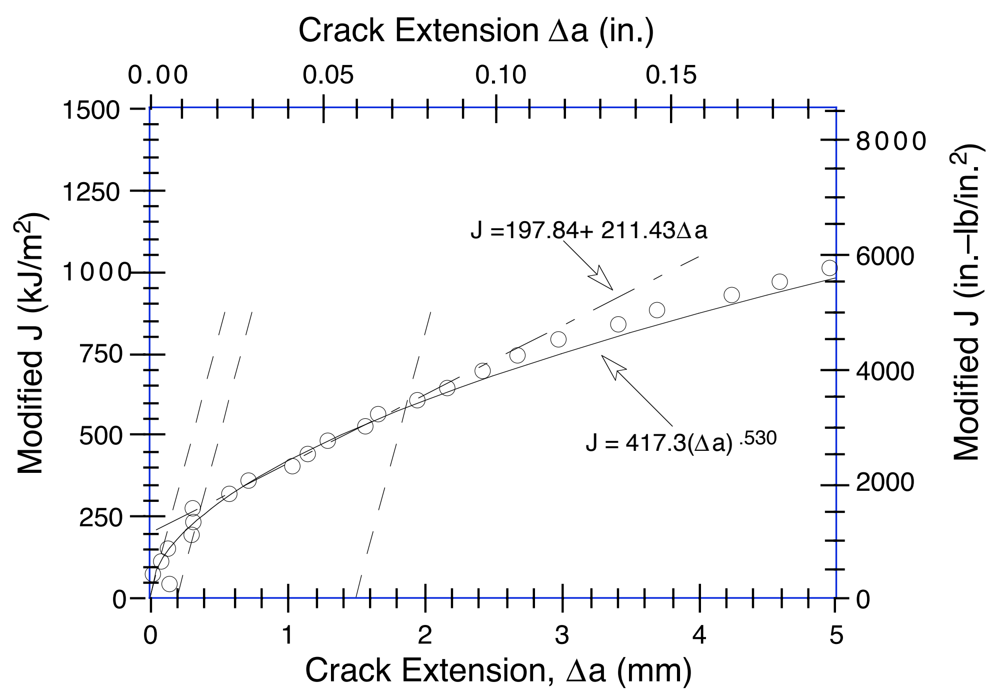

Figure A–18. Modified J–R curve for unaged weld metal specimen PWWO–01 tested at 290°C. Blunting, 0.2–mm offset, and 1.5–mm offset lines are shown as dashed lines.

Table A–19. Test data for specimen PWWO–04

Test Number	: 0128	Test Temp	: 290˚C
Material Type	: Weld Metal	Heat Number	: PWWO
Aging Temp	: 400˚C	Aging Time	: 7,700 h
Thickness	: 22.85 mm	Net Thickness	: 18.20 mm
Width	: 50.81 mm	Flow Stress	: 409.00 MPa

Unload Number	J_d (kJ/m^2)	J_m (kJ/m^2)	Δa (mm)	Load (kN)	Deflection (mm)
1	13.40	13.40	-0.0456	19.223	0.251
2	47.73	47.82	0.0516	31.277	0.502
3	92.07	91.74	-0.0899	36.179	0.754
4	144.59	146.09	0.2313	38.228	1.006
5	193.78	196.10	0.3302	39.176	1.256
6	236.04	240.70	0.5459	39.512	1.459
7	287.38	294.25	0.7041	39.441	1.709
8	328.01	336.63	0.8106	39.193	1.907
9	366.71	382.05	1.1671	38.973	2.106
10	402.81	425.26	1.5010	38.061	2.309
11	435.56	468.56	1.9490	37.500	2.508
12	467.46	509.09	2.2816	36.304	2.707
13	497.52	551.59	2.7202	34.899	2.908
14	524.13	592.40	3.1849	33.871	3.110
15	549.66	630.37	3.5639	32.410	3.307
16	581.33	666.88	3.7014	31.862	3.506
17	607.64	710.43	4.1601	30.839	3.710
18	630.54	748.81	4.5476	29.376	3.918
19	644.64	784.94	5.0753	28.491	4.108
20	663.72	820.03	5.4390	26.850	4.314
21	682.90	853.66	5.7522	25.984	4.508
22	696.65	900.16	6.4259	24.490	4.757
23	716.78	938.28	6.7777	23.311	5.011
24	745.18	1007.55	7.5163	21.719	5.408
25	772.28	1068.00	8.0774	20.143	5.809
26	790.29	1128.74	8.7521	18.615	6.207
27	797.59	1184.41	9.4739	16.729	6.605
28	795.67	1236.86	10.2483	15.274	7.006
29	808.74	1299.16	10.9049	13.672	7.506
30	823.99	1358.76	11.4612	12.533	8.006
31	821.26	1417.30	12.1900	11.294	8.506
32	837.00	1468.40	12.5876	10.347	9.006
33	856.34	1522.71	12.9590	9.622	9.506
34	867.50	1577.34	13.3962	8.848	10.022

Table A–20. Deformation J_{IC} and J–R curve results for specimen PWWO–04

Test Number	: 0128	Test Temp	: 290˚C
Material Type	: Weld Metal	Heat Number	: PWWO
Aging Temp	: 400˚C	Aging Time	: 7,700 h
Thickness	: 22.85 mm	Net Thickness	: 18.20 mm
Width	: 50.81 mm	Flow Stress	: 409.00 MPa
Modulus E	: 171.79 GPa	(Effective)	
Modulus E	: 180.00 GPa	(Nominal)	
Init. Crack	: 27.9188 mm	Init. a/w	: 0.5495 (Measured)
Final Crack	: 41.7750 mm	Final a/w	: 0.8223 (Measured)
Final Crack	: 41.3150 mm	Final a/w	: 0.8132 (Compliance)
Linear Fit	**$J = B + M(\Delta a)$**		
Intercept B	: 150.815 kJ/m^2	Slope M	: 179.85 kJ/m^3
Fit Coeff. R	: 0.9695	(6 Data Points)	
J_{IC}	: 169.4 kJ/m^2	(967.5 in.-lb/in.^{2})	
Δa (J_{IC})	: 0.104 mm	(0.0041 in.)	
T average	: 184.7	(J_{IC} at 0.15)	
Power–Law Fit	**$J = C(\Delta a)^n$**		
Coeff. C	: 338.84 kJ/m^2	Exponent n	: 0.5051
Fit Coeff. R	: 0.9872	(6 Data Points)	
J_{IC}(0.20)	: 189.3 kJ/m^2	(1080.7 in.-lb/in.^{2})	
Δa (J_{IC})	: 0.316 mm	(0.0124 in.)	
T average	: 179.3	(J_{IC} at 0.20)	
J_{IC}(0.15)	: 169.4 kJ/m^2	(967.4 in.-lb/in.^{2})	
Δa (J_{IC})	: 0.254 mm	(0.0100 in.)	
T average	: 183.5	(J_{IC} at 0.15)	
K_{jc}	: 279.0 MPa–$m^{0.5}$		
J_{IC} Validity & Data Qualification (E 813–85)			
J_{max} allowed	: 624.03 kJ/m^2	($J_{max} = b_o \sigma_f/15$)	
Data Limit	: J_{max} Ignored		
Δa (max) allowed	: 1.777 mm	(at 1.5 exclusion line)	
Data Limit	: 1.5 Exclusion line		
Data Points	: Zone A = 2	Zone B = 1	
Data Point Spacing	: OK		
B_{net} and b_o size	: OK		
dJ/da at J_{IC})	: OK		
Initial crack shape	: OK		
Final crack shape	: OK		
Crack size estimate	: Inadequate	(by Compliance)	
E Effective	: OK		
J_{IC} Estimate	: Invalid		
J–R curve Validity & Data Qualification (E 1152–86)			
J_{max} allowed	: 372.11 kJ/m^2	($J_{max} = B_{net}\, \sigma_f/20$)	
Δa (max) allowed	: 2.289 mm	($\Delta a = 0.1 b_o$)	
Δa (max) allowed	: 4.662 mm	($\omega = 5$)	
Data Points	: Zone A = 3	Zone B = 7	
Data Point Spacing	: Inadequate		
J-R Curve Data	: Invalid		

Table A–21. Modified J_{IC} and J–R curve results for specimen PWWO–04

Linear Fit	**$J = B + M(\Delta a)$**		
Intercept B	: 146.094 kJ/m^2	Slope M	: 197.36 kJ/m^3
Fit Coeff. R	: 0.9763	(6 Data Points)	
J_{IC}	: 166.1 kJ/m^2	(948.7 in.-lb/in.^{2})	
Δa (J_{IC})	: 0.102 mm	(0.0040 in.)	
T average	: 202.7	(J_{IC} at 0.15)	
Power–Law Fit	**$J = C(\Delta a)^n$**		
Coeff. C	: 351.67 kJ/m^2	Exponent n	: 0.5325
Fit Coeff. R	: 0.9897	(6 Data Points)	
J_{IC}(0.20)	: 190.6 kJ/m^2	(1088.3 in.-lb/in.^{2})	
Δa (J_{IC})	: 0.316 mm	(0.0125 in.)	
T average	: 195.1	(J_{IC} at 0.20)	
J_{IC}(0.15)	: 169.4 kJ/m^2	(967.0 in.-lb/in.^{2})	
Δa (J_{IC})	: 0.254 mm	(0.0100 in.)	
T average	: 199.4	(J_{IC} at 0.15)	
K_{jc}	: 287.1 MPa–$m^{0.5}$		

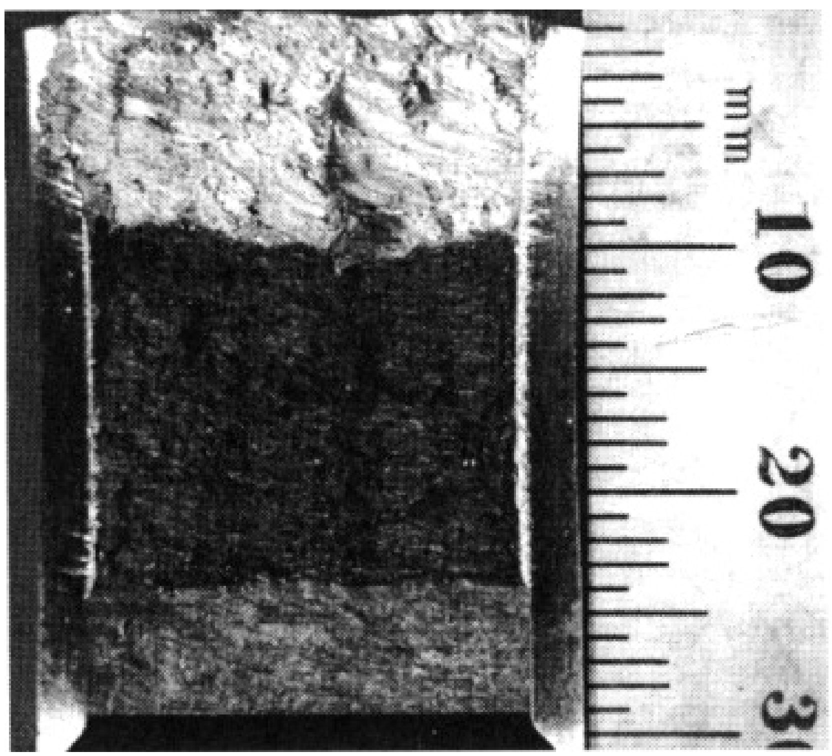

Figure A–19. Fracture surface of aged weld metal PWWO tested at 290°C

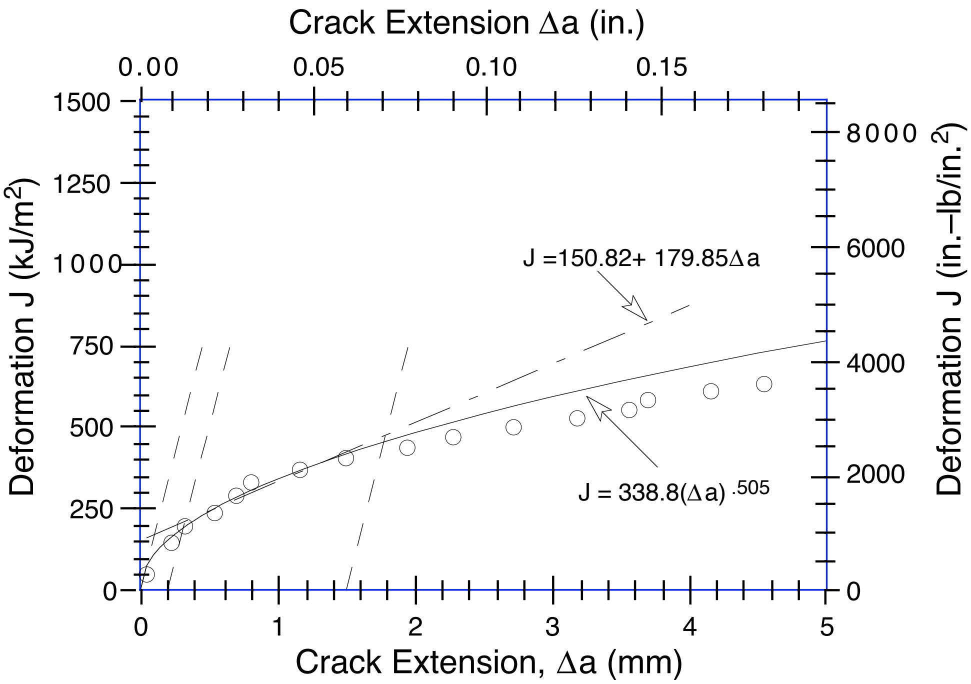

Figure A–20. Deformation J–R curve for weld metal specimen PWWO–04 aged at 400°C for 7,700 h and tested at 290°C. Blunting, 0.2–mm offset, and 1.5–mm offset lines are shown as dashed lines.

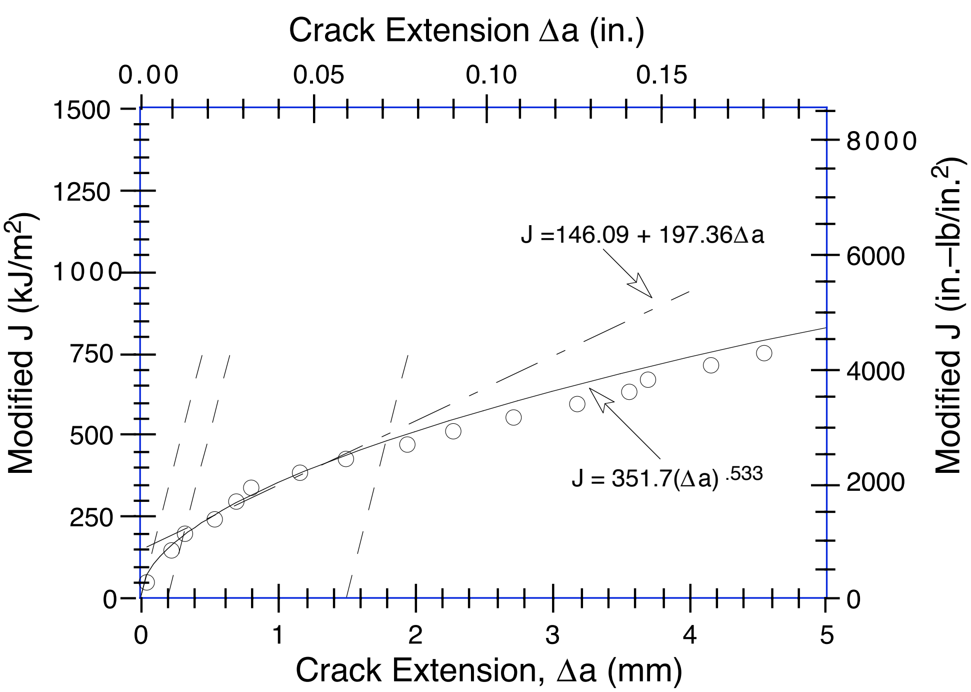

Figure A–21. Modified J–R curve for weld metal specimen PWWO–04 aged at 400°C for 7,700 h and tested at 290°C. Blunting, 0.2–mm offset, and 1.5–mm offset lines are shown as dashed lines.

Table A–22. Test data for specimen PWWO–02

Test Number	: 0126	Test Temp	: 290°C
Material Type	: Weld Metal	Heat Number	: PWWO
Aging Temp	: 400°C	Aging Time	: 7,700 h
Thickness	: 22.84 mm	Net Thickness	: 18.25 mm
Width	: 50.75 mm	Flow Stress	: 409.00 MPa

Unload Number	J_d (kJ/m^2)	J_m (kJ/m^2)	Δa (mm)	Load (kN)	Deflection (mm)
1	13.54	13.54	0.0195	18.816	0.251
2	46.86	46.92	0.0824	29.863	0.502
3	104.46	104.16	-0.0157	35.332	0.826
4	141.63	143.09	0.2938	36.521	1.006
5	190.13	192.42	0.3915	37.441	1.257
6	245.43	251.61	0.7218	37.577	1.528
7	280.46	284.68	0.5809	37.735	1.707
8	321.85	331.83	0.9298	37.440	1.904
9	358.97	373.42	1.1657	37.215	2.108
10	396.27	415.94	1.4102	36.676	2.308
11	428.64	460.78	1.9358	36.078	2.510
12	464.21	495.68	1.9102	35.242	2.708
13	502.69	541.39	2.1608	34.758	2.911
14	536.61	582.55	2.3914	33.899	3.113
15	563.10	624.27	2.8438	32.901	3.310
16	574.73	665.58	3.6785	31.035	3.509
17	599.36	694.23	3.7855	30.069	3.706
18	627.89	735.82	4.1106	29.032	3.910
19	647.42	773.49	4.5391	28.000	4.109
20	666.73	808.84	4.9003	27.134	4.310
21	676.77	845.08	5.4653	25.673	4.506
22	696.31	887.41	5.9308	24.324	4.761
23	700.25	930.89	6.7034	22.719	5.009
24	723.90	993.49	7.4071	20.493	5.411
25	733.33	1052.86	8.2530	18.355	5.807
26	744.51	1107.26	8.9417	16.557	6.213
27	750.04	1158.83	9.6365	15.031	6.606
28	763.97	1207.24	10.1289	13.918	7.005
29	775.01	1270.72	10.8293	12.507	7.506
30	775.96	1326.60	11.5211	10.970	8.005
31	779.86	1378.73	12.0967	9.975	8.507
32	786.84	1429.87	12.5959	9.114	9.014
33	792.04	1478.72	13.0649	8.398	9.510
34	776.02	1527.03	13.7284	7.734	10.007

Table A–23. Deformation J_{IC} and J–R curve results for specimen PWWO–02

Test Number	: 0126	Test Temp	: 290˚C
Material Type	: Weld Metal	Heat Number	: PWWO
Aging Temp	: 400˚C	Aging Time	: 7,700 h
Thickness	: 22.84 mm	Net Thickness	: 18.25 mm
Width	: 50.75 mm	Flow Stress	: 409.00 MPa
Modulus E	: 176.10 GPa	(Effective)	
Modulus E	: 180.00 GPa	(Nominal)	
Init. Crack	: 28.5000 mm	Init. a/w	: 0.5615 (Measured)
Final Crack	: 42.5438 mm	Final a/w	: 0.8382 (Measured)
Final Crack	: 42.2284 mm	Final a/w	: 0.8320 (Compliance)
Linear Fit	**$J = B + M(\Delta a)$**		
Intercept B	: 108.016 kJ/m^2	Slope M	: 214.54 kJ/m^3
Fit Coeff. R	: 0.9604	(7 Data Points)	
J_{IC}	: 124.3 kJ/m^2	(709.9 in.-lb/in.^{2})	
Δa (J_{IC})	: 0.076 mm	(0.0030 in.)	
T average	: 225.9	(J_{IC} at 0.15)	
Power–Law Fit	**$J = C(\Delta a)^n$**		
Coeff. C	: 330.22 kJ/m^2	Exponent n	: 0.6207
Fit Coeff. R	: 0.9690	(7 Data Points)	
J_{IC}(0.20)	: 154.6 kJ/m^2	(882.9 in.-lb/in.^{2})	
Δa (J_{IC})	: 0.295 mm	(0.0116 in.)	
T average	: 219.3	(J_{IC} at 0.20)	
J_{IC}(0.15)	: 133.1 kJ/m^2	(760.1 in.-lb/in.^{2})	
Δa (J_{IC})	: 0.231 mm	(0.0091 in.)	
T average	: 223.2	(J_{IC} at 0.15)	
K_{jc}	: 288.9 MPa–m$^{0.5}$		
J_{IC} Validity & Data Qualification (E 813–85)			
J_{max} allowed	: 606.79 kJ/m^2	($J_{max} = b_o\sigma_f/15$)	
Data Limit	: J_{max} Ignored		
Δa (max) allowed	: 1.790 mm	(at 1.5 exclusion line)	
Data Limit	: 1.5 Exclusion line		
Data Points	: Zone A = 3	Zone B = 1	
Data Point Spacing	: OK		
B_{net} and b_o size	: OK		
dJ/da at J_{IC})	: OK		
a_f Measurement	: Near-surface	Outside Limit	
Initial crack shape	: OK		
Crack size estimate	: Inadequate	(by Compliance)	
E Effective	: OK		
J_{IC} Estimate	: Invalid		
J–R curve Validity & Data Qualification (E 1152–86)			
J_{max} allowed	: 373.11 kJ/m^2	($J_{max} = B_{net}\ \sigma_f/20$)	
Δa (max) allowed	: 2.225 mm	($\Delta a = 0.1b_o$)	
Δa (max) allowed	: 5.605 mm	($\omega = 5$)	
Data Points	: Zone A = 2	Zone B = 10	
Data Point Spacing	: OK		
J-R Curve Data	: Invalid		

Table A–24. Modified J_{IC} and J–R curve results for specimen PWWO–02

Linear Fit	**$J = B + M(\Delta a)$**		
Intercept B	: 103.460 kJ/m^2	Slope M	: 230.95 kJ/m^3
Fit Coeff. R	: 0.9668	(7 Data Points)	
J_{IC}	: 120.5 kJ/m^2	(687.9 in.-lb/in.^{2})	
Δa (J_{IC})	: 0.074 mm	(0.0029 in.)	
T average	: 243.1	(J_{IC} at 0.15)	
Power–Law Fit	**$J = C(\Delta a)^n$**		
Coeff. C	: 341.93 kJ/m^2	Exponent n	: 0.6451
Fit Coeff. R	: 0.9730	(7 Data Points)	
$J_{IC}(0.20)$	: 155.6 kJ/m^2	(888.6 in.-lb/in.^{2})	
Δa (J_{IC})	: 0.295 mm	(0.0116 in.)	
T average	: 234.9	(J_{IC} at 0.20)	
$J_{IC}(0.15)$	: 133.0 kJ/m^2	(759.3 in.-lb/in.^{2})	
Δa (J_{IC})	: 0.231 mm	(0.0091 in.)	
T average	: 238.9	(J_{IC} at 0.15)	
K_{jc}	: 296.9 MPa–$m^{0.5}$		

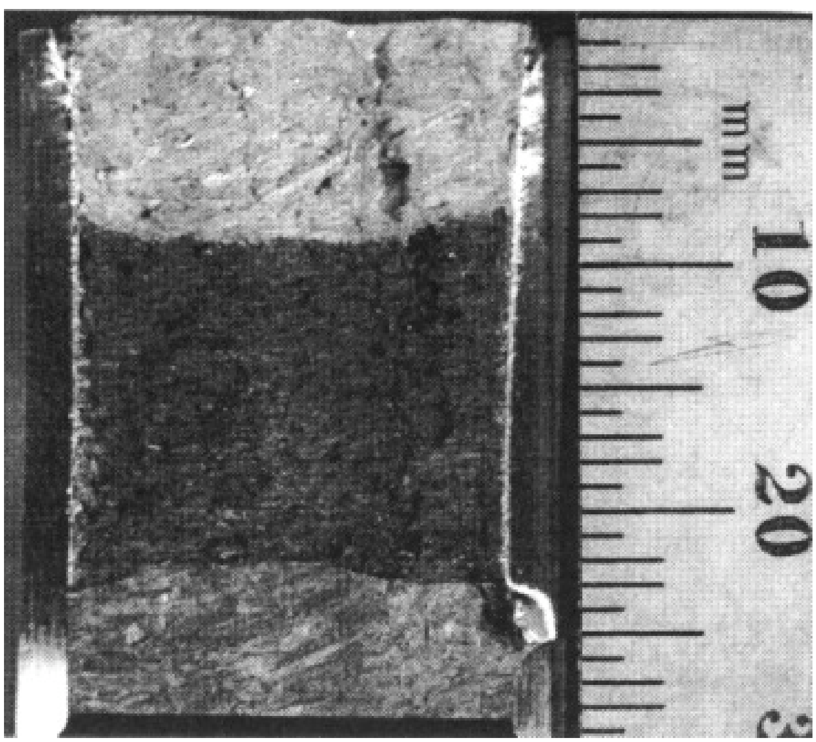

Figure A–22. Fracture surface of aged weld metal PWWO tested at 290°C

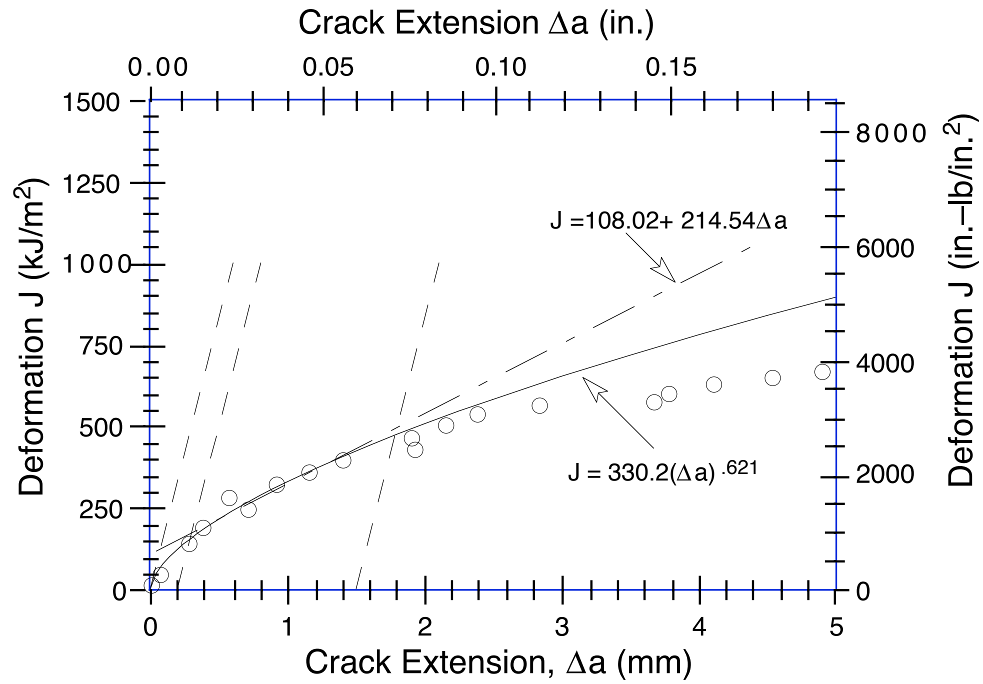

Figure A–23. Deformation J–R curve for weld metal specimen PWWO–02 aged at 400°C for 7,700 h and tested at 290°C. Blunting, 0.2–mm offset, and 1.5–mm offset lines are shown as dashed lines.

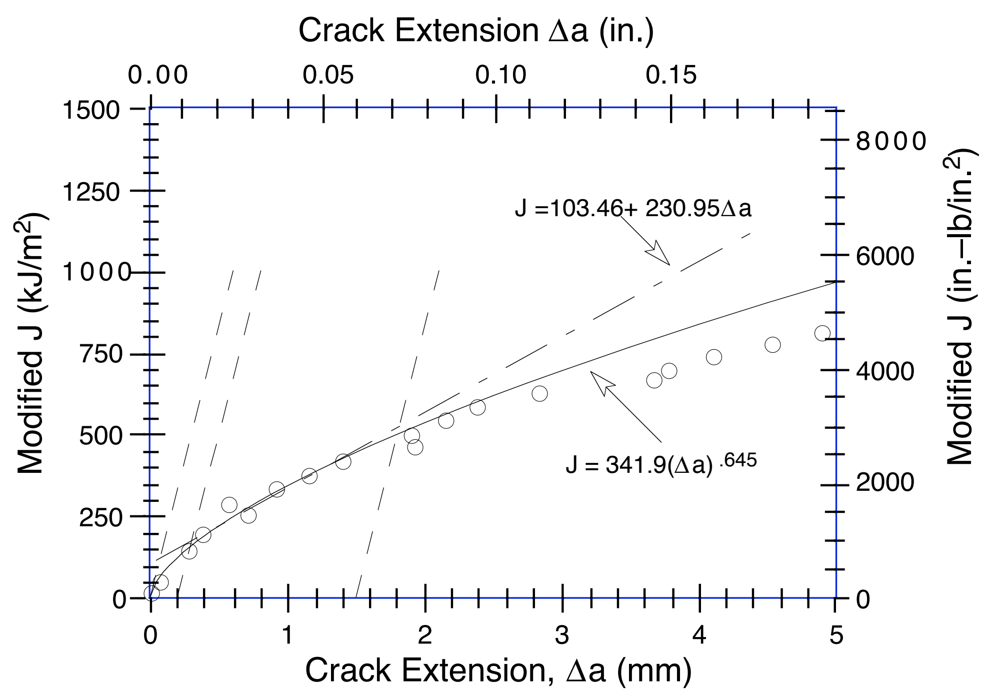

Figure A–24. Modified J–R curve for weld metal specimen PWWO–02 aged at 400°C for 7,700 h and tested at 290°C. Blunting, 0.2–mm offset, and 1.5–mm offset lines are shown as dashed lines.

Table A–25. Test data for specimen PWER–01

Test Number	: 0124	Test Temp	: 290°C
Material Type	: Weld Metal	Heat Number	: PWER
Aging Temp	: 400°C	Aging Time	: 10,000 h
Thickness	: 25.38 mm	Net Thickness	: 20.23 mm
Width	: 50.82 mm	Flow Stress	: 409.00 MPa

Unload Number	J_d (kJ/m^2)	J_m (kJ/m^2)	Δa (mm)	Load (kN)	Deflection (mm)
1	12.77	12.78	0.1408	20.967	0.251
2	35.40	35.22	-0.1580	31.170	0.442
3	63.39	63.48	-0.0061	35.990	0.602
4	91.23	91.75	0.1304	38.466	0.760
5	127.66	127.64	0.0252	40.155	0.957
6	198.54	199.40	0.1229	41.692	1.306
7	279.37	283.71	0.3753	42.390	1.707
8	360.83	365.44	0.3895	42.499	2.107
9	437.53	455.32	0.9520	42.220	2.508
10	512.00	535.78	1.1642	41.331	2.907
11	583.66	622.77	1.6278	40.579	3.310
12	647.88	704.84	2.1016	39.436	3.706
13	718.76	785.96	2.3418	38.515	4.110
14	771.03	871.84	3.0574	37.640	4.507
15	841.60	945.24	3.1118	36.280	4.908
16	896.63	1029.82	3.6325	34.991	5.307
17	950.21	1106.43	4.0083	33.939	5.708
18	997.64	1184.50	4.4740	32.668	6.108
19	1048.57	1259.07	4.8094	31.402	6.512
20	1096.75	1332.20	5.1418	30.192	6.909
21	1129.40	1406.41	5.6667	29.198	7.309
22	1175.69	1479.02	5.9806	28.118	7.730
23	1198.75	1546.87	6.4910	26.822	8.108
24	1231.72	1613.37	6.8557	25.792	8.508
25	1250.47	1681.51	7.3701	24.365	8.908
26	1291.77	1743.02	7.5710	23.214	9.311
27	1322.93	1807.13	7.8847	22.092	9.707
28	1335.63	1869.39	8.3400	21.036	10.107
29	1344.44	1927.58	8.7790	19.808	10.506
30	1353.94	1984.58	9.1879	18.855	10.908
31	1375.00	2039.54	9.4697	18.038	11.308
32	1380.96	2095.58	9.8737	17.166	11.707
33	1394.53	2147.78	10.1758	16.205	12.107

Table A–26. Deformation J_{IC} and J–R curve results for specimen PWER–01

Test Number	: 0124	Test Temp	: 290˚C
Material Type	: Weld Metal	Heat Number	: PWER
Aging Temp	: 400˚C	Aging Time	: 10,000 h
Thickness	: 25.38 mm	Net Thickness	: 20.23 mm
Width	: 50.82 mm	Flow Stress	: 409.00 MPa
Modulus E	: 178.03 GPa	(Effective)	
Modulus E	: 180.00 GPa	(Nominal)	
Init. Crack	: 28.1094 mm	Init. a/w	: 0.5532 (Measured)
Final Crack	: 38.4531 mm	Final a/w	: 0.7567 (Measured)
Final Crack	: 38.2852 mm	Final a/w	: 0.7534 (Compliance)

Linear Fit	**$J = B + M(\Delta a)$**		
Intercept B	: 197.746 kJ/m^2	Slope M	: 248.00 kJ/m^3
Fit Coeff. R	: 0.9890	(4 Data Points)	
J_{IC}	: 233.1 kJ/m^2	(1330.9 in.-lb/$in.^2$)	
Δa (J_{IC})	: 0.142 mm	(0.0056 in.)	
T average	: 263.9	(J_{IC} at 0.15)	

Power–Law Fit	**$J = C(\Delta a)^n$**		
Coeff. C	: 459.43 kJ/m^2	Exponent n	: 0.5092
Fit Coeff. R	: 0.9974	(4 Data Points)	
$J_{IC}(0.20)$	: 276.5 kJ/m^2	(1579.1 in.-lb/$in.^2$)	
Δa (J_{IC})	: 0.369 mm	(0.0145 in.)	
T average	: 243.8	(J_{IC} at 0.20)	
$J_{IC}(0.15)$	: 250.1 kJ/m^2	(1427.9 in.-lb/$in.^2$)	
Δa (J_{IC})	: 0.303 mm	(0.0119 in.)	
T average	: 249.2	(J_{IC} at 0.15)	
K_{jc}	: 336.2 MPa–$m^{0.5}$		

J_{IC} Validity & Data Qualification (E 813–85)

J_{max} allowed	: 619.11 kJ/m^2	($J_{max} = b_o\sigma_f/15$)
Data Limit	: J_{max} Ignored	
Δa (max) allowed	: 1.888 mm	(at 1.5 exclusion line)
Data Limit	: 1.5 Exclusion line	
Data Points	: Zone A = 1	Zone B = 1
Data Point Spacing	: OK	
B_{net} and b_o size	: OK	
dJ/da at J_{IC})	: OK	
a_f Measurement	: Near-surface	Outside Limit
Initial crack shape	: OK	
Crack size estimate	: OK	(by Compliance)
E Effective	: OK	
J_{IC} Estimate	: Invalid	

J–R curve Validity & Data Qualification (E 1152–86)

J_{max} allowed	: 413.62 kJ/m^2	($J_{max} = B_{net}\ \sigma_f/20$)
Δa (max) allowed	: 2.271 mm	($\Delta a = 0.1b_o$)
Δa (max) allowed	: 4.697 mm	($\omega = 5$)
Data Points	: Zone A = 5	Zone B = 5
Data Point Spacing	: Inadequate	
J-R Curve Data	: Invalid	

Table A–27. Modified J_{IC} and J–R curve results for specimen PWER–01

Linear Fit	**$J = B + M(\Delta a)$**		
Intercept B	: 190.581 kJ/m^2	Slope M	: 275.59 kJ/m^3
Fit Coeff. R	: 0.9922	(4 Data Points)	
J_{IC}	: 229.2 kJ/m^2	(1308.7 in.-lb/in.^{2})	
Δa (J_{IC})	: 0.140 mm	(0.0055 in.)	
T average	: 293.3	(J_{IC} at 0.15)	
Power–Law Fit	**$J = C(\Delta a)^n$**		
Coeff. C	: 480.32 kJ/m^2	Exponent n	: 0.5409
Fit Coeff. R	: 0.9979	(4 Data Points)	
J_{IC}(0.20)	: 281.3 kJ/m^2	(1606.4 in.-lb/in.^{2})	
Δa (J_{IC})	: 0.372 mm	(0.0146 in.)	
T average	: 269.2	(J_{IC} at 0.20)	
J_{IC}(0.15)	: 252.4 kJ/m^2	(1441.0 in.-lb/in.^{2})	
Δa (J_{IC})	: 0.304 mm	(0.0120 in.)	
T average	: 274.8	(J_{IC} at 0.15)	
K_{jc}	: 348.7 MPa–m$^{0.5}$		

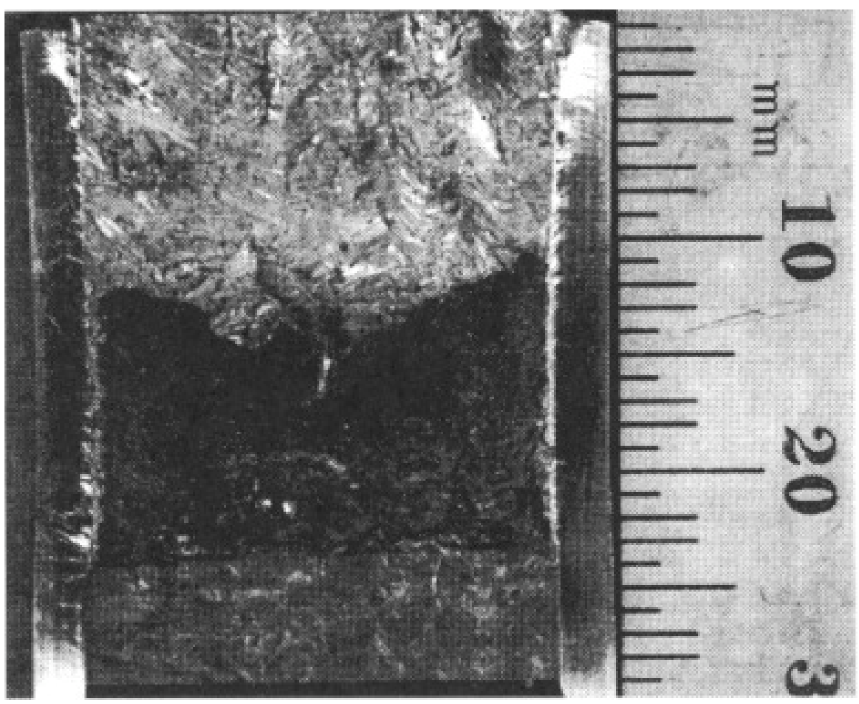

Figure A–25. Fracture surface of aged weld metal PWER tested at 290°C

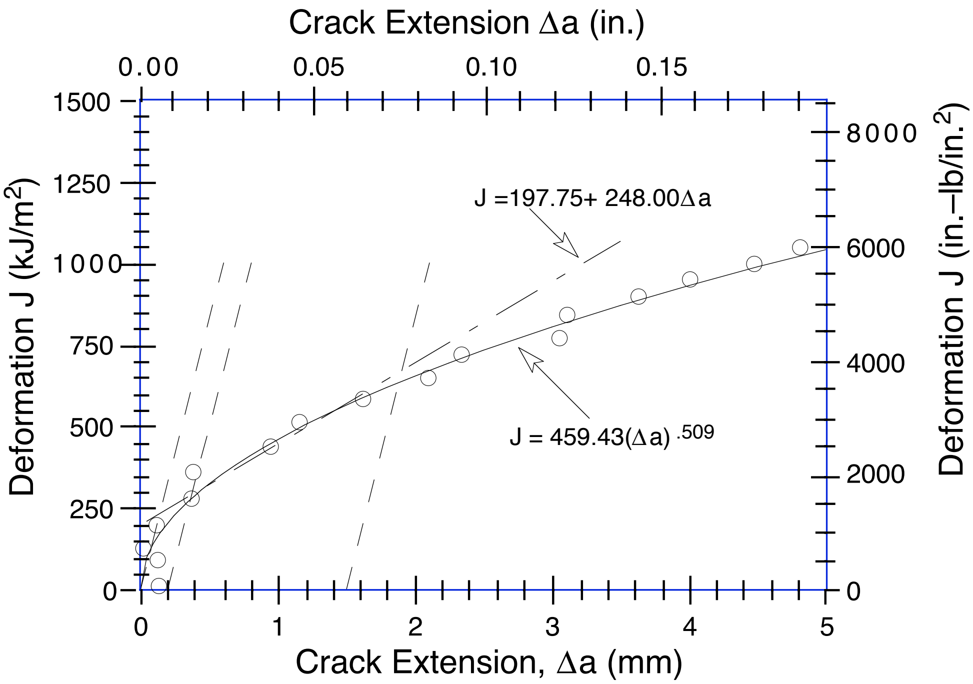

Figure A–26. Deformation J–R curve for weld metal specimen PWER–01 aged at 400°C for 10,000 h and tested at 290°C. Blunting, 0.2–mm offset, and 1.5–mm offset lines are shown as dashed lines.

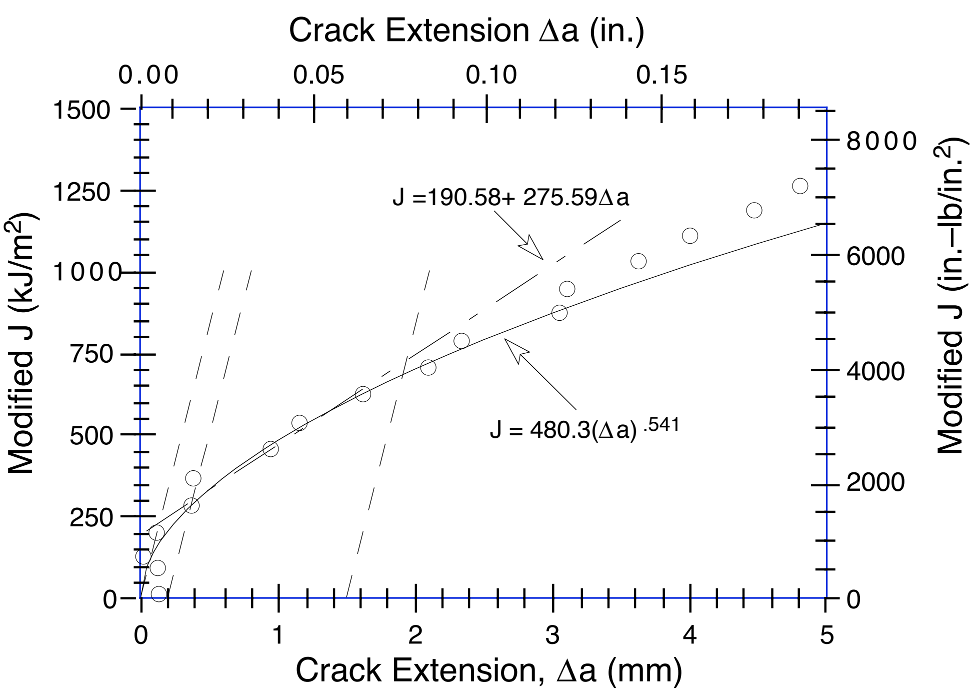

Figure A–27. Modified J–R curve for metal specimen PWER–01 aged at 400°C for 10,000 h and tested at 290°C. Blunting, 0.2–mm offset, and 1.5–mm offset lines are shown as dashed lines.

Distribution for NUREG/CR–6428 (ANL–95/47)

Internal:

W. F. Burke
O. K. Chopra (20)
T. M. Galvin
D. J. Gavenda (5)
T. F. Kassner
C. Malefyt
W. F. Michaud
R. B. Poeppel
W. J. Shack
C. E. Till
R. W. Weeks
TIS Files

External:

NRC, for distribution per R5
ANL Libraries
    ANL–E (2)
    ANL–W
Manager, Chicago Field Office, DOE
Energy Technology Division Review Committee
    H. K. Birnbaum, University of Illinois, Urbana
    R. C. Buchanan, University of Cincinnati, Cincinnati, OH
    S.-N. Liu, Fremont, CA
    H. S. Rosenbaum, Fremont, CA
    R. K. Shah, University of Kentucky, Lexington
    S. Smialowska, Ohio State University, Columbus
    R. E. Smith, Altran Corp., Huntersville, NC
D. Atteridge, Battelle Pacific Northwest Laboratory
W. H. Bamford, Westinghouse Electric Corp., Pittsburgh, PA
K. K. Bandyopadhyay, Brookhaven National Laboratory
J. A. Christensen, Battelle Pacific Northwest Laboratory
A. Cowan, Risley Nuclear Power Development Labs., Risley, Warrington, UK
W. H. Cullen, Materials Engineering Associates, Inc., Lanham, MD
B. J. L. Darlaston, Berkeley Nuclear Laboratories, Berkeley, Gloucestershire, UK
G. Gage, AEA Technology, Harwell Laboratory, Oxfordshire, UK
J. Gilman, Electric Power Research Inst., Palo Alto, CA
W. Gysel, Georg Fischer, Ltd., Schaffhausen, Switzerland
G. E. Hale, The Welding Institute, Abington, Cambridge, UK
P. Hedgecock, APTECH Engineering Services, Inc., Palo Alto, CA
B. Hemsworth, HM Nuclear Installations Inspectorate, London, UK
C. Hoffmann, ABB CE Nuclear Power, Windsor, CT
J. Jansky, Büro für Technische Beratung, Leonberg, Germany
C. E. Jaske, CC Technologies, Cortest, Columbus, OH
G. J. Licina, Structural Integrity Associates, San Jose, CA
T. R. Mager, Westinghouse Electric Corp., Pittsburgh, PA
H. Mehta, General Electric Co., San Jose, CA
Y. Meyzaud, Framatome, Paris La Defense, France
M. Prager, Materials Properties Council, Inc., New York, NY
D. Quiñones, Robert Cloud & Associates, Berkeley, CA
C. Y. Rieg, Electricité de France, Villeurbanne Cedex, France
V. N. Shah, EG&G Idaho, Inc., Idaho Falls, Idaho

G. Slama, Framatome, Paris La Defense, France
D. M. Stevens, Lynchburg Research Center, Babcock & Wilcox Co., Lynchburg, VA
L. Taylor, Nuclear Electric plc., Chelsford Rd., Knutsford, Cheshire, UK
J. C. Van Duysen, Electricité de France, Moret–Sur–Loing, France
S. Yukawa, Boulder, CO

NRC FORM 335
(2–89)
NRCM 1102,
3201, 3202

U. S. NUCLEAR REGULATORY COMMISSION

BIBLIOGRAPHIC DATA SHEET

(See instructions on the reverse)

1. REPORT NUMBER
(Assigned by NRC. Add Vol., Supp., Rev., and Addendum Numbers, if any.)
NUREG/CR–6428
ANL–95/47

2. TITLE AND SUBTITLE
Effects of Thermal Aging on Fracture Toughness and Charpy–Impact Strength of Stainless Steel Pipe Welds

3. DATE REPORT PUBLISHED

MONTH	YEAR
May	1996

4. FIN OR GRANT NUMBER
A2212

5. AUTHOR(S)
D. J. Gavenda, W. F. Michaud, T. M. Galvin, W. F. Burke, and O. K. Chopra

6. TYPE OF REPORT
Technical

7. PERIOD COVERED *(Inclusive Dates)*

8. PERFORMING ORGANIZATION – NAME AND ADDRESS *(If NRC, provide Division, Office or Region, U.S. Nuclear Regulatory Commission, and mailing address; if contractor, provide name and mailing address.)*
Argonne National Laboratory
9700 South Cass Avenue
Argonne, IL 60439

9. SPONSORING ORGANIZATION – NAME AND ADDRESS *(If NRC, type "Same as above": if contractor, provide NRC Division, Office or Region, U.S. Nuclear Regulatory Commission, and mailing address.)*
Division of Engineering
Office of Nuclear Regulatory Research
U.S. Nuclear Regulatory Commission
Washington, DC 20555

10. SUPPLEMENTARY NOTES

11. ABSTRACT (200 words or less)
The degradation of fracture toughness, tensile, and Charpy–impact properties of Type 308 stainless steel (SS) pipe welds due to thermal aging has been characterized at room temperature and 290°C. Thermal aging of SS welds results in moderate decreases in Charpy–impact strength and fracture toughness. For the various welds in this study, upper–shelf energy decreased by 50–80 J/cm^2. The decrease in fracture toughness J–R curve or J_{IC} is relatively small. Thermal aging had little or no effect on the tensile strength of the welds. Fracture properties of SS welds are controlled by the distribution and morphology of second–phase particles. Failure occurs by the formation and growth of microvoids near hard inclusions. Such processes are relatively insensitive to thermal aging. The ferrite phase has little or no effect on the fracture properties of the welds. Differences in fracture resistance of the welds arise from differences in the density and size of inclusions. The mechanical–property data from the present study are consistent with results from other investigations. The existing data have been used to establish minimum expected fracture properties for SS welds.

12. KEY WORDS/DESCRIPTORS *(List words or phrases that will assist researchers in locating this report.)*

13. AVAILABILITY STATEMENT
Unlimited

14. SECURITY CLASSIFICATION
(This Page)
Unclassified
(This Report)
Unclassified

15. NUMBER OF PAGES

16. PRICE